

Mechanisms of Confined Explosions and The Effects of Afterburn – The
Consistency of Experimental Measurement and Thermochemical
Prediction.

Scott Woolford



This thesis is for consideration towards the degree of Doctor of Philosophy
in

The Department of Civil and Structural Engineering, University of Sheffield

Date: 26/01/2024

Declaration

I, Scott Woolford, certify that all the material contained within this document is my own work, except where it is clearly referenced to others.

Date: 26/01/2024

Singed:

Abstract

Developing an improved understanding of explosions occurring in confined spaces is becoming of increasing importance. This is due to the increase in storage silo explosions and ammunition store development and the need to ensure that accidental explosions in these situations can be minimised in terms of effects or risk of occurring. To gain a better understanding of these scenarios, there have been investigations into the confined environments, but with differing conclusions about the repeatability and processes occurring in these confined environments.

A testing regime and methodology was created for this thesis to allow confined experiments to be conducted, investigating the consistency of explosive events and the ability to measure the quasi-static pressures generated. These pressures are generated post initial shock pressures generated by the explosion due to build up of pressure in the system from an increased temperature in the confined space and gas formation increasing the amount of gas in the system. This causes an increase in overall pressure over a longer timeframe in the order of seconds. Using differing masses of explosive in the same volume of confined chamber, a profile for consistency was generated which shows considerable levels of repeatability. Following developing this experimental method, an infra-red thermometer was used to determine the temperatures generated in an explosive event and compared to the ideal gas equation to determine if the assumptions would hold.

A thermochemical model was then generated using the ideal gas equation, predicting the pressures generated in a confined explosion using a chemistry-based approach. This model allows the prediction of maximum quasi-static pressures (QSP) accurately for the charge to volume ratios tested. This model was then tested rigorously by investigating other scenarios such as altered explosive types as well as altered surrounding atmospheres in the chamber, to investigate if the model could cope with other conditions.

These trials were then investigated to understand the processes occurring during the early stage of the explosive event as well as the late time effects such as energy loss through heat transfer. This provided a better understanding of the explosive process and an insight into future work that could be performed in this field.

This leads to a thesis that can be used to show that improvements need to be made in the field of confined explosive measurements and modelling, before outlining and developing the ways to start that process and the impact they could have on the future of this subject.

Acknowledgements

I would like to firstly take the chance to thank my supervisory team, Professor Andrew Tyas, Professor Sam Clarke and Dr Sam Rigby. They have created a welcoming group of researchers that allowed the interest we all share in blast and impact dynamics to prosper and grow with each other's input. I would also like to thank Dr Andrew Barr for his help and motivation towards the end of the thesis, without which I would not have made it to the end.

I would like to add a special mention to Dain Farrimond for keeping me on track when times were hard throughout the PhD process. Always lending an ear when I needed advice on work or with life in general. Without his support throughout the multiple years of being in the north, I would not have made it to the point I have today.

I would like to thank the staff at Blastech for welcoming me into their small, tight knit family and providing a place where I could learn and experience a lot more than an average PhD student gets the chance to withing the course of their studies. Without the help of these staff to teach me the ropes of how the explosives research is conducted thoroughly, my results and data would not have been of the level we managed to achieve.

A special thanks go to Jack Hibbert and Andrew Hibbert for making the north feel more like home, instead of just a place I had to be for work. Without them I would not have enjoyed my time half as much as they made it.

To my family, I want to say thank you for putting up with my seemingly constant complaining and issues and always encouraging me to keep going even when I felt like it was pointless. I would never have imagined I would be able to complete a piece of work such as this if it wasn't for their constant support and encouragement.

Nomenclature

- P = pressure
- V = Volume
- n = moles
- R = ideal gas constant
- T = Temperature
- E = energy
- γ = specific heat capacity ratio
- C_p = specific heat capacity at constant pressure
- C_v = specific heat capacity at constant volume
- Z = scaled distance
- W = charge mass
- R = stand-off distance
- W_{Eg} = equivalent charge weight for gas pressure
- W_{EXP} = weight of the examined explosive
- EF = equivalency factor
- H_{EXP}^c = Heat of combustion of examined explosive
- H_{TNT}^c = Heat of combustion of TNT
- H_{EXP}^d = Heat of detonation of examined explosive
- H_{TNT}^d = Heat of detonation of TNT explosive
- \emptyset = TNT conversion factor
- OB = Oxygen balance
- M = Mass of explosive
- $MW(X)$ = Molecular weight of target molecule (X)
- β_{exp} = total number of moles of O_2 required for full combustion of the fuels from a specific explosive
- ρ_{air} = ambient air density
- Γ_{exp} = volume of air per 1 kg of explosive needed for the full combustion of the fuel in the detonation products
- ΔH_{ab} = afterburn energy
- $\Delta H_r(i)$ = energy released in the full chemical combustion of each component (i)
- ΔH_{tot} = total energy of the reaction
- ΔQ = total heat that is generated by the chemical reaction
- E_{det} = detonation energy
- E_{def} = deflagration energy
- E_0 = initial energy
- T_f = Adiabatic flame temperature at constant pressure

- D = diameter of pipe
- σ =Yield stress of pipe wall
- t = pipe wall thickness
- DLF = dynamic load factor for suddenly applied load

Contents

Table of Contents

Abstract	4
Acknowledgements	6
Nomenclature.....	7
Contents	9
List of Figures.....	12
List of Tables	15
Chapter 1 – Introduction	16
1.1 Background and Motivation	16
1.2 Aim of the Thesis.....	19
1.3 Outline of the Thesis	19
Chapter 2 – Literature Review and Background.....	21
2.1 What are Explosions?	21
2.2 The formation of a shock wave	23
2.3 Free field shock waves.....	26
2.4 Shock Wave Interactions with Structures.....	28
2.5 The Chemistry of Explosives.....	34
2.5.1 The Ideal gas Equation.....	34
2.5.2 Determination of Energy Release.....	36
2.5.3 Specific Heat Capacity	39
2.6 Consistency of Explosive measurements	39
2.6.1 Free-field consistency.....	39
2.6.2 Consistency in Soil	46
2.7 Scaling Laws.....	48
2.8 Charge shape influence	49
2.9 Confined Explosions	51
2.10 Afterburn	55
2.11 Gaps in the literature.....	59
Chapter 3 - Experimental Methodologies	61
3.1 The confined chamber	61
3.2 Data acquisition.....	64

3.3 Pressure gauge set up.	67
3.4 Capability to alter the atmosphere.	70
3.5 The explosive charge	71
3.6 Infra-Red Thermometer set up.....	73
3.7 Step by Step Experimental Procedure	75
Chapter 4 – Theoretical Thermochemical Modelling of Pressure.....	77
4.1 - Introduction.....	77
4.2 The Edri model	79
4.3 The Modified Edri Model.....	81
4.4 Degrees of Freedom and Internal Energy of Gases.....	85
4.5 Worked Examples	87
4.5.1 Nitrogen Atmosphere Example	89
4.5.2 Air Atmosphere Adjustment Example	93
4.5.4 Comparisons of pure explosive to including a binder/plasticiser.....	97
4.5.5 Sensitivity Analysis	98
Chapter 5 - Experimental Results	102
5.1 Test Plan	102
5.2 Thermal Stability	104
5.3 Consistency of Trial Data	108
5.4 Effects of charge shape.....	112
5.5 Atmospheric variation and its effects on QSP	113
5.6 Infrared Thermometry.....	118
Section 6 - Discussion	120
6.1 The Consistency of QSP Explosions	120
6.2 Charge and Chamber Shape Discussion	122
6.3 Ideal Gas Assumptions	123
6.4 Thermochemical model.....	133
Chapter 7 – Conclusions and Future Work.....	143
7.1 Conclusions.....	143
7.1.1 Repeatability of Confined Explosions	143
7.1.2 Afterburn Effects	143
7.1.3 Thermochemical Modelling.....	144
7.1.4 Infrared Thermometry.....	145
7.1.5 Validation of the Model.....	145

7.2 Future work	146
7.2.1 Non ideal explosives.....	146
7.2.2 The use of aluminised explosives that would increase the temperature.	146
7.2.3 Mitigation factors such as water and how these affect afterburn and QSP.	147
7.2.4 Further development of the model to include these facets.	147
7.2.5 DIC of confined chamber	148
7.2.6 Charge size to chamber volume expansion.....	148
Bibliography.....	150

List of Figures

Figure 1 - Shock waves propagating through a medium and coalescing into a discontinuous shock wave. (Kinney & Graham, 1985). a) initial stage of shock generation. b) middle stage of shock formation as the high pressure zone moves towards the front of the wave. c) the final formation of the shock wave with high pressure at the front and lower pressure tail.....	24
Figure 2 - Fireball tracking to show instabilities in the fireball/air boundary in the near field. (Rigby, 2020).....	25
Figure 3 - Far field shock wave tracking to illustrate smooth shock waves in far field. a) real time image of shock wave. b) shock tracking reduction image of shock wave. (D. Farrimond, 2022)	26
Figure 4- An idealised version of free field pressure-time history (Pichandi, 2013)	27
Figure 5– Various forms of shock waves interacting with a plane wedge. (T.V. Bazhenova, 1984). a) single Mach reflection, b) Complex Mach reflection with a kink on the reflected shock, c) double Mach reflection with a second triple point, d) regular reflection.	29
Figure 6 - Relationship between pressure impulse amplification and angle of incidence (Barnat, 2014).	30
Figure 7 - Schematic shock front distance-time diagram for a series of clearing waves travelling across the target face. Subplots show shock front progression at the times indicated. (S.E. Rigby, 2014)	32
Figure 8 - Clearing corrections to UFC-3-340-02 (S.E. Rigby, 2014)	33
Figure 9 - Bomb Calorimeter. A, quartz thermometer; B, nickel resistance thermometer; C, mercury-in-glass thermometer; D, calorimeter bucket with lid; E, Styrofoam support blocks; F, support cable; G, Styrofoam insulation; H, firing-lead connector; I, knife blade heater; J, stirrer; K, bomb; and L, constant-temperature jacket. (Ornellas, 1982)	36
Figure 10 - Bomb calorimeter designed to study the heat of explosion of HE charges of mass up to 100 g (development of the ICP RAS): 1) electric lead; 2) valve; 3) self-sealed cover of the bomb; 4) Teflon or rubber seal; 5) changeable metal liners protecting the bomb walls from being damaged by debris; 6) HE charge; 7) bomb casing. (Pepekin, 2007)	37
Figure 11 - Energy changes during a reaction. (I. Edri, 2013).....	38
Figure 12 - Site layout of (Formby & Wharton, 1996).	42
Figure 13 - Detonation product cloud after 75ms after detonation. (Tyas A, 2016)	44
Figure 14 - Effect of DPC instabilities on pressure loading. (Tyas A. , 2018).....	45
Figure 15 - Controllability of geotechnical conditions Vs repeatability of measured impulse. (Clarke, 2015)	47
Figure 16 - Charge detonation locations a, b and c - (Xiao, 2020).....	49
Figure 17- Regions of highest shock wave velocity surrounded in red lines for four different shaped charges. Sphere (a), cylinder (b), tetrahedron (c), and cube (d) respectively. (Catherine Johnson, 2018)	50
Figure 18 - A more complex pressure distribution that indicates pressure increases at the corner of a confined space. (Baker, 1983).....	52
Figure 19 - Chemical structures of different explosives. (Doble Mukesh, 2005).....	56
Figure 20 - Pressure traces 0.9 m radially from TNT in 1D and 3D. (Balakrishnan Kaushik, 2010)	57
Figure 21 - TNTe factor (EF) of (a) RDX and (b) PETN. (Edri I.E., 2019).....	59

Figure 22 - QSP pipe schematic	61
Figure 23 – 25 mm thickness end plate face on showing the holes and a plug next to it showing how they attach.....	63
Figure 24 – diagram of the inner face of the end plate showing how a rod is held in place. (not to scale)	64
Figure 25 - Comparison of 17-bar gauge and 35 bar gauge for a 30 g PE10 detonation.	65
Figure 26- Diagram of the static pressure pump connected with a pressure gauge and tie-pie system.	66
Figure 27- Schematic diagram for Kulite pressure gauge (KULITE SEMICONDUCTOR PRODUCTS, 2022)	67
Figure 28 – Full schematic for the pipe system. (D. G. Farrimond, 2024)	67
Figure 29 – Gauge bolt mounting system, greased and ungreased. (D. G. Farrimond, 2024) ...	69
Figure 30- Alternate atmosphere chamber configuration.	71
Figure 31 - A PE10 charge with detonator hole.	73
Figure 32 - Schematic drawing of IRT.	74
Figure 33 - PETN thermodynamic model comparison of (Edri I.E., 2019) and the thermochemical model used in this work.....	87
Figure 34 -RDX thermodynamic model comparison of (Edri I.E., 2019) and the thermochemical model used in this work.	88
Figure 35 - Percentage change vs normalised change for mass of PE4.....	100
Figure 36 - Percentage change vs normalised change for Volume of PE4.	100
Figure 37 - Percentage change vs normalised change for Temperature of PE4	101
Figure 38 - Raw pressure-time history plot for test P1. The 35-bar gauge was mounted with a lithium grease filled reservoir and a 17-bar, with a standard air-filled reservoir.	105
Figure 39 - Gauge bolt located inside of the chamber with no separating chamber.	106
Figure 40- Raw pressure-time history plot for 50 g sphere of PE4 detonated within an air atmosphere with pressure gauges taking measurements from direct line of sight to the fireball, installed on the chamber wall, and a gauge mounted in the protective bolt.	107
Figure 41 - Raw pressure-time history plots for nominally identical 50 g PE4 spherical detonations within the described confined chamber, within an air atmosphere across three different timescales of interest.	109
Figure 42- Raw pressure-time history plots and time dependant smoothed average for 50 g PE4 spherical detonations for Test 1.	110
Figure 43-Raw pressure-time history plots for both 50 g sphere and cylinder PE4 detonations within the described confined chamber, denoted by red and blue lines are the TDSA for each test evaluating a peak QSP pressure.	112
Figure 44 - Raw pressure-time histories of 50 g PE4 spherical detonations within a confined chamber with air and nitrogen atmospheres.....	114
Figure 45 - Raw Pressure-Time history of 30 g PE10 spherical charges detonated withing air, nitrogen and argon atmospheres with a TDSA fit for each plot.....	115
Figure 46 – Raw Pressure-Time History of 30 g PE10 over the first few shocks in differing atmospheres.....	116
Figure 47 – Compiled processed maximum QSP data from three explosives, with different atmospheres and different mass to chamber volume ratios.	117
Figure 48 - PE10 trendline and equation through use of a cubic polynomial line of best fit....	118

Figure 49 - Infrared Thermometry of an explosive event in air, argon and nitrogen respectively.	119
Figure 50 – A comparison of 4 50 g PE4 experimental tests showing the consistency of data.	121
Figure 51 - Raw pressure-time history plots for both 50 g sphere and cylinder PE4 detonations within the described confined chamber.....	123
Figure 52 – A comparison of Infra-red thermometry inferred pressure against pressure gauge direct measurements.	124
Figure 53 - Time history of total energy release against energy-release rates of fuel rich explosive (Xiangshao Kong, 2019).	126
Figure 54 – Temperature history for 120 g TNT charge with and without water mist.	127
Figure 55 - Pressure-time history of 120 g TNT with and without mist.	128
Figure 56 - Pressure measurements generated from IRT data compared to direct pressure measurements from a 30 g PE10 charge in an argon atmosphere (D. G Farrimond, 2024).	129
Figure 57 - Pressure measurements derived from IRT temperature data Vs Direct pressure measurements of a 30 g PE10 charge in air (D. G Farrimond, 2024).	130
Figure 58 - Pressure inferred from temperature measurements Vs Direct pressure measurements of a 30 g PE10 charge in a nitrogen atmosphere (D. G Farrimond, 2024).....	131
Figure 59 - Long term behaviour of IRT inferred pressure and gauge pressure.....	133
Figure 60 – Comparison of 50 g PE4 in air against the thermochemical model prediction.	134
Figure 61 – Comparison of thermochemical model with and without plasticiser of a 50 g PE4/pure RDX charge and experimental data.	135
Figure 62 – Comparison of a 30 g PE10 experimental pressure vs predicted pressure.	136
Figure 63 - A comparison of 10 g up to 40 g PE10 charges with comparisons to the thermochemical model.	138
Figure 64 – Comparison of a 50 g PE4 charge detonating in nitrogen and air with thermochemical model prediction lines.	139
Figure 65 - Comparison of a 50 g PE4 charge detonating in argon and air with thermochemical model prediction lines.....	140
Figure 66 - QSP prediction comparisons of PE10 to smoothed data sets for air, argon and nitrogen.	141

List of Tables

Table 1 - Wave speed through different media. (Toolbox, 2024)	23
Table 2 - TNT scaled impulse with and without 3D mixing.	58
Table 3- Heat of reaction of fuel.....	80
Table 4– Detonation reactions and detonation energy.....	80
Table 5 - molecular weight, detonation reaction and detonation energy, adapted from (Edri, 2019).	83
Table 6 - Explosives and corresponding heat of detonation, heat of afterburn and afterburn reaction.	84
Table 7 - Explosive compositions.....	84
Table 8 - Chamber atmosphere pre and post detonation with a nitrogen atmosphere	90
Table 9 - Heat capacity ratios and gamma values for different temperatures of H ₂ O between 750 K and 2000 K. ((The Engineering Toolbox, 2024)).....	91
Table 10 – Iterative solving of temperature values.	92
Table 11 – Chamber atmosphere pre and post detonation in air.....	94
Table 12- Chamber atmosphere pre and post detonation in nitrogen.	95
Table 13 – Iteration of temperature values for air test.	96
Table 14 - Pressure and Temperature ratios comparison at different charge mass to volume ratios for pure explosives and those including binders and plasticisers.	97
Table 15 – Percentage change of mass and normalised change for 40 g of PE4.....	98
Table 16 – Percentage change of volume and normalised change for 40 g of PE4.....	99
Table 17 – Percentage change of temperature and normalised change for 40 g of PE4.	99
Table 18 - Test summary (Tests P1 and P2 were part of a different study so details on charge type and mass cannot be included so have been denoted as X and Y.).....	103
Table 19 – Maximum QSP values determined from experimental data.....	111
Table 20 - Max QSP from experimental vs theoretical for a PE4 in air tests.	137
Table 21 - Max QSP from experimental vs theoretical for a PE10 in air tests.	137
Table 22 - Max QSP from experimental vs theoretical for PE4 and PE10 in nitrogen and argon.	142

Chapter 1 – Introduction

In this thesis, the influence of confinement on an explosion will be explored through theoretical modelling and experimental testing and validation. The main focus will be on plasticised versions of ideal explosives, RDX and PETN in a fully confined environment, investigating consistency and the influence of changes to the system. This work will be put into context by providing an analytical tool for prediction of confined explosion events and comparing this to previous and current modelling of these scenarios.

This chapter gives an outline of the thesis structure and motivations behind the investigations undertaken later in the thesis.

1.1 Background and Motivation

Explosions occur for many reasons, from accidental detonations in storage locations and manufacturing facilities to terrorist attacks. These can occur in many location types such as mines and tunnels, vehicles and boats. Among the most notable terror attacks related to this work were the 7/7 bombings, where multiple explosions occurred in confined environments, resulting in the loss of 52 lives and damage to structures (H.D.L. Patel, 2012). Much research into free-air explosions has been undertaken in the past, as they are common when dealing with historic scenarios (Baker, 1983) (Dewey, 1964) (Cooper, 2018). However, when looking at accidental or terrorist explosions in recent history, a number of them occurred in confined spaces (Hu Y, 2011), where reflections of the shock waves interact with the surrounding structures/boundaries (Alex M. Remennikov, 2005). Confinement is also used to aid in the disposal of high-hazard explosive devices to contain or confine the explosives output (UFC-3-340-02, 2008), often when they contain hazardous materials and cannot be disposed of in controlled demolitions externally. It is especially important in these cases that the confinement is strong enough that it will not fail due to the pressures generated in the explosive event, as this would lead to the dispersal of dangerous chemicals. In cases where there is no additional risk of chemical release or similar, less robust barriers can be used to protect from explosive events such as HESCO or water barriers through absorbing kinetic energy out of the system.

When investigating blast parameters, there can be two types in terms of confinement. The first is free field, where there is no boundary or obstacle to the shock wave expansion and the detonation product cloud (DPC) is free to expand in space. Then there are confined explosions, (which can be fully or partially confined) where there is interference from an object or containing system to the expansion of a shock wave causing reflections and mixing

of the detonation product cloud. These are normally partially confined in the real world such as buildings with doors but can still be full confined in some situations.

It is important to understand the differences between a fully confined chamber compared against a partially confined chamber; the venting present in a partially confined chamber will allow the pressure to reduce at a higher rate than if there was no venting due to the increase in energy that can be expelled from the system through pressure loss and temperature loss. This venting of pressure reduces damage to the structure compared to full confinement, which usually causes more severe damage (Xiangshao Kong, 2019). The reduction in damage to structures by using venting in the case of an explosion is created by including design features covering vent holes in materials or systems that will begin venting when the pressure wave interacts with them, such as scored glass, hinged panels or lighter sections of wall or roof (V.R. Feldgun, 2011). If a structure experiences significant damage to some members due to a confined explosion, it can occur that this damage causes other supporting members of a structure to fail (Griffiths, 1968), which is why it is important to understand the pressures that may be generated in a confined explosion so that they can be predicted effectively and avoid excess damage to structures or total collapse.

When a structure is exposed to a blast, the variation in the pressures experienced can be large depending on the confinement of the surrounding structure. Even if two charges at an equal scaled distance from a surface occurred, they would have different pressures if those surfaces were differently confined (Salvado, 2017). This is due to the confinement causing an increase in duration that the load will be imparted on the structure, this increase in duration causes an increase in the impulse load acting on the structure which could cause a significant amount more damage than a short duration load.

When these venting capabilities can't be introduced to a structure, a fully confined explosion occurs. (Feldgun V.R., 2016) shows the difference between early-time pressures in a chamber when comparing vented to unvented. It is shown that pressure significantly decreases when there is venting available for the gas pressure to escape through. This lack of drop-off in pressure over the first instances after a confined explosion causes more stress to be imparted on the structure. This occurs through the temperature and pressure increase in a sealed environment having limited ways to escape to the surrounding environment and the ways it can such as conduction through the chamber or through any leaks in the system occur slower than in the free field, causing the pressure and temperature to remain higher in the confinement for longer, which leads to more damage or failure.

This thesis provides further insight into the mechanisms behind confined explosions and attempts to contribute to this insight by creating a fast-running model that can predict quasi static pressures generated from confined explosions without need for complex modelling

solutions. It is also part of a larger series of work looking into the repeatability of explosive testing as a whole, with work such as (Farrimond, 2023) being completed on free field variability, as well as other research papers being developed on quasi-static pressure in manuscript currently. Once this overarching project known as MACE (mechanisms and characterisation of explosives) has been completed, there should be a greater understanding of blast testing and the methods to achieve repeatable testing regimes in many circumstances.

1.2 Aim of the Thesis

The Objectives of this PhD thesis are as follows:

- 1) Investigate the use of the ideal gas equation and determine whether it can be used to estimate the pressure generated from a confined explosion of an ideal explosive.
- 2) Derive a predictive model based on the ideal gas equation.
- 3) Develop an experimental procedure to accurately and reliably measure the output from confined explosions in order to generate validation data for the predictive model.
- 4) Demonstrate the validity of the model for a number of unseen scenarios, such as different explosives and environments.
- 5) Use a combination of experimental data and predictive model to comprehensively investigate the effect of afterburn and identify the mechanisms that cause this phenomenon.

1.3 Outline of the Thesis

- Chapter 1 – An introduction to the background and motivation of the thesis, as well as the objectives that are aimed to be completed during the thesis.
- Chapter 2 – The development of a comprehensive understanding of the current state of research dealing with confined explosions and the ideal gas equation in these circumstances. This will be presented in the form of a literature review, discussing how current research has developed and the gaps in the knowledge that need to be addressed and considered for this thesis. This prior understanding is vital to develop models and experiments that are of value to fill in these gaps and explore into the topics further.
- Chapter 3 – An explanation of the design of the testing regime and the methodologies for carrying out the tests with a comprehensive discussion of how and why things were done.
- Chapter 4 – The development of a thermochemical predictor that can be used to estimate maximum QSP values for differing circumstances and the chemistry it is based on.

- Chapter 5 – A description of the results, explaining the features and mechanisms discovered through a closer look at the pressure traces generated through the different series of tests. These discussions aim to answer the effects of the afterburn phenomenon as well as the effects of thermal sinks and the capability of the model to work with these additional influences.
- Chapter 6 – Discussion of the results, going into further detail about the link between the experimental data and the thermochemical model to explore the usefulness of the model and accuracy of the testing.
- Chapter 7 – Final conclusions and an overview of the main topics discussed in the thesis to summarise the findings and discuss the possible future work that could be done to further the development.

Chapter 2 – Literature Review and Background

2.1 What are Explosions?

A chemical explosion in an explosive material occurs when a chemical reaction occurs rapidly enough that the energy is passed through the material as a wave. When this reaction wave travels at a speed between 1500 and 9000 ms⁻¹ this is classified as a detonation. This reaction results in the exothermic release of energy and formation of gaseous products in a very small timeframe which causes a very hot, very dense gas in the space occupied by the previously solid explosive (Akhavan, 2022). The speed at which this reaction (conversion of solid explosive to gaseous detonation products) occurs at is dependent on the charge itself, composition of the explosive being the main factor that affects this reaction wave speed. Because this reaction happens in the order of microseconds, it causes extreme pressures and temperature of 10-30 GPa and 3000-4000 degrees respectively due to it being confined to such a small volume and being such an exothermic reaction. As the reaction wave passes through the solid explosive, the reaction of the material constantly provides energy to the reaction in front of it allowing it to be self-sustaining once initiated until it reaches an outer bound of the explosive substance.

This reaction wave occurring through the explosive material releases energy through the breaking of intermolecular bonds during oxidisation of the substance. This change from molecules in the substance to individual atoms or much smaller molecules is favourable in terms of entropy, creating more molecules than it began with.

Pioneering explosive research was focused on free field testing and understanding the generation of shock waves and prediction methods for them. (Taylor, 1950) proposed that an explosion could be considered as a finite amount of energy being released at an infinitely concentrated point, and then the motion and pressure of the surrounding air can be calculated. This assumption is based on the explosion process occurring at such speeds that the conversion of solid to gas can be assumed to be instantaneous, allowing a more simplistic approach to be developed.

Some early work by (J. A. Zukas, 2013) introduced some assumptions for creating a more simplistic approach to explosions being generated. This approach considered the event as one dimensional, using assumptions where there was no loss of energy to the surroundings as the shock wave propagated through mediums. Another assumption is that the detonation wave is planar and doesn't have any curvature on the shock front, which is not possible when considering the loss of energy at a boundary. This loss will cause the outer edge of the shock wave to have less energy than the internal side from the point source of expansion. This difference in energy causes the surface of the shock wave to be pushed by the internal component of the shock wave.

(J. A. Zukas, 2013) also assumed the chemical reaction is completed instantly with zero reaction zone length and products behind the shock wave are in chemical and thermodynamic equilibrium. In practice, this is not realistic as there is some time discrepancy between the shock wave starting and reaching the bounds of the explosive, and due to the nature of the explosion process the process is not in equilibrium. Velocity of the wave is also considered constant even though this is dependent on the explosive in question as different explosives have different shock wave velocities.

The current accepted structure of a high explosive event is given by (S. Paterson, 1955). He describes three separate zones, the first of which is the pre-detonation region before a part of the explosive has been subjected to the energy required to cause it to propagate the shock wave. This is still the composition it was before any explosive event started to occur in the substance.

The second section is the leading shock front. This shock front is composed of the compressed explosive material that is in the initial stages of exothermic reaction releasing considerable amounts of energy and transferring this energy to the unreacted zone. Chapman and Jouguet's detonation theory (JACOBS, 1968) has the reaction occurring instantaneously with the shock becoming supersonic at the Chapman-Jouguet point (C-J point). To contrast this theory, Von Neuman argued that this reaction at the shock front occurs over a finite time with a reaction zone length (Sollier, 2016). This results in a significant difference between the pressure and temperature on either side of this shock wave reaction zone. They then took this further to develop the theory of an induction period between reaction initiation and the compression of the detonation wave.

After the chemical reaction completes, the third section is formed where the detonation products are no longer confined by the inertia from the previous medium of the explosive. This leads to the products being able to expand freely from the rear of the shock wave path.

The density of an explosive also contributes to its reaction speed and shock wave propagation, this is dependent on the composition of the explosive as each different explosive will have an optimal density at which it can transfer this shock energy through the substance. Even small changes in density of an explosive within a charge can affect the effectiveness of the explosive and also the energy required to detonate it (S. Davis Herring, 2010).

Another factor affecting the efficiency of the shock wave propagation through an explosive is whether the explosive is considered to be an ideal explosive or a non-ideal explosive. An ideal explosive is one that can be considered to transfer from shock wave in the explosive to air instantaneously upon detonation because the time frame between this occurring and the shock transferring to air can be considered instantaneous. A non-ideal explosive is one where this time of detonation cannot be considered instantaneous and there is a significant time for a reaction to occur, this often happens when there is oxygen produced by the explosive that then

can react instantaneously with the fuels produced by the explosion, causing a fireball as these reactions take place during initial expansion. Non ideal explosives can also include those where the explosive generates additional fuel which reacts with oxygen in the atmosphere outside of the initial fireball causing an even longer reaction time of detonation. These could be denoted as ideal, non-ideal and fuel rich respectively.

Explosives can also be split into primary and secondary. These are categorised by their sensitivity to external initiation sources. A primary explosive is the most sensitive to external initiation and often can be initiated by sparks, heat, friction or impact. An example of a primary explosive is lead azide and lead styphnate. These sensitive explosives are often used to initiate the secondary explosives that are less sensitive and require more energy to initiate due to the increased sensitivity of their structure. An example of a secondary explosive would be TNT, RDX or HMX. This use of primary explosives to initiate secondary ones is often referred to as an explosive train, causing a chain reaction from the most sensitive explosive to the least sensitive.

2.2 The formation of a shock wave

When an explosive has completed detonation and the detonation wave has reached the boundary of the charge and free air, this causes a discontinuity between the charge and the surrounding medium. Because of this discontinuity, the detonation wave starts to expand out into this new medium as well as causing a reflection wave that travels back through the previously detonated material to its centre. This expansion of the detonation products will occur at a rate dependant on the medium that it is expanding into. This thesis considers three gasses; air, argon and nitrogen, each with a different speed at which this wave would propagate. The standard wave speeds through each medium between 20 °C and 30 °C are shown in Table 1 below.

Table 1 - Wave speed through different media. (Toolbox, 2024)

Medium	Wave speed m/s
Air	343 (20 °C)
Nitrogen	354.4 (29°C)
Argon	323 (27°C)

All three of the gasses considered in this thesis are compressible fluids, which means that as this rapid expansion of the compressed detonation products break out into the compressible medium, they cause the propagation of this pressure as a shock wave by compressing the external medium. This occurs almost instantaneously at the border between the charge and the medium since we are considering ideal explosives and propagates outwards

forming the shock wave (Kinney & Graham, 1985). Shown in Figure 1 is a diagram from Kinney and Graham that shows the compression of the shock wave as it travels through a medium that is providing a force against its direction of travel. Part (a) of the figure shows the initial pressure profile of the wave, where the highest-pressure zone is at the centre of the wave. Because this high-pressure is denser than the surroundings it will have a faster wave speed through the air and will subsequently travel faster than the lower pressure in front of it, it will start to skew this pressure profile as it travels to part (b). At this point the higher pressure section is closer towards the front of the wave but will continue faster than the front due to its higher pressure until it reaches the front of the wave, creating a flat front at part (c). As it is in part c it has the maximum pressure at the front of the wave and so when coming into contact with a structure will deliver maximum pressure instantly followed by the lower pressure tail.

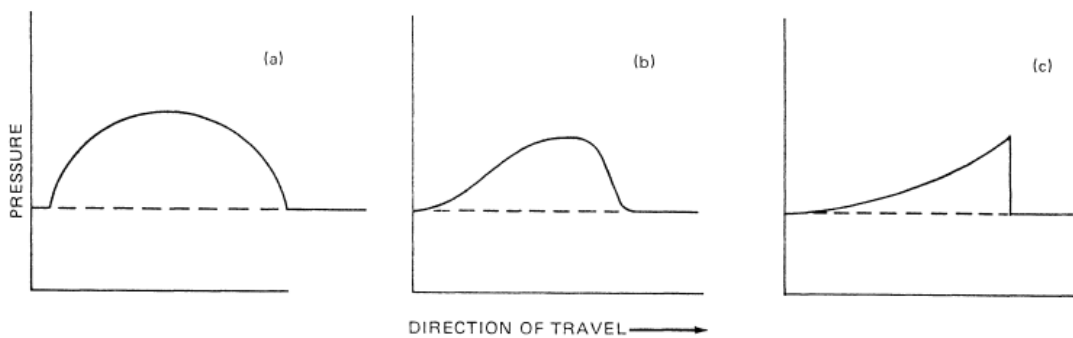


Figure 1 - Shock waves propagating through a medium and coalescing into a discontinuous shock wave. (Kinney & Graham, 1985). a) initial stage of shock generation. b) middle stage of shock formation as the high-pressure zone moves towards the front of the wave. c) the final formation of the shock wave with high pressure at the front and lower pressure tail.

As a shock wave propagate out from the detonating explosive, it will be accompanied by the expanding detonation products from the chemical reaction. This is due to the fact that the detonation products that are now gasses are at a much higher pressure than the surrounding medium. In the early stages of a detonation, both the fireball and the shock wave travel at approximately the same speed as one another until the detonation products are slowed too much by their own expansion, losing energy and beginning to slow. The shock wave continues to travel and compress the surrounding medium separating from the fireball/detonation products.

As a spherical or hemispherical charge detonates, it produces a spherical shock wave surrounding the charge (assuming that it was detonated in the centre of the explosive). As this shock wave expands out through the medium it will slowly lose energy due to having to force its way through the surrounding medium that is yet to be compressed. This loss of energy causes a decay in the pressure as it tends back towards ambient pressure. Whilst the shock wave is still “attached” to the expanding fireball, this is considered the near field, and when the shock wave separates from the fireball, this is considered to then be the far field. Separation typically occurs

once expansion has reached approximately 10 times the original charge, with the near field thereby loosely being defined as the region within 10 charge radii.

The difference between a shock that is near field compared to far field, is the effect that the fireball is said to be having on the shock wave. Whilst the shock is expanding with the fireball, it will be affected by the instabilities and temperature changes of the fireball, which can vary over the fireball surface, whereas when this has separated from the fireball it has no influence from this fireball and so will smooth out and become a uniform shock wave. The instabilities of a fireball are shown in Figure 2 below.

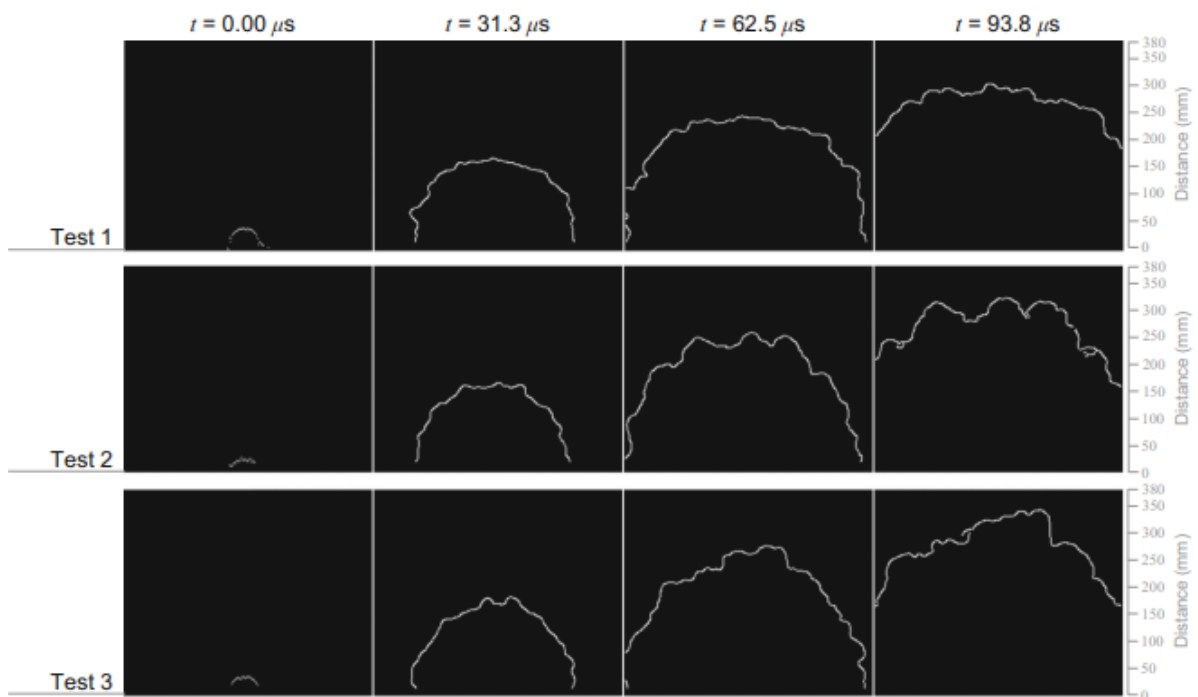


Figure 2 - Fireball tracking to show instabilities in the fireball/air boundary in the near field. (Rigby, 2020)

After this separation, when the fireball has stopped interacting with the shock wave, the shock wave will start to coalesce back into a smooth shock wave through the force of the air that its pushing against causing the different instabilities to equilibrate between them (Figure 3). The very early stages (few microseconds) straight after detonation are also in this spherical shape for a short time before they start to develop instabilities, so it is a process from smooth to unstable to smooth again within this near field. This process of stability to instability is why blast load parameters in the near field are more difficult to accurately quantify than those of the far field (alongside the considerably higher magnitudes and shorter durations).

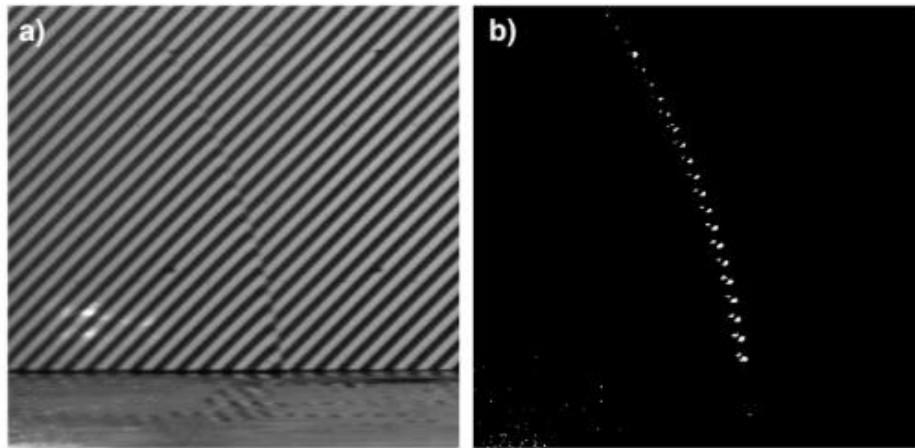


Figure 3 - Far field shock wave tracking to illustrate smooth shock waves in far field. a) real time image of shock wave. b) shock tracking reduction image of shock wave. (D. Farrimond, 2022)

2.3 Free field shock waves

A shock wave reaching the boundary of its solid structure causes a discontinuity between the wave and the surrounding medium resulting in the rapid expansion of the detonation products into the surroundings (Davison, 2008). This expansion forces the external medium out with a force dependant on the wave's energy. In this thesis a few different external mediums are considered, air, nitrogen and argon. In terms of nitrogen gas, it is compositionally very similar to air as nitrogen makes up approximately 78% of it (Brimblecombe, 1996), meaning it will have very similar properties to that of air tests. Argon on the other hand has a higher density of 1.603 g/L at 26.9°C compared to air at 1.184 g/L at 25°C. This difference in density will likely cause the wave to transfer at a different speed through the medium as the frequency of a wave doesn't change, but this just means that the wave will start to travel at a different speed.

When considering an explosion event, the characteristics are also dependant on external factors, not just the explosive itself. When an explosive detonation in free air occurs (where there are no obstacles or structures affecting shock wave travel), there is a characteristic increase in air pressure that increases above ambient conditions due to the shock pressure expanding up to a maximum peak overpressure, followed by a pressure decay back down to ambient pressure (Tyas A. , 2018). Considerable research has been carried out to establish a well-rounded understanding of this explosion process including the formulation of a series of predictors using semi-empirical formulae (Swisdak, 1994) (S. E. Rigby, 2014). These are based on large amounts of experimental data from sources such as (Kingery & Bulmash, 1984) who first created the K-B model to calculate overpressure generated in the positive phase of an explosion.

After the initial pressure rise of a free field explosion, the pressure starts to decay back to atmospheric pressure, however due to the rapid expansion that has taken place, there will occur a phenomenon called the negative phase where the pressure goes below atmospheric pressure for a duration dependant on the initial shock as described by (Rigby SE, 2014). This is due to the rapid expansion causing an under-pressure system inside the expanding shock wave. This overexpansion from the shock wave leaves the low-pressure zone in the centre of the explosive event, causing the pressure to need to further equilibrate even after the shock reaches its outer bound, this is known as the negative phase and can cause further displacement of debris or equivalent when passing over objects. The different stages of a free field detonation can be seen in Figure 4 by (Pichandi, 2013) which points out the different phases of a blast wave.

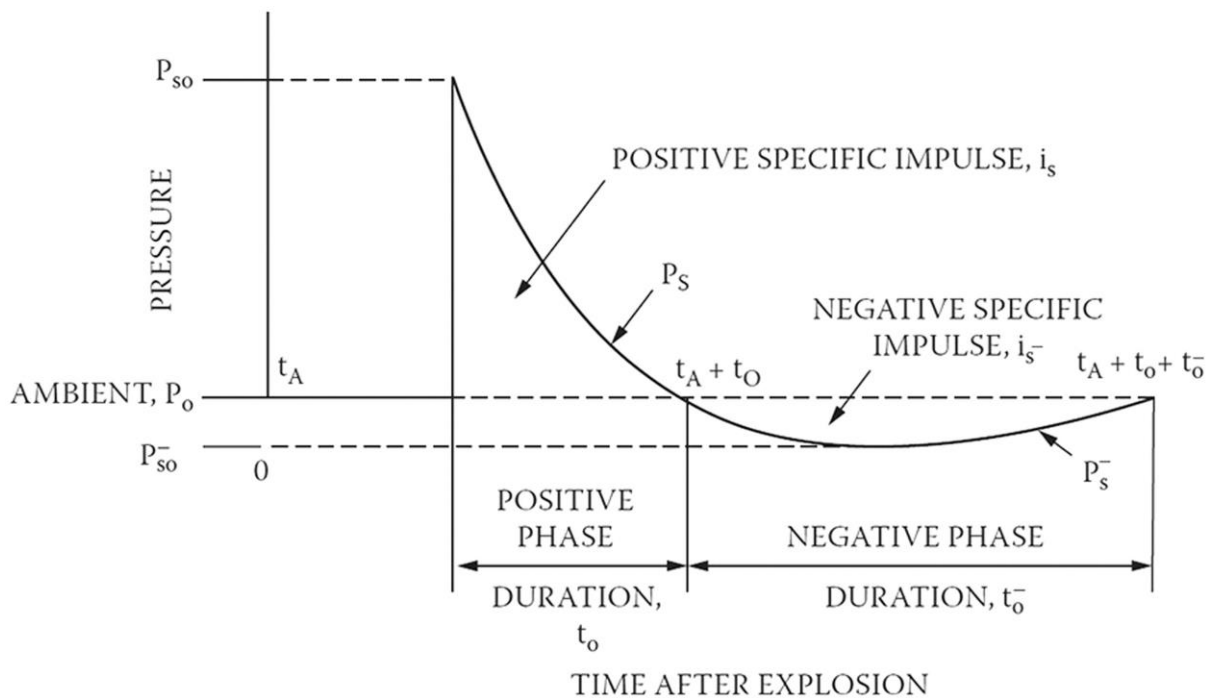


Figure 4- An idealised version of free field pressure-time history (Pichandi, 2013)

The ambient pressure is the pressure of the environment, which in most cases is around 1 bar, the positive phase duration is the length of time that the pressure is above the ambient pressure before returning to the ambient pressure which leads into the negative phase where the pressure reduces due to overexpansion of the shock wave and the duration is the time it takes for this reduction in pressure to return to the ambient pressure. The positive and negative specific impulse are the integral of the pressure over the positive or negative phase with respect to time. The time of detonation is given by t_A and the distance between that and the positive phase occurring is the arrival time.

2.4 Shock Wave Interactions with Structures

After a shock wave has been generated by an explosion, it expands out in all directions. The chance of this expansion not interacting with any surface is therefore very low in a real-world scenario. The mechanisms of shock expansion are well known by an analysis of mathematical equations of propagating shocks with empirical information on the blast wave's speed Vs distance relationship for different sizes of explosive. It is therefore relatively straightforward to predict pressure in the shock front and if that front reflects from a normal flat rigid surface (Dewey, 1964) (Obad Samuelraj Isaac, 2023). Comparatively, when a shock wave is produced that interacts with structures, especially complex structures where they are not flat, rigid or normal to the shock wave, this creates a very difficult and less understood set of problems for modelling and for experimental research (Cheval, 2003). The most common reason to predict blast loads on structures or complex structures is to predict blast loads on cityscape geometries to provide increased protection. Often when there are structures involved, the position and scale of these structures can increase or decrease the pressure seen at a target as shown by (Alex M. Remennikov, 2005), these could be caused by clearing effects decreasing the pressure at certain locations along a structure or through structure failure like glass breaking or walls failing that would reduce the pressure due to effective venting. The pressure could be increased by multiple waves interacting with a structure at the same time due to reflections from other surfaces and building in one location. This work shows the importance of understanding the surroundings of a building and the ability to model the shock waves in urban areas effectively.

(T.V. Bazhenova, 1984) showed how the shape of a structure and the angle that the shock wave hits that structure can affect how the shock wave reacts to that structure, often causing Mach stems. A Mach stem occurs when the reflected blast wave coalesces with the incident wave combining into a singular wave. For example, on a plane wedge, depending on the angle of the wedge and the speed of the shock wave, it can develop into four different shock reflections. These different reflections are shown in Figure 5 taken from their paper to provide a better understanding of these differences. For the context of this thesis, the exact types of reflections are not considered due to the overall system being the main focus, but this is to provide evidence of how complex the interactions with structures can become. Part a of Figure 5 shows a single Mach reflection, b shows a complex Mach reflection with a kink on the reflected shock, c shows a double Mach reflection with a second triple point and figure d shows a regular reflection. The different sections of the diagram are labelled as follows, AI is the incident wave, AM is the Mach stem, ARP is the reflected wave, AE is the slipstream, RS and RE' are secondary shock wave and secondary slipstream respectively.

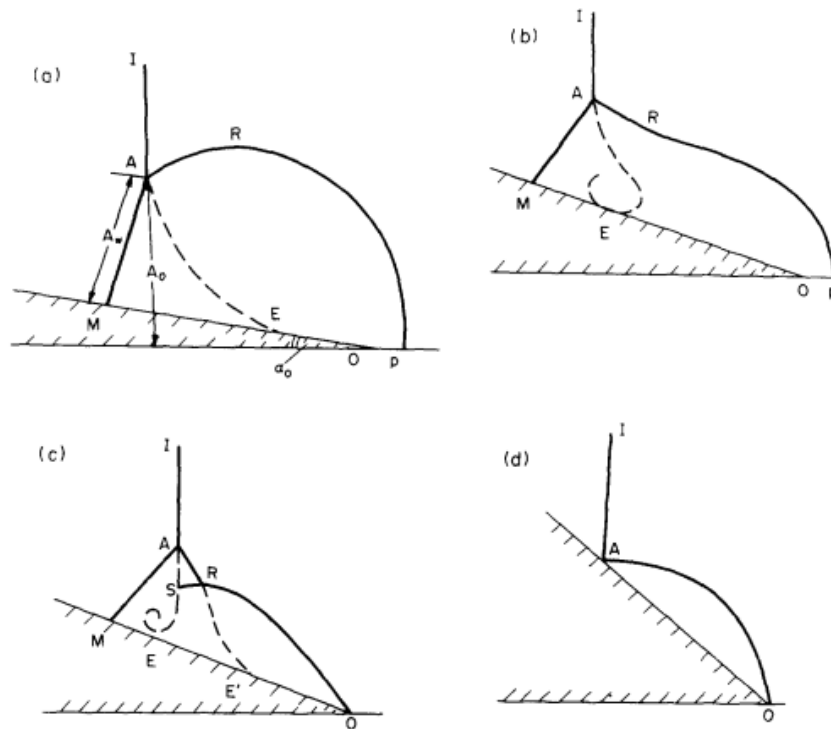


Figure 5– Various forms of shock waves interacting with a plane wedge. (T.V. Bazhenova, 1984). a) single Mach reflection, b) Complex Mach reflection with a kink on the reflected shock, c) double Mach reflection with a second triple point, d) regular reflection.

Further complications occur when shock waves interact with surfaces at different angles of incidence. This is a phenomenon that occurs when a shock wave interacts with an infinite surface that is not perpendicular to the direction of travel of the shock wave, causing an angular surface for the shock to reflect off between purely reflected or purely incident. These reflections can lead to the amplification of the pressure impulse. The relationship between the angle of incidence and the amplification of the pressure is shown in Figure 6, where the C_r is the amplification factor and α_1 is the angle of incidence (Barnat, 2014).

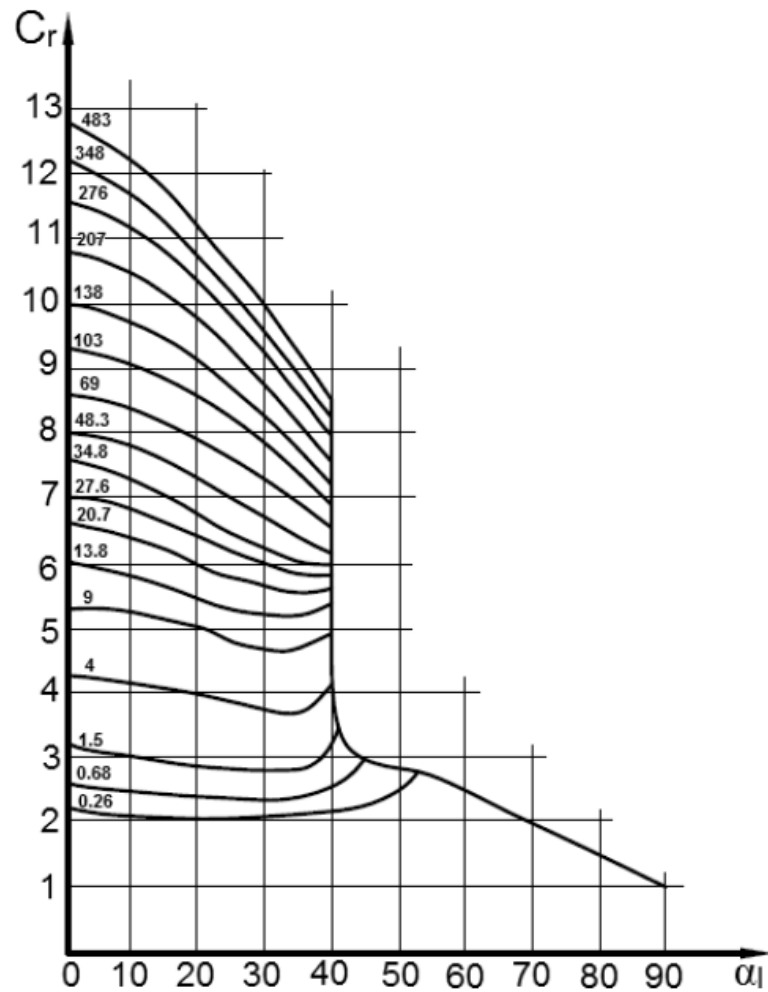


Figure 6 - Relationship between pressure impulse amplification and angle of incidence (Barnat, 2014).

When looking at just the positive phase parameters of a shock wave, the effects of the angle of incidence are generally considered well known and defined by (UFC-3-340-02, 2008) where they use graphical analysis from semi-empirical data sets. Also, analytical solutions of shock equations are used by (Kinney & Graham, 1985) or the use of simplified expressions that calculate these effects. Through this work and that of (S.E Rigby, 2015), it is known that when the angle of incidence is equal to or greater than 45 degrees, the impulse and positive phase duration decreases significantly with the increasing angle. For example, a roughly 20% decrease in positive phase duration was observed when the angle of incidence was equal to 56.3° compared to normally reflected phase duration.

Though there are lots of ways to remedy the effects of the angle of incidence and its effects on shock interactions, such as the effect on pressure and impulse, most of these methods ignored the effect of the negative phase of the shock wave. This was remedied by (S.E Rigby, 2015) who conducted experiments that showed the effects of the negative phase were

independent to the angle of incidence of the target and that the main effect was on the positive phase of the wave.

When there is a finite amount of surface that the shock wave is interacting with, there is another phenomenon known as clearing that takes place (Whittaker, 2019). This occurs when the shock wave strikes the finite target and the free edges of the target cause a rarefaction wave to propagate along the loaded face of the finite surface which relieves some of the pressure acting upon it. This occurs because as the shock wave impacts the surface, that part of the shock wave is impeded by the surface, yet the rest of the wave continues past the reflecting surface unimpeded, which causes diffraction around the edge of the surface, lowering the pressure over the edge of the surface. At the same time as this diffraction, the pressure is increasing at the surface as the wave is being reflected. This change in relative pressure between the edge of the surface and on the surface causes the low-pressure rarefaction wave, as it's driven by the pressure imbalance occurring between the surface and off the surface. Since the higher-pressure area will want to stabilise with the lower pressure area, this means that the overall pressure on that surface will start to decrease. This is shown in Figure 7 below to help illustrate that point.

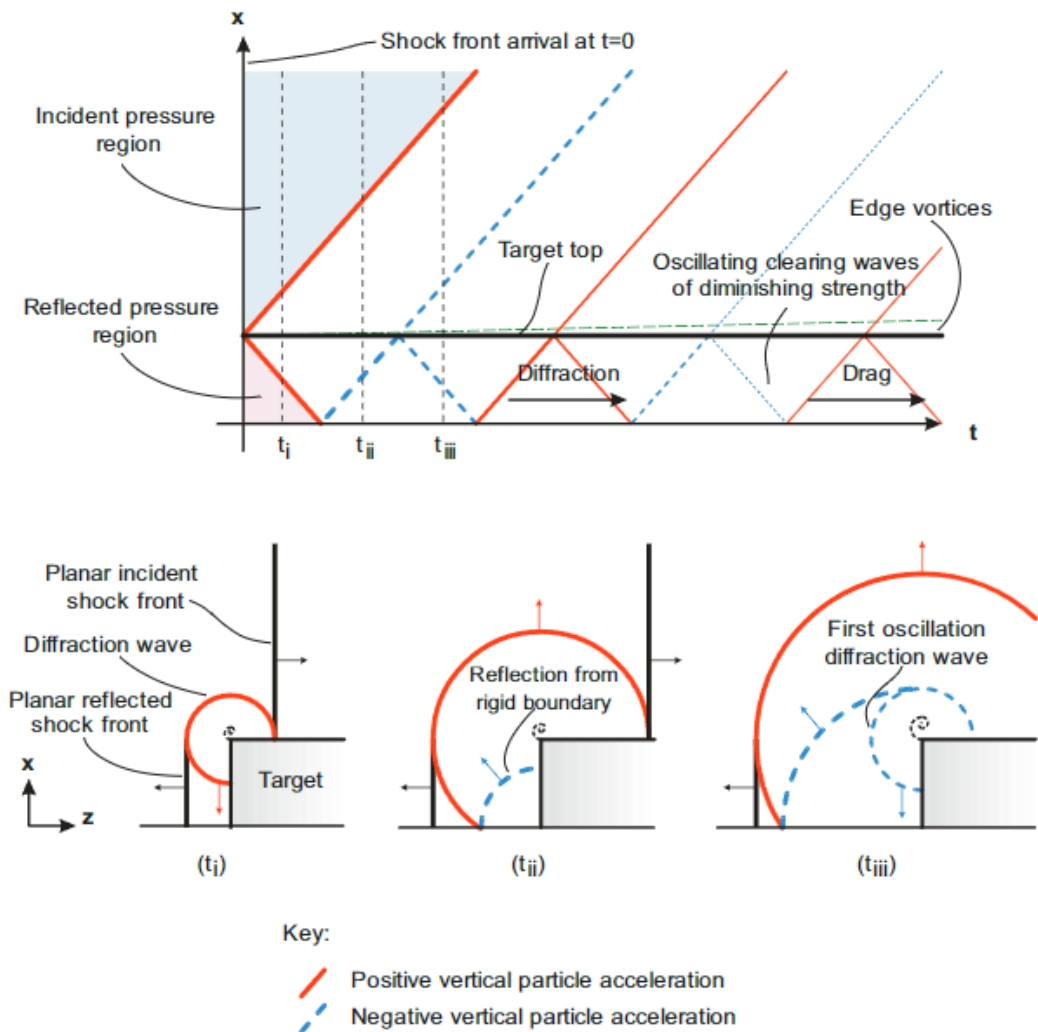


Figure 7 - Schematic shock front distance-time diagram for a series of clearing waves travelling across the target face. Subplots show shock front progression at the times indicated. (S.E. Rigby, 2014)

This clearing effect has been predicted in the (UFC-3-340-02, 2008) codes and shown below in Figure 8 is a diagram of the effect of corrections for a plate undergoing the effects of clearing, showing the reduction in pressure that this causes. This effect is most pronounced in surfaces where the distance from the loaded surface/area to the free edge is small enough that the diffraction phase resolves early whilst the loading is still prevalent on the surface.

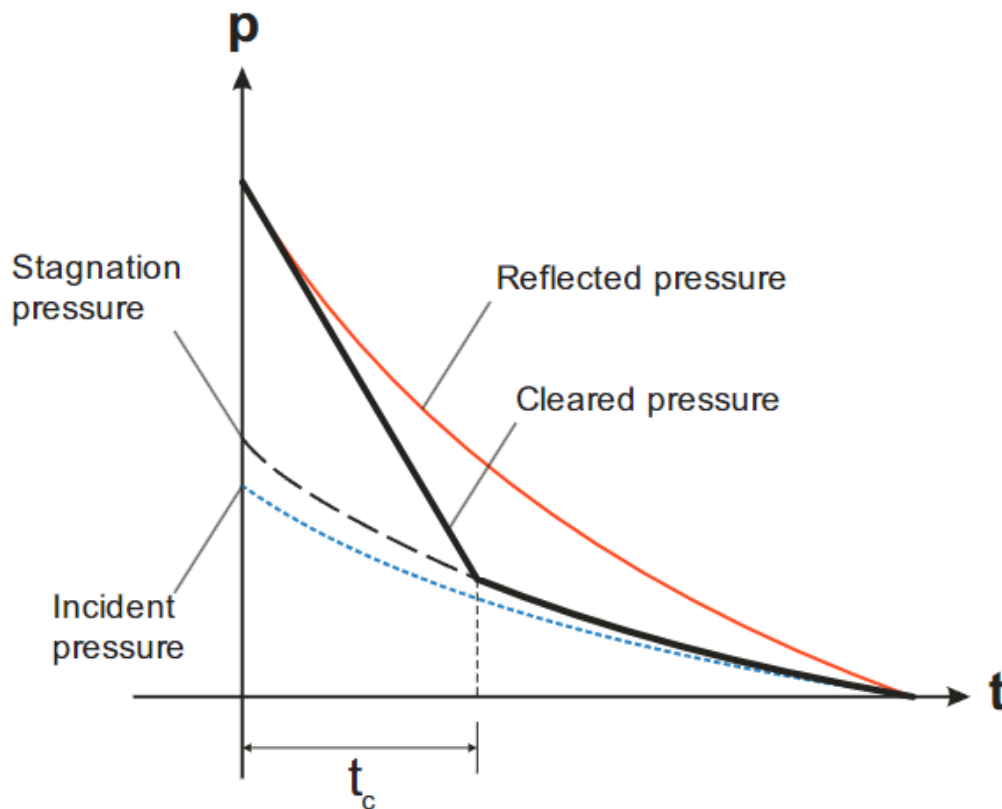


Figure 8 - Clearing corrections to UFC-3-340-02 (S.E. Rigby, 2014)

impulse is the pressure experienced by the surface caused by the interaction with the shock wave and the incident pressure is the pressure experienced at the sides of the finite wall where the shock wave travels at 90 degrees to the surface. The cleared pressure is the pressure change that occurs due to pressure being imparted on a finite size target, where the reflected pressure is reduced by the pressure equalisation process of reflected waves and incident waves at the side of the finite wall trying to equalise the overall pressure (P. D. Smith, 1999). This process of clearing leads to the formation of the stagnation pressure of the system. “Stagnation (or total) pressure is the pressure measured at a point in a fluid flow at which the fluid comes to rest and has the highest value found anywhere in the flow field.” (Reza Hedayati, 2016). Predictions of this clearing pressure using ConWep have been validated by (A. Tyas, 2011) through an experimental regime.

There has been work done to increase the understanding of explosions around complex structures, such as the work done by (Ian G. Cullis, 2010) where they used a QinetiQ developed modelling software (EAGLE-Blast) to simulate shock pressures over a model of a tank, considering the complex structures involved. This would involve the understanding and application of all these types of interactions to build a complex model that can use each type effectively and accurately.

So far, this work has just talked about interactions with rigid structures as they are what is focused on in this thesis, but it should be noted that if a structure is not rigid and is able to flex, this analysis becomes even more complex as the structures need to be considered or modelled accurately with this flexibility to allow the shock to react realistically to those changes and for energy to be transferred to the non-rigid components.

2.5 The Chemistry of Explosives

Understanding the chemical composition and the way these chemicals react is an important part of learning how different explosives work. This has been a topic of much research in the past with development of new explosives and gaining a better understanding of old ones and is still researched today (Urbanski, 1964) (Jai Prakash Agrawal, 2007). There are many facets that need to be understood so each will be given its own section so that each part can be understood.

2.5.1 The Ideal gas Equation

The ideal gas equation is a simple equation that relates the pressure, temperature and volume of gasses which was developed from Charles's Law, Boyle's Law and Gay-Lussac's Law. Charles's Law shows that at a constant pressure, there is a direct proportionality between volume and temperature. Boyle's Law shows that the pressure and volume are inversely proportional when at a constant temperature. Gay-Lussac's Law shows that there is a direct proportionality between pressure and temperature when the gas is at a constant volume (Poling, 2001). These correlations were then turned into the ideal gas equation (Equation 2.1)

$$PV = nRT$$

Equation 2.1

Where P is pressure in (Pa), V is the volume in (L), n is the number of moles of gas(mol), R is the universal gas constant (J/K/mol) and T is the absolute temperature (K).

The gas constant R is used to satisfy the proportionalities of the P, V and T relationship. The units of the gas constant are dependant on the units used for the pressure, volume and temperature so can be denoted as different values to allow the use of different units. These different versions can be found on online databases, for example (The Engineering Toolbox, 2024) and can also be calculated from one another using dimensional analysis. The gas constant is 8.314 J/K/mol to 3 decimal places. The number of moles in this equation is used in the units of moles, a mole of a substance is determined by the amount of a substance it takes to be equal

in mass to its relative atomic mass, so for example 12 grams of carbon would equal 1 mole because the relative atomic mass of carbon is 12. The same is true for molecules, so 44 g of CO₂ would be equal to 1 mole as that is the total relative atomic mass of each part of the molecule summed together. When considering a single mole of a substance, Avogadro's law states that this will always have the same number of molecules/atoms no matter what the molecule or atom is (Leonard, 2011). The absolute temperature is used in units of kelvin (K). The units that can be user dependant are pressure and volume which is why R must have multiple possible values.

The ideal gas equation is a theoretical based relationship that uses some assumptions when calculating values. These assumptions are impossible to achieve in real world practical scenarios. These assumptions are given below (Poling, 2001):

- The gas particles have negligible volume.
- The gas particles are equally sized and do not have intermolecular forces with other gas particles.
- The gas particles move randomly in agreement with Newton's Laws of Motion (they move in straight lines).
- The collisions between particles with other particles or the chamber walls are completely elastic (there is no energy loss).

These assumptions are said to hold unless the gas is close to a temperature at which the gas molecules are close to a transition state, for example between going from gas to liquid or from solid to gas. Also, if the temperature of a gas increases past certain bounds, there can be dissociation of any gas molecules into their constituent parts, increasing the number of moles that should be in the equation, hence at very high temperatures, these assumptions also do not hold. This will be explored later in the thesis to investigate the effect of temperature on the ideal gas equation.

For an explosion of HMX (C₄H₈N₈O₈) the detonation temperature has been recorded at maximum values of around 2273 K through the use of infrared measurements by (Wang, 2019) of 3 kg of explosive. These were obtained using their infrared thermometer and also a compensation formula based on geometrical optics and infrared radiation theory. This temperature is lower than the dissociation temperatures of the molecules expected to be formed by the explosives used in this thesis as well as less mass of explosive being used in this thesis which should cause a lower temperature. The dissociation of molecules likely formed by explosive detonation are 2200 K or higher. For example, CO₂ starts to dissociate at 2400K (Kwak, 2015).

2.5.2 Determination of Energy Release

To determine the energy release of an explosive, an understanding of the processes involved in the explosion are needed. To calculate the energy release in an explosive event, a typical way to measure that is to use a process of calorimetry, which measures the energy release from a chemical reaction occurring.

A calorimeter is an apparatus for measuring the amount of heat involved in a chemical reaction of other processes. For the case of assessing the heat of combustion of an explosive,, the type of calorimeter considered is a bomb calorimeter, which has a constant volume. This was chosen as previous studies on heat of detonation has been conducted using them (Ornellas, 1982) (Trzcinski, 2006). These can be used to determine the amount of energy produced by an explosive upon detonation, since when detonated inside this type of calorimeter, the energy is all focused on heating the inside of the chamber, which is measured from the inside of the calorimeter but outside of the chamber containing the material in question. This process works through measuring the heating of a liquid surrounding the chamber through the use of very accurate thermometers. These instruments are normally well insulated to ensure a correct reading of the temperature change. Schematics for two different bomb calorimeters are shown in Figure 9 and Figure 10 .

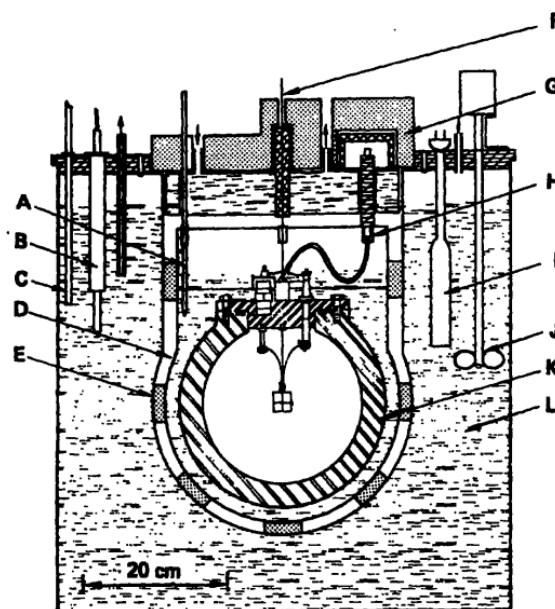


Figure 9 - Bomb Calorimeter. A, quartz thermometer; B, nickel resistance thermometer; C, mercury-in-glass thermometer; D, calorimeter bucket with lid; E, Styrofoam support blocks; F, support cable; G, Styrofoam insulation; H, firing-lead connector; I, knife blade heater; J, stirrer; K, bomb; and L, constant-temperature jacket. (Ornellas, 1982)

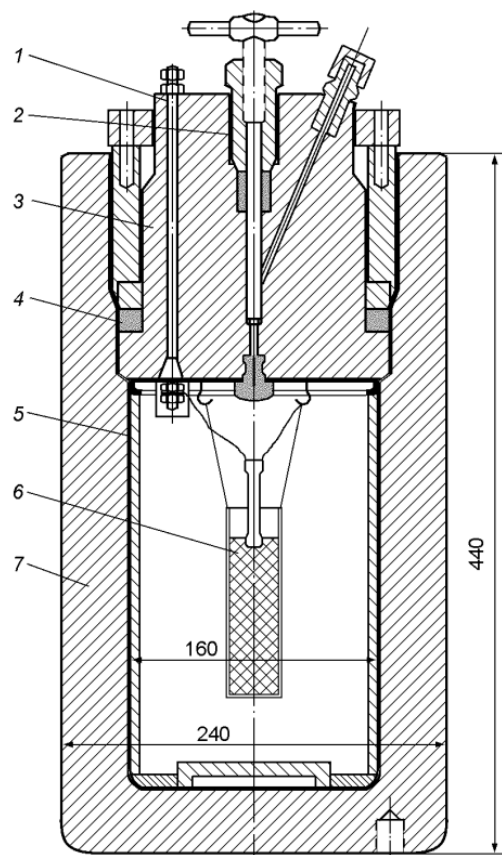


Figure 10 - Bomb calorimeter designed to study the heat of explosion of HE charges of mass up to 100 g (development of the ICP RAS): 1) electric lead; 2) valve; 3) self-sealed cover of the bomb; 4) Teflon or rubber seal; 5) changeable metal liners protecting the bomb walls from being damaged by debris; 6) HE charge; 7) bomb casing. (Pepekin, 2007)

The change in energy (enthalpy) between the initial state and the final state of a reaction, does not depend on the chemical pathway that the reaction goes through, instead it depends on its starting composition and final composition. This is known as Hess's Law for constant volume transitions. This means that if an explosive detonates in a confined space, no matter the reactions occurring through the initial stages, as long as the final products are the same, the energy released will be the same. This is the theory that the calorimeter is partly based on since the energy released will provide the same total energy release into the surrounding medium. Most of the work undertaken of this type with explosives is done with the raw explosive (RDX or PETN in the case of this thesis) before binders and plasticisers have been added to them. This means that to determine the energy of a plasticised explosive there should be a consideration of the other components present.

For a reaction to occur, it often requires some form of activation energy, this is the energy required before a reaction will be self sustaining and go to completion. This is different for each reaction, as each reaction has different pathways that it goes through before it gets to the

products of the reaction. This can be through multiple intermediate steps or minimal other steps depending on the reaction. An example of this process is shown in Figure 11 showing the activation energy and intermediate step for an arbitrary reaction. In an explosion, this activation energy is most commonly provided by the use of a detonator, inputting energy into an explosive in the form of a shock or an electrical current. The reactants have an initial energy that they are stable at, in this case that is a value of 0.7. To cause a reaction to occur, enough energy needs to be introduced to the system to cause a jump in energy, this is denoted as E_a . The energy change between the initial energy of the system and the intermediate products, where there is a middle stage of the reaction where the explosive has been atomised is denoted as ΔH_{det} or the enthalpy of detonation. Between the intermediate products and the final products is where afterburn occurs and this energy change is denoted as ΔH_{ab} . The energy difference between the initial energy and the energy of the products is denoted as the ΔH_c which is the enthalpy of combustion which includes the enthalpy of detonation and afterburn. Each explosive will provide a different magnitudes of these pathways due to differences in activation energies, enthalpy of detonation and afterburn which creates unique processes for different explosives.

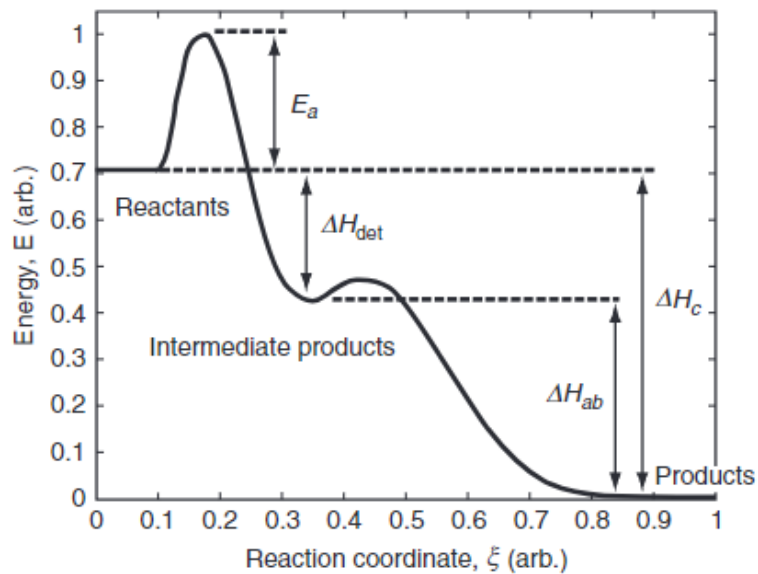


Figure 11 - Energy changes during a reaction. (I. Edri, 2013)

2.5.3 Specific Heat Capacity

Specific heat capacity is the energy required to raise the temperature of 1 mole of a substance by 1 degrees Kelvin (Le-Ping Zhou, 2010).

When investigating the energy of an enclosed system, the specific heat capacities of a gas are dependent on the environment of the gas (Waples, 2004). The specific heat capacity under constant volume (C_V) is used when a gas cannot expand, it is fixed in a volume of space. The specific heat capacity under constant pressure (C_P) is used when the gas remains at a constant pressure through the ability to expand the volume through work on a frictionless piston. Once these two factors are known, the ratio of specific heats can be calculated by dividing C_P by C_V (Equation 2.2).

$$\gamma = C_P/C_V$$

Equation 2.2

Where γ is the specific heat capacity ratio, and C_P the specific heat capacity at constant pressure ($\text{Jkg}^{-1}\text{K}^{-1}$) and C_V is the specific heat capacity at constant volume ($\text{Jkg}^{-1}\text{K}^{-1}$).

2.6 Consistency of Explosive measurements

The ability to measure pressures generated from an explosive has been a contentious topic, from early work in the 60's getting accurate data to build models from (Dewey, 1964) to some current research that suggests a much larger variability (Locking, 2011). This section will discuss aspects relating to variability of explosive loading, and attempts to find evidence either in support of, or in opposition of the notion that the explosive process is inherently unpredictable and chaotic. With some people claiming that explosions contain inherent variability and are fundamentally unpredictable and chaotic, and some people who claim that explosions are fundamentally deterministic and predictable. This section will discuss both sides of this.

2.6.1 Free-field consistency

The first detailed scientific investigations on the topic of quantifying the loading from blast waves began in 1914 with experimental work conducted by (Hopkinson B. , 1913) and the key contributions thereafter were from (Friedlander, 1946) who established the shape of a free field air blast followed by a large contribution of work by (Dewey, 1964) etc quantifying the blast parameters which lead to the (Kingery & Bulmash, 1984) work that underpins CONWEP to this day. There were many different ways to measure these different phenomena over the years, one

of the simplest, as described in a book by (Shelton, 1988) which discussed the early accounts of weapons development, where he spoke of a fellow scientist Dr Fermi who described his experiment as follows:

“About 40 seconds after the (Trinity) explosion the air blast reached me. I tried to estimate its strength by dropping from about six feet (height) small pieces of paper before, during, and after passage of the blast wave. Since, at that time, there was no wind, I could observe very distinctly and actually measure the displacement of the pieces of paper that were in the process of falling while the blast was passing. The shift was about 2-1/2 meters, which, at the time, I estimated to correspond to the blast that would be produced by ten thousand tons of TNT.”

Though this method seems crude and unreliable, at the time, it was just as accurate a method as some of the others being utilized as he had created tables to reference from for these different distances to determine the yield of the explosive relative to TNT.

The methods for measuring the explosion parameters from 1943 – 1993 were all collated and reviewed by (Reisler, 1995) after going through innumerable reports to assemble all the information possible from public and classified documents. He provides an extensive description of each of the methods used and how they measured different parameters. After describing these methods, he also gave values for accuracy of some of the methods employed. Passive devices such as bursting diaphragms, cube displacement and deformation gauges were found to provide an accuracy of 10-20 % from maximum parameters. Electronic transducers were found useful due to their resistance to environmental effects and were believed to have an accuracy of 3-5%. Mechanical self-recording gauges had an adequate sensor response for long duration blast waves and were used extensively but only were believed to have an accuracy of 5-10 %.

Also described by (Shelton, 1988) was the skill required to use the different instrumentation that was available to the scientific community at the time. The ability to go from no idea about the existence of such materials, to being able to quantify them and understand how to measure and predict these events in such a short space of time was something that should be noted for its progress. These early predictions around nuclear explosions and their prediction had accuracies quoted of 3-5% which is very close to what some more recent researchers claim such as (S. E. Rigby, 2014) which shows how well they understood the phenomena they were predicting and the effort that was put into a goal of gaining more understanding of the phenomenology of blast from nuclear explosions.

After the initial years of testing and development, was an era that is widely regarded as when the best experimental data was recorded. This was when many of the semi-empirical tools were developed for the prediction of free-air blasts. (Kingery & Bulmash, 1984) developed a set of semi-empirical curves that are still regarded as standard practice for blast predictions and are used in (UFC-3-340-02, 2008) as a reference for the design manual as well as multiple computer

codes including CONWEP (Hyde, 1991) as well as being used in LS-DYNA (Glenn Randers-Pehrson, 1997).

The use of these prediction methods for explosive events would indicate that a blast event is deterministic and predictable since the data that these systems are based on are shown to be accurate between 3-5% as described previously.

Though this data is still used today, there are some that claim that these predictions are not as accurate as they were believed to be previously. Some researchers have since reported an experimental lack of repeatability when it comes to blast pressure measurements when comparing their results to those of Kingery and Bulmash. (Formby & Wharton, 1996) had experimental variability of around 15-30% when using hemispherical secondary explosives which is relatively high compared to those of the past. They also bring up the possibility that blast parameters are variable at closer scaled distances and less variable at further scaled distances, which is also mentioned by (Michael M. Swisdak, 1975) where he mentions a transition region between the two low variability regions.

Compared to the older data that had an accuracy of 3-5 %, some work conducted by (Bogosian D., 2002) has a much higher level of uncertainty, values between 70-150 % for peak pressures and 50-130 % for peak impulse values from nominally identical tests in the far field, where $1 < Z < 40 \text{ m/kg}^{1/3}$. These are much higher uncertainty than the previously stated data, which provides evidence that maybe there is some inherent chaotic and unpredictable nature to the shock waves causing variability in these blast parameters.

The work of (Netherton & Stewart, 2008) was done to develop a probabilistic analysis of risks associated with explosive blast loading, where they took into account many factors that can cause uncertainty in explosive results, stating "Given the highly unstable nature of explosives and that uncertainty of blast loading may dominate probability of failure calculations, an understanding of blast variability is an important area for future research."

To gain an understanding of possible variability in explosive testing, (Locking, 2011) investigated multiple sources and experiments and collated the different TNT equivalency factors given by different work. This shows a wide range of equivalencies up to a difference of 50% error. These pieces of work would suggest that the nature of an explosive is chaotic and unpredictable and that there is a randomness associated with explosive events.

The work of Formby and Wharton displayed uncertainty in their results, however when looking at their methodology for taking these measurements, they are possibly the reason for the variation from the data previously presented by KB predictions. In their paper, they show the layout of the site along with the heights and elevations of the pressure gauges relative to the charge location (Figure 12). This figure shows that they have natural embankments and obstacles in the way of the gauges. They then even mention that these factors could cause reflections of

the blast waves. Even though they mention this, they do not take that into account when determining this variability that they are seeing.

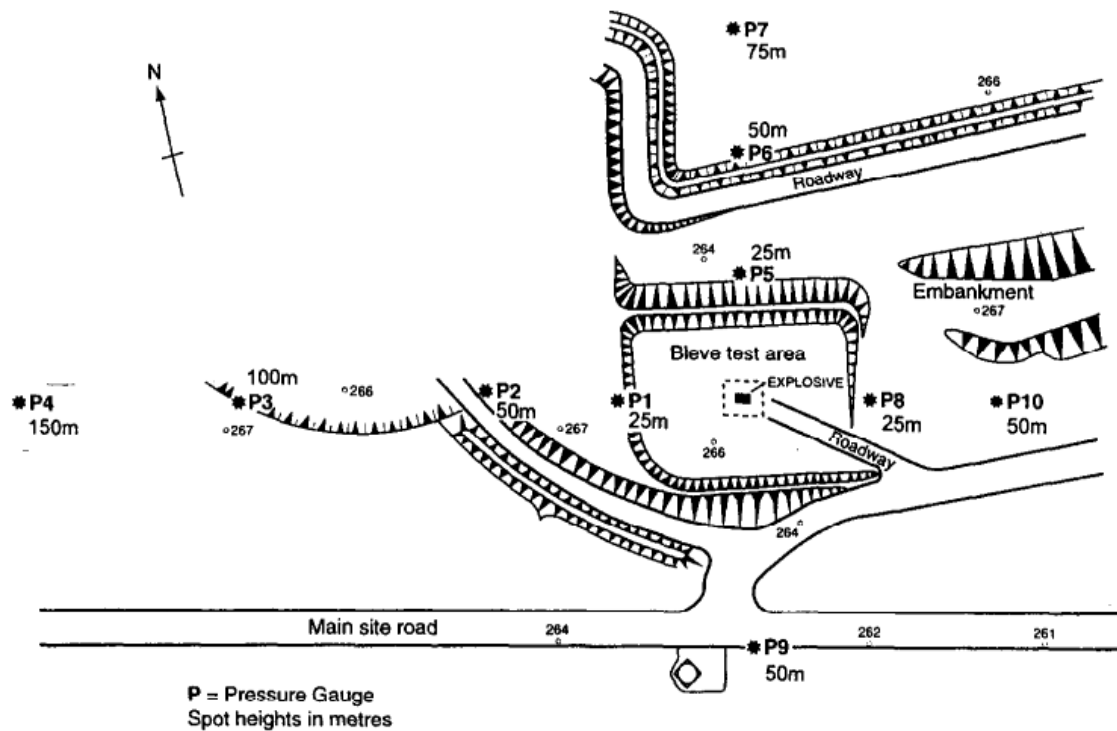


Figure 12 - Site layout of (Formby & Wharton, 1996).

An investigation into the data presented by (Bogosian D., 2002), was done by (Borenstein, 2009) who performed a sensitivity study of the blast parameters which consisted of different explosive shapes, sizes and compositions which were scaled directly to TNT. He then concluded that the experiments by Bogosian were analysed collectively, which resulted in the quantification as a representation of the data that was not representative of the actual phenomena occurring, which has since, by the community, been attributed to random inherent variability.

Some experimental tests undertaken by (Esparza, 1986) included experiments of a range of explosive compositions presenting blast parameters with respect to scaled distance, which from a visual inspection hold agreement between nominally identical tests even though no analysis was conducted by the writer. Though these are just visual inspections into the data, there are others who provide variability values in their testing such as (Richard G. Stoner, 2004) who reported a variability in pressure between +/-0.6-6.5% when looking at nominally identical tests, even though they still see a difference when the scaled distance increases, causing lower variability. Similar to the variability seen by Stoner and Bleakney, (Tang, 2017) conducted a

variety of incident and reflected measurements from spherical and hemispherical PE4 charges and saw similar magnitudes of variability.

The data gathered by (Tang, 2017) was compared to Kingery and Bulmash predictors as well as other software and had reasonable levels of agreement for the medium and large scale charges shown in (Tang L., 2018). The incident measurements were not as accurate when compared to the reflected pressures, but these differences were put down to the difficulty of measuring incident pressures compared to the reflected pressure. (A. Tyas, 2011) Also presented well controlled small scale experimental tests in the far-field that provided good agreement to Kingery and Bulmash predictions when looking at normally reflected conditions.

An in-depth review of literature was performed by (S. E. Rigby, 2014) where he considered many articles looking at experimental variability of far field parameters and compared them to Kingery and Bulmash predictions investigating the errors that may have been missed. This review came to the conclusion that the reason for these large differences to previous data, is likely to be systematic experimental or analytical errors to get such large variabilities, not inherent variability in explosive events.

There has also been well documented and controlled experimental work using the optical features of a blast such as shock wave tracking to determine parameters (D. Farrimond, 2022). This work accurately determines blast loading parameters from video footage of the shock wave when the point of detonation is known. This method allows the accurate prediction of TNT equivalency of explosives through this technique which also has excellent agreement with the Kingery and Bulmash predictions. This paper also suggests the idea of more accurate predictions for larger scaled distances compared to smaller ones as there is less instabilities when the shock has travelled further.

Work by (Tyas A. , 2018) (Tyas A, 2016), looking at near field blast measurement, investigated the repeatability and predictability of a detonation in the near field. This work showed that in the near field there is variability in the fireball surface as it expands caused by Rayleigh-Taylor and Richtmyer-Meshkov instabilities. These Richtmyer-Meshkov instabilities occur between the interface of the detonation product cloud and the surrounding shocked air. The cause of these instabilities is when a fluid comes into contact with a different fluid that has different properties. For example, when a heavy fluid is placed on top of a lighter fluid causing gravity to destabilize the boundary between the two fluids causing turbulent mixing. This also occurs when a lighter fluid is accelerated into a heavier fluid or a heavy one decelerated by a lighter one. The Rayleigh-Taylor instabilities at a fluid-filled boundary are caused when two superimposed fluids of different densities are accelerated perpendicularly to the interface between them, the surface can be stable or unstable dependant on if the acceleration is originating in the lighter or heavier fluid (Taylor, 1949). An example of these instabilities in small scale charges is shown in Figure 13

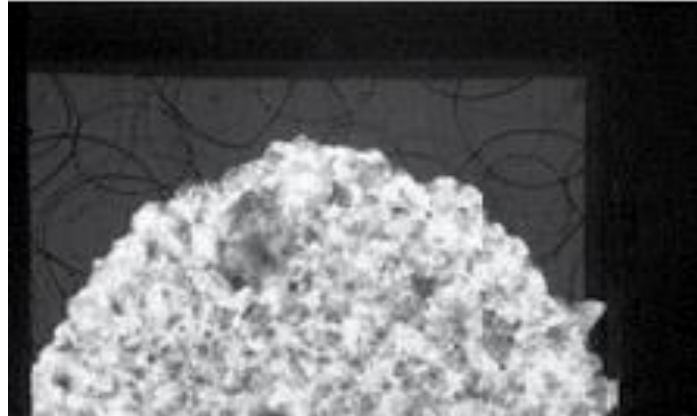


Figure 13 - Detonation product cloud after 75ms after detonation. (Tyas A, 2016)

This test series looked at the impact of these instabilities on the pressure profile through the use of an array of Hopkinson pressure bars. Using an array of 21 bars, spatial measurements of pressure could be taken over multiple locations. When analysing the data from separate bars from the same test, it can be seen that there is a significant difference between the two locations caused by jets protruding from the detonation product cloud (Figure 14). This is suggesting instabilities can cause the pressure to be unpredictable. Though this may be the case when looking at a single bar in the test, when all bars are collated and an integrated impulse is used instead, generated through temporal integration of pressure-time traces, and spatially integrated over annular areas between each bar offset, the impulse seen between tests is very repeatable with impulse ranging from 9.8 N.s to 9.1 N.s through 5 separate nominally identical tests (broadly +/- 5% from the mean). This means that the overall pressure generated by the shock wave averages out over a given surface area, but does have some variability when looking at a single point on that wave or a very small area. This is due to instabilities causing changes in pressure where they occur but with every increased zone of pressure there is a decreased zone of pressure.

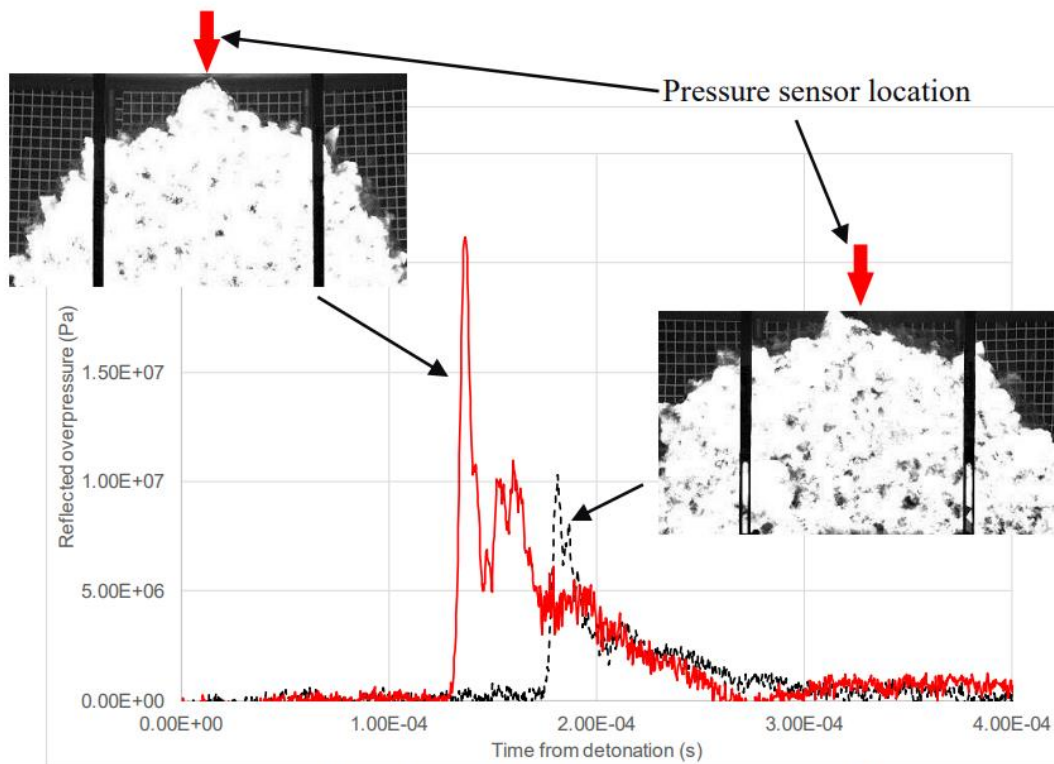


Figure 14 - Effect of DPC instabilities on pressure loading. (Tyas A. , 2018)

This shows that though there are localised instabilities the overall energy release as pressure from the detonation is still predictable and consistent when considering the whole event, instead of just a part of it.

Work using cylindrical charges has also been completed by (Langran-Wheeler C., 2021) in which a series of trials were completed to investigate the effects of charge shape and orientation on the pressures and impulses generated. Through the analysis of data from these tests, it was shown that even though they are more complex than a spherical charge due to different shock interactions occurring with a target plate, they were still incredibly consistent, and this assessment of near-field blast and these results could be used to provide a benchmark for future numerical modelling.

These research articles and conference proceeding suggest heavily that there is in fact very little variability and chaotic nature when looking at an explosive event. They would suggest that an explosive event is in fact fundamentally deterministic and predictable, at least in terms of energy release and pressure generation. Therefore, in the free field, it should be noted that seemingly good experimental practice and control should be able to provide accurate data of blast parameters.

These studies of repeatability show that more complex or near field scenarios will provide lower repeatability, through phenomena such as fireball effects in the near field or shock wave reflections from objects. This will be further discussed in a later section for the confined explosions as this is the main focus of this thesis.

2.6.2 Consistency in Soil

Compared to the scenarios in the free field, there are more complex interactions that have been investigated such as those in soils, where the shock wave must pass through a complex medium which will affect the passage of the shock wave through it. This added complexity is likely to cause consistency and predictability to be lessened. Experimental tests have been conducted at small laboratory scale where they use compressed gas to simulate the loading (McShane, 2013) experienced by a plate due to the sand being thrown from the surface. This however is an oversimplification of the problem of buried charges as it ignores the loading effects of the air shock as well as the thermal and geometrical aspects of the detonation. This causes the effects of soil interactions with shock and the effect of shock reflections and clearing to be ignored, lessening the usefulness of the data when considering these scenarios.

In geotechnical engineering it is generally accepted that the geotechnical properties of a soil are of major importance when considering the variation in output of a buried charge. There are many factors that can differ between soil types such as bulk density, moisture content, particle size distribution and burial depth of the explosive charge. The ability to control these properties/parameters is a major part in being able to understand the relationships between them and how they affect their relationships to impulse.

A series of tests conducted by (Fox, 2011) investigated the effect of shallow buried explosives beneath target plates through computational and experimental analysis. This work proposed that a computational model based solely on quasi-static test evaluations gave close agreement to experimental data. However, when the experimental data is discussed, it is noted that when investigating identical tests being performed, there was variability that they did not quantify but attributed to differences in charge mass, soil moisture content and positioning of the charge within the soil. This should be something that is considered and understood before these tests took place so that variability can be attributed to features not just unsure experimental set up.

Though there is work again suggesting that there is a large variability in buried explosives testing, work by (Clarke, 2015) shows that when controlled experimental procedures are in place for soil testing, a much greater repeatability can be achieved, where the majority (80%) of data was within 3.7% of the mean for each test series. This is due to well controlled experimental procedures for identical tests. This work even evaluated different soil types to allow the most

consistent to be used for future testing so that variations can be known to be caused by other phenomena, not just a difference in soils. Shown in Figure 15 is the standard deviations of moisture content and bulk density compared to the mean normalised impulse ranges of the different soils tested, showing that the most consistent soil is the fully saturated Leighton Buzzard 14/25 (LBa,b and c) which gave repeatable impulse and deflections.

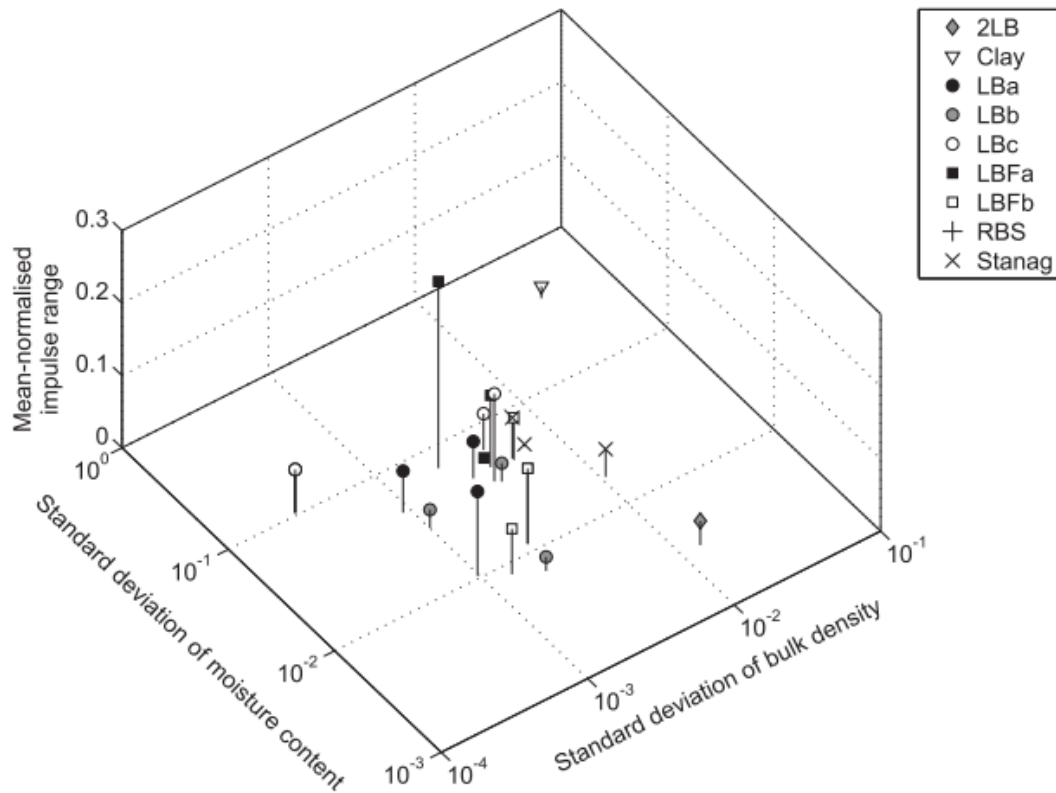


Figure 15 - Controllability of geotechnical conditions Vs repeatability of measured impulse. (Clarke, 2015)

2.7 Scaling Laws

Scaled distance is a commonly used function for free field explosions, to generalise the blast pressures that are likely to be generated by high explosives, often used to predict pressures for large scale tests from small scale experiments. This is done by comparing explosives of the same material and geometry in the same atmosphere but different in size/mass. This was developed by (Hopkinson B. , 1915) and (Cranz, 1926) where scaled distance is defined as (Equation 2.3):

$$Z = \frac{R}{W^{1/3}}$$

Equation 2.3

Where Z is the scaled distance, R is the distance between the centre of the explosive and the point of interest (m), W is the TNT equivalent mass of the charge (kg).

This cube root scaling assumes that the energy released by the explosive charge is directly proportional to the pressure generation and so doesn't need scaling, though time related parameters will require scaling by the cube-root of the explosive mass as stated by (Kinney & Graham, 1985). This means that for any mass of explosive, at any distance, pressure can be predicted since it can be related back to a known scaled distance that is more practical to perform testing at that scale. This is an invaluable tool for predictions in the free field as it allows the impact of large scale explosives to be experimentally measured using small scale trials.

These scaling laws however do not work for confined explosions, or very complex shock interactions, as the pressures are altered by these obstacle interactions and wall interactions. This means that it was necessary for people to attempt to deduce a new way that can predict these confined pressures generated. To do this the scaling has been based off the charge weight to volume ratio of the chamber as explained in (Edri I.E., 2019) which was based off (UFC-3-340-02, 2008). This is shown in Equation 2.4.

$$\frac{W_{EG}}{W_{EXP}} = EF = \frac{\emptyset [H_{EXP}^c - H_{EXP}^d] + H_{EXP}^d}{\emptyset [H_{TNT}^c - H_{TNT}^d] + H_{TNT}^d}$$

Equation 2.4

Where W_{EG} is the equivalent charge weight for gas pressure (kg); H_{TNT}^c , H_{TNT}^d are the heat of combustion and heat of detonation of TNT (kJ/kg), respectively, and H_{EXP}^c and H_{EXP}^d are the heat of combustion and the heat of detonation of the examined explosive (kJ/kg), respectively and \emptyset is the TNT conversion factor.

2.8 Charge shape influence

Most blast research is done using spherical charges, as noted by (Simoens, 2015), which means less is known about the behaviours of other shapes since there is less experimental data and verification of modelling for these shapes. It is however important to consider other shapes of charges as it can affect the pressure generated as discussed by (Hryciów, 2014) when they looked at free field blast profiles of cylindrical charges. Several other researchers have considered this effect, and this section is about the experimental and numerical methods that have been used to investigate this.

Through numerical analysis using LS-DYNA, (Xiao, 2020) presented results that showed in the near field, a cylindrical charge compared to a hemispherical charge can have large differences in peak overpressure (maximum impulse) by a factor of up to 6.6. Similarly, the maximum impulse in the near field can be increased by a factor of 2.0 when dealing with a cylindrical charge. However, in the far field the factor changes down to roughly 1.2 times that of a hemisphere. They also showed that the detonation location for a cylinder affects the overpressure generated by the explosion with a charge detonated at top-centre being the highest yield then middle centre and finally bottom centre, these detonation locations are shown below in Figure 16.

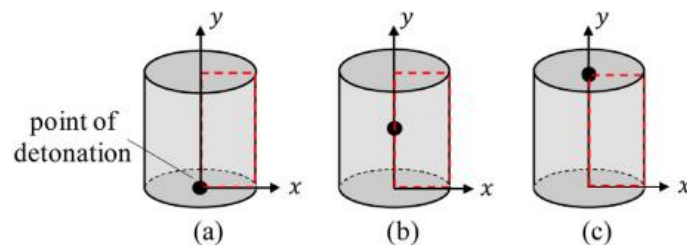


Figure 16 - Charge detonation locations a, b and c - (Xiao, 2020).

Through numerical modelling of spherical and cylindrical charges, (Wu C., 2010) presented comparisons between their models and the (UFC-3-340-02, 2008) standards for spheres and cylinders of masses between 0.24 kg to 8.0 kg of different length to diameter ratios. This work presented the influence that the differing length and diameter, as well as the detonation point effects the reflected peak overpressure and impulse in the immediate vicinity of the detonation. They also showed that (UFC-3-340-02, 2008) standards underpredict these pressures when a cylinder of aspect ratio 1.0 is facing axially towards the gauge zone being investigated. This difference in peak overpressure generation was further expanded upon by (Rigby S., 2021) who performed a detailed numerical study into the deflection of loaded plates when exposed to different shaped charges, and subsequently developed an equivalence factor for charge shape to allow a cylinder to be represented as a different mass spherical charge.

Research by (Wisotski, 1965) showed that with a cylindrical charge, the greatest pressure generation would come from the regions of the charge with the largest surface area and this was then confirmed and expanded upon by (Catherine Johnson, 2018), who conducted experiments on not only cylinders and spheres, but also cubic and tetrahedron shaped charges (Figure 17). These additional shapes all had differing effects on the pressure generation at different locations surrounding the charge, where there are larger surface areas of explosive often being the locations of high pressures, and all the shapes having at least one dimension where the pressure was higher than that of the spherical charge. The explanation of this additional pressure from the large surface area locations is due to the overdriven state of the shock wave expanding from the facets, due to continual detonation of material along the vertices but this process is not fully defined yet.

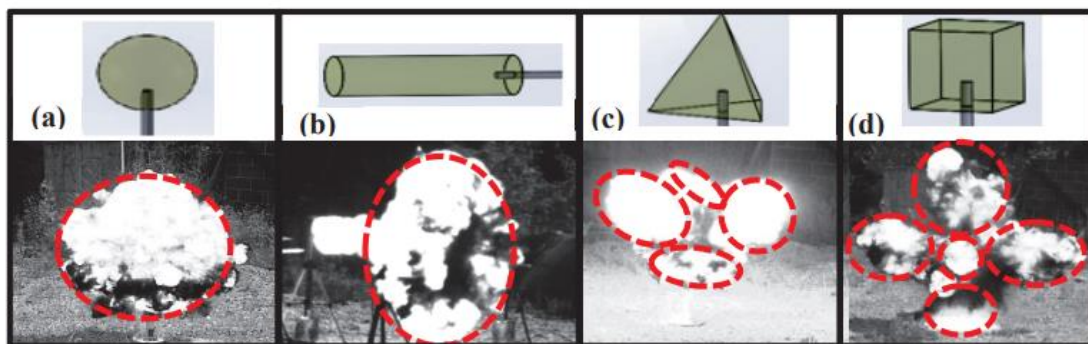


Figure 17- Regions of highest shock wave velocity surrounded in red lines for four different shaped charges. Sphere (a), cylinder (b), tetrahedron (c), and cube (d) respectively. (Catherine Johnson, 2018)

Scaled distance is a factor that largely effects the influence of the shape of an explosive, as described by (Shi, 2022) who through experimental and numerical testing showed that over a scaled distance of less than $5.0 \text{ m/kg}^{1/3}$, the effect of a cylindrical charge shape can be ignored in terms of peak overpressure, as the pressure distribution has stabilised over this distance and performs the same as a spherical explosive. This distribution of the pressure is also known as attenuation and is explained by (Ahn, 2017) to occur as the geometrical spreading of the surface that a vibration is taking place over, so as the pressure wave expands, its surface area increases, causing an attenuation over the surface of the wave which equalises the pressure over the area.

Work completed by (C. Knock N. D., 2015) showed the formation of side and end shock waves and how the interactions of these waves caused the formation of Mach stems (bridge waves) and reflected shock waves. The pressures of these waves were also measured and the secondary shock was found to contribute to the axial impulse significantly. At scaled distances (Z) greater than $3.9 \text{ m kg}^{-1/3}$ this secondary shock produced accounts for over half of the measured impulse, with greater peak overpressure than the primary shock. More work has also been completed looking at the effects of holes in the centre of cylindrical charges compared to solid charges allowing for the implementation of electronics inside the cavity that doesn't affect

the shock formation (C. Knock, 2016) as well as more work understanding the effects of cylindrical charges at different diameter to length ratios and masses (C Knock, 2013).

This research shows that the shape of an explosive charge has a significant effect on the pressure and impulse in the near field but is less of a factor when investigating the far field. For this reason, it is considered in the later sections of this thesis when experimental work is conducted.

2.9 Confined Explosions

A confined explosion is one that occurs where there is constraining obstacles or limits to the expansion of the shock wave that causes multiple reflections. This differs from a free field explosion where there are no obstacles or limits causing turbulent mixing of the shock waves and air. Confined explosions cause a build-up of pressure inside the confinement due to the inability of the energy from the shock waves to escape the enclosing medium and this increase in energy is what makes confined explosions a more complex situation than the standard free field explosion.

There are many situations that can cause a confined explosion, from ammunition storage explosions to a terrorist explosion within a building (Feldgun, 2012). This is why the investigation into the effects of confined explosions and gaining an understanding of the mechanisms behind them is important to better develop protective structures. There has been significantly less research into these confined scenarios mainly due to the added complexity for analysis (Salvado, 2017). Gaining a better understanding of these cases is important due to the likelihood of having higher energy concentrations due to their confined nature (Silvestrini, 2009).

When an explosive is confined into a chamber, the interactions that occur between this containing structure and the shock waves causes a more complex interaction than occurs in the free field. When the shock wave comes into contact with the walls/confinement, it causes an enhanced turbulent mixing (A. L. Kuhl, 1998). This additional turbulence within the shock front, mixing in additional oxygen from the atmosphere causes the fuels generated by the detonation such as carbon and carbon monoxide to mix with the atmospheric oxygen generating afterburn. Shortly after this discovery, (Kuhl A. I., 2000) simulated this scenario and determined that the combustion rates of a confined explosive are dependent on the charge mass to chamber volume ratio. This shows the beginnings of understanding that the turbulence and forced mixing have an important impact on the pressures occurring, since the larger that ratio, the faster and more efficient reflections will occur in theory.

Work by (Baker, 1983) provided a lot of the initial understanding of how confined explosions would interact with their environment. They compiled a sizeable quantity of data to

obtain duration and impulse of an explosion occurring within a structure. During this work the peak quasi-static pressure was found to be a function of the charge weight to the volume of the chamber. The data compiled data was of multiple orders of magnitude. After performing curve fits to the experimental data which allows the use of those curves to predict the specific impulse.

These are fairly simplistic relations and this is the case in most manuals, such as (UFC-3-340-02, 2008) since they are based on an assumption of a uniform pressure distribution. However (Baker, 1983) described the qualitatively complex distribution relationships, but did not provide further quantitative ways to predict these pressures and distributions, yet he did suggest the mechanisms causing a pressure increase in the corners of rooms as shown in Figure 18.

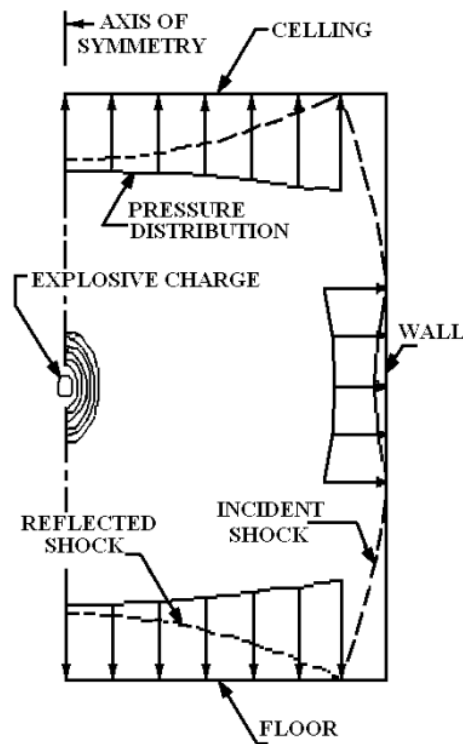


Figure 18 - A more complex pressure distribution that indicates pressure increases at the corner of a confined space. (Baker, 1983).

Taking these initial thoughts and findings of Baker, (Edri I, 2011) performed tests to further understand these phenomena and characteristics. He noted the difficulty in measuring these phenomena and the differences between their data and the UFC 3-340-02 model being consistently 27% lower when considering gas pressures. He concluded that the gas pressure parameter is not an unmistakable physical value, since it actually depends on the methods chosen for analysis and their characteristics. This work focussed on the effects of charge size on blast pressures in regard to pressure distribution on the walls as well as pressure attenuation.

In work by (Anderson Jr CE, 1983), they performed a model analysis to investigate the functional forms of quasi-static pressure (QSP) with respect to different parameters of a vented structure. According to this work the peak value of QSP is a function of the ratio of energy released on detonation (usually denoted as the equivalent mass of TNT) to the volume of the chamber. If the chamber is vented, the time for decay of QSP is related to the peak QSP, the area of the vent and the speed of sound in air.

Experimental tests were undertaken by (Wu Chengqing, 2013), performing 4 experimental tests to determine the effects of a cylindrical charge compared to a spherical one. In this series, three cylindrical tests were compared to one spherical one, as well as the UFC-3-340-02 model. These tests showed that the codes over and underpredicted the pressures generated depending on the orientation of the cylinder. They recorded high pressures for axially oriented cylinders compared to values of a spherical charge on the same chamber location. This shows the complexity of these interactions and how the change in orientation can change the pressures generated, though these were looking at peak reflected overpressures and impulse on the wall instead of the QSP. This study also only included 4 non-identical tests, which makes further interpretation difficult due to the unknown effects of experimental variability, noise, uncertainty, etc.

Many of these complex mechanisms are localised mechanisms that affect the pressures generated at specific points of the confining chamber, which means they would have some, but not considerable influence on the overall QSP generation being developed in the chamber. This means that a small part of a chamber was to be sampled, such as a bolt holding on a plate and what pressures that would experience, a more comprehensive understanding of these more complex events would be required to properly interpret the data. However, when considering the chamber quasi-static pressure as a whole, these may not need to be considered.

Explosive events can also be partially confined, and in this case, there is a venting scenario that needs to be considered as the energy from the explosion will be lost through the loss of pressure out of the venting area. A partially confined explosion adds new complexities for this reason and new mechanisms that should be considered when evaluating pressures and temperatures generated. This additional loss of energy would then be in addition to the losses through heating of the confining boundary as explained in (Feldgun V.R., 2016) through experimental testing and numerical simulations of the pressure decay mechanisms and relationships.

Confined trials with different chamber volumes and geometries were conducted in an attempt to characterise the temporal behaviour of explosives with respect to the mass to volume ratio of charge to chamber (Weibull, 1968). This data showed a clear and significant link between maximum QSP values and the chamber volume. This data was fundamental in the production of the predictive curves used in (UFC-3-340-02, 2008).

Confined experimental tests completed by (W. A. Trzcinski, 2007) investigated the quasi-static pressure generated by aluminium enriched RDX explosives in two chamber sizes, 0.15 m³ and 7 m³ volume. these were then compared to thermochemical calculations. These comparisons showed increases in QSP compared to pure RDX explosives and changes between the aluminium mixture of the explosive using flakes or powder also causes change to the QSP formed in the system.

A sizeable quantity of data was compiled by (C. E. Anderson, 1983) and analysed, obtaining peak quasi-static pressures as well as time durations and impulse measurements for confined explosions. Through the use of similitude analysis, appropriate parameters were chosen for graphically displaying the data obtained, as QSP was found to be a function of explosive energy to chamber volume. This allowed least square curve fit to be used with experimental data to allow predictions of values of QSP within the limits of the experimental data analysed. They envisioned the event as an instantaneous energy release inside a vented chamber but with no thermal losses from the conduction of heat into the structure's walls. In there analysis they state that "Provided the flow through the vent is small relative to the rate of energy release, the maximum pressure will occur before significant venting has transpired." which allows them to calculate the ratio of maximum absolute QSP to ambient pressure using equation 2.5.

$$\bar{p} = f \left[\frac{W}{p_0 V} \right]$$

Equation 2.5

Where \bar{p} is the ratio of maximum absolute QSP to ambient pressure, f is the functional relationship, W is the unit of energy, p_0 is ambient pressure and V is the enclosure volume.

Though not considered in the experimental work in this thesis, nuclear explosions do not generate afterburn in this way as they develop through different processes, and the same is considered true for explosives with a high oxygen balance as they should have little to no fuels remaining after detonation (Dewey, 1964).

Some research into modelling the pressures generated in a confined explosion on aircraft as well as development of characteristic blast load parameters associated with confined explosions when wall failure occurs. This was designed to be usable for aircraft design engineers. This has been undertaken by (Proctor, 1972). This process ignores the loss of energy through heat due to the long duration involved on pressure. However, they state that for generic use outside of aircraft, in larger structures such as compartments in ships or building rooms uses they need to consider more inputs or would need to make more modifications, such as multiple shock reflections, heat loss from interactions with walls as well as processes occurring upon wall

confinement failures (Proctor, 1972). This is an important part of understanding the full picture of confined explosions when considering venting processes from breakout of chambers.

These complex mechanisms and difficulties to measure the pressures and temperatures inside confined chambers mean that there are still gaps in the understanding of the processes occurring in confined explosions and the time scales that they occur over. The large use of TNT equivalence and TNT explosives also causes differences in literature since it has such different compositions to other common explosives which leads to differences in modelling and predictions that are based on TNT.

2.10 Afterburn

The phenomenon of afterburn is a well-established occurrence when an explosive detonates. This phenomenon occurs when detonation products react with external oxygen to cause a further reaction and release of energy. Modern high explosives are typically 'oxygen deficient', this means that they do not have enough oxygen within the molecular structure of the explosive to fully oxidise all the products made from the detonation reaction (Tyas A, 2016). Since these explosives produce additional fuel, they continue to react/burn after the initial reaction when they encounter oxygen. This additional reaction is called afterburn.

Oxygen balance (OB) can be defined as an equation, shown by Equation 2.5, where a, b, c and d represent the corresponding atoms in the molecule $C_aH_bN_cO_d$ and M is the molecular mass. The value of 1600 is used to convert from a fraction to a percentage since it is being calculated in terms of 100 g of substance, so 100 g of O_2 gives a mass of 1600. An oxygen balance of 0 is obtained when a molecule has just enough oxygen to form carbon dioxide from carbon and water from hydrogen as well as any other atoms that could be oxidised in the composition (though only considered in this thesis are carbon and hydrogen containing explosives) with no excess. An explosive with a positive oxygen balance has enough oxygen to react all the carbon and hydrogen as well as having some left over as excess. An explosive with a negative oxygen balance has less oxygen than needed to react with the carbon and hydrogen present in the molecule so fuel gasses such as carbon monoxide will be left over post detonation (Lobry, 2021).

$$OB = \frac{1600(d - 2a - \frac{b}{2})}{M}$$

Equation 2.5

The effects of oxygen balance on free air blasts have been modelled by (Genetier, 2014) through looking at three different liquid explosives. Though this was done considering liquid explosives, it still provides insight into the differences between explosives with varying amounts

of oxygen to fuel ratios. The main differences from these models and tests are shown to be the secondary shock and fireball emergence and speed.

The fuels present in conventional explosives are mostly carbon and carbon monoxide as they are normally some forms of hydrocarbon with additional oxygen and nitrogen attached to allow the reactions to take place within the explosive. For example, the structure of some common explosives is shown below in Figure 19. Each of these explosives is purely composed of carbon, nitrogen, oxygen and hydrogen, so the products they can create are limited to those constituents.

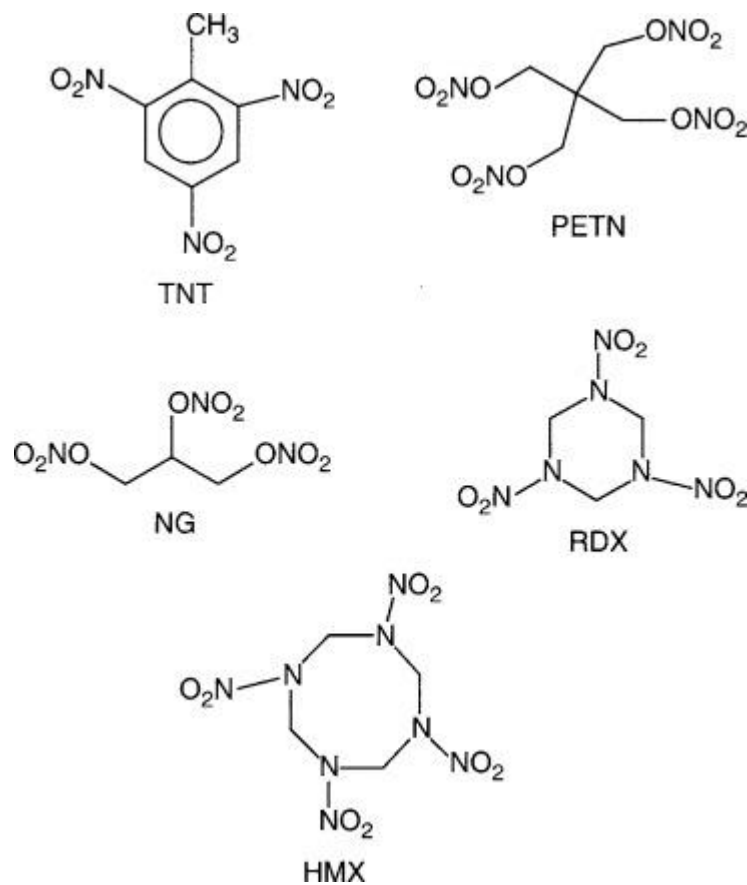


Figure 19 - Chemical structures of different explosives. (Doble Mukesh, 2005)

Different explosives have different reaction mechanisms, which means that each one will have a varying amount of reactive products that are produced by their detonation. These different reactions mean that the afterburn from each explosive is also different, and the work of (McNesby, 2010) showed that having a hydrogen rich set of products generated, causes a lower temperature that the afterburn will ignite at. They also summarise that afterburn occurs in the middle-time of a detonation, which they describe as when the charge has expanded to around 10 charge radii and ends when shock wave separation occurs from the fireball. The method of afterburn theorised here occurs due to the leading shock being reflected back through the detonation products which causes the mixture to further heat and mix.

A typical TNT explosion contains 2.5 times the initial energy release within the afterburn compared to initial detonation energy (Milne, 2016) so for this to be even partially contained would result in a much different effect on these structures than a free field explosion due to the reflections and mixing and hence requires a better understanding of the phenomena occurring.

Through the use of 1-dimensional and 3-dimensional models, (Balakrishnan Kaushik, 2010) gained a better understanding of afterburns impact on impulsive loading. Shown in Figure 20 are the differences when modelling the pressure generated at a point when using a 1-dimensional model and 3-dimensional models. This shows a major difference in the time of arrival of the secondary shock as well as the decay in pressure being more significant in the 1-dimensional model. This shows that afterburn and mixing has an impact on not only late time features but also the acceleration of the secondary shock, the strength of the secondary shock, and a lesser decay of the primary shock. Though there are these differences, the primary shock pressures are equal, it would just be an alteration for the impulse.

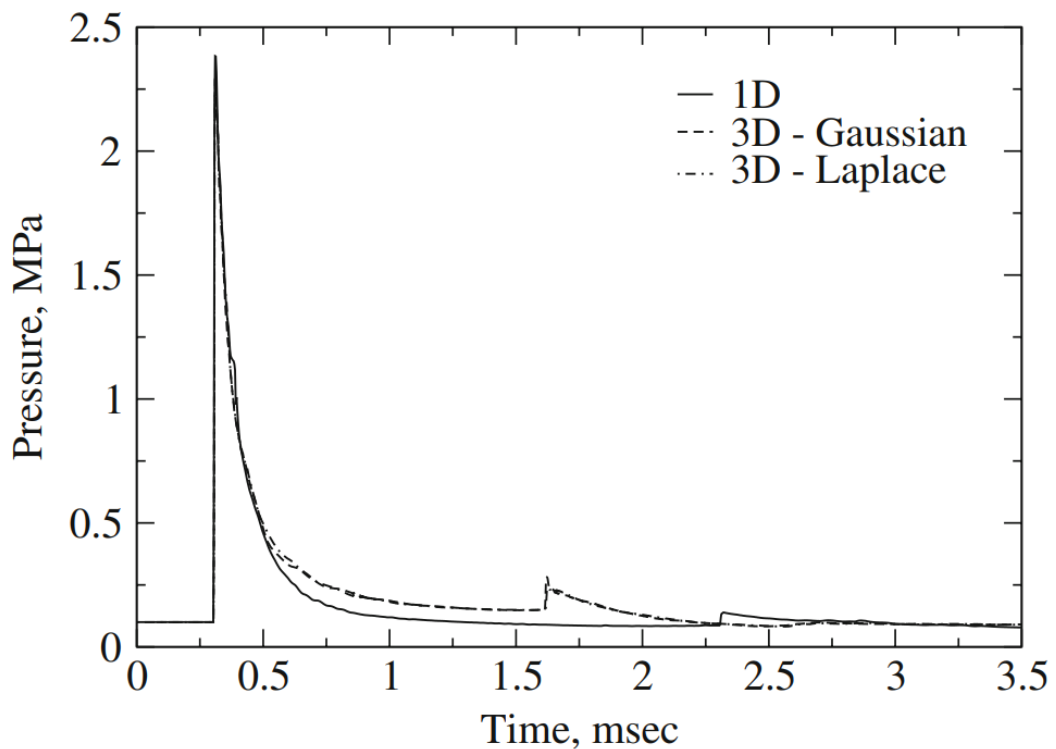


Figure 20 - Pressure traces 0.9 m radially from TNT in 1D and 3D. (Balakrishnan Kaushik, 2010)

Values for the difference in impulse generated using these 1-Dimensional and 3-Dimensional models is shown below in Table 2 for reference.

Table 2 - TNT scaled impulse with and without 3D mixing.

Scaled radius ($\text{mkg}^{-1/3}$)	Positive pressure impulse ($\text{Pa sec kg}^{-1/3}$)			Total impulse ($\text{Pa sec kg}^{-1/3}$)		
	1D	3D-11.25°	3D-22.5°	1D	3D-11.25°	3D-22.5°
0.80	208.9	334.4	335.5	425.9	572.6	611.5
1.38	121.4	177.8	177.5	219.6	296.7	293.0

This difference in 1-dimensional modelling and 3-dimensional modelling shows that there are complex interactions associated with the afterburning which affect the pressure generation and the development of the quasi-static pressure (QSP). This is because the 3-dimensional models include turbulent mixing of the products with the surrounding air, whereas the 1-dimensional models do not include this turbulent mixing as they do not have the ability to. This shows that if there can be turbulent mixing forced upon an expanding detonation product cloud, this would increase the amount of turbulent mixing and hence the time of onset of this afterburning effect.

The effect of afterburn has an effect on the production of energy and hence pressure when considering the QSP of a system. For example, an explosive with an oxygen balance of 0 or greater than 0 would have enough internal oxygen to cause the full reaction, leaving little or no fuels to react with external oxygen, this would mean that the afterburn would not cause an increase in the QSP as it does not have any additional energy. Compared to an explosive with a negative OB which would gain additional energy and pressure from afterburning reactions that would affect the QSP and likely make it higher and last for longer.

Work by (Edri I.E., 2019) looked at this effect by comparing the confined TNTe factors of different explosives in a confined environment. This work compared the weight to volume (W/V) ratio of explosive to chamber size and investigated the influence that this ratio had for different explosives. When comparing the three explosives, RDX, PETN and ANFO to TNT, he discovered that the equivalency factor to TNT of these other explosives was dependant on the W/V ratio. This means that at different W/V ratios, the TNT equivalency factor changed. For RDX and PETN the TNTe was lower than 1.0 for low values of W/V but when the ratio is higher, the TNTe is also higher. This is attributed to the increased effect that afterburning will have on a TNT explosion because there is more fuel that can react with external oxygen compared to the other explosives. Though not used in this thesis, this work also investigated the oxygen-rich explosive ANFO, which produces a full reaction with the fuel contained within the explosive, leaving oxygen remaining that can react with excess fuel in the fuel oil component of the explosive, however its TNTe still varies due to the variation in TNT's afterburn effects. The changing equivalency factors for RDX and PETN are shown below in Figure 21.

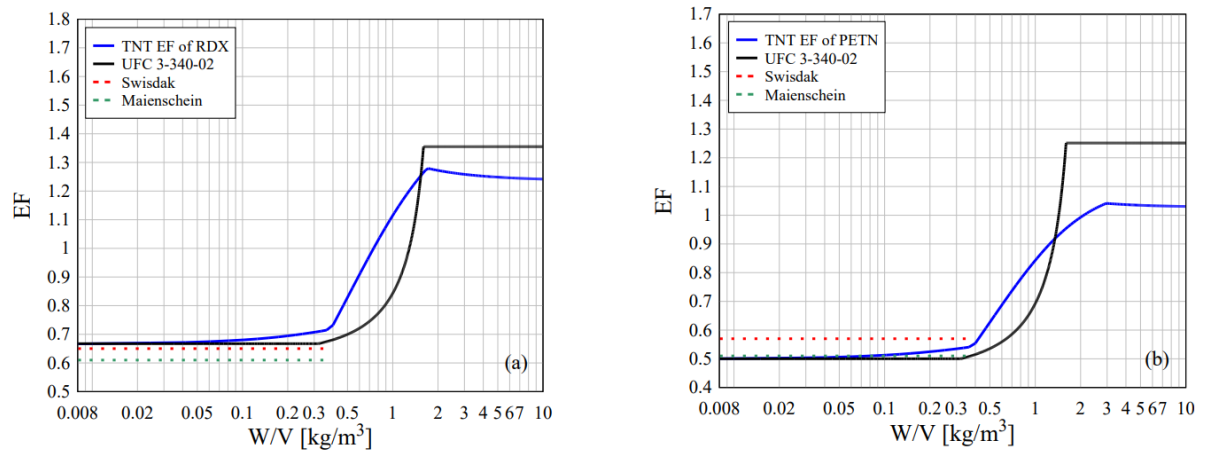


Figure 21 - TNTe factor (EF) of (a) RDX and (b) PETN. (Edri I.E., 2019)

These works show that there is a considerable effect on the onset and effectiveness of afterburn depending on the amount of turbulent mixing that can occur. From 3-dimensional models that can involve this turbulent mixing of detonation products, to TNTe factors that depend on the amount of available oxygen for these turbulent reactions. Therefore, it should be noted that turbulent mixing is an important part of any explosion's development.

2.11 Gaps in the literature

Through this extensive literature review, it can be seen that there are some main issues and areas that require further investigation to get a better understanding of the processes and mechanisms occurring. Below is a list of these main findings and areas of interest.

- Is blast loading fundamentally deterministic and predictable or is it fundamentally unpredictable and chaotic? Though there is some evidence in the literature to suggest such processes are naturally variable, it has been shown that the events can be considered deterministic in the free field at certain scaled distances when the experiments are well defined and controlled.
- Can blast loading be deterministic in more complex situations and scenarios? Though some work has been done on this area, much of the experimental data shows inconsistencies within more complex environments, though newer work has started to increase the consistency of complex scenarios such as soils. Will explosions in confined environments exhibit high degrees of determinism, or variability?

- When examining explosive reactions, do the assumptions of the ideal gas equation hold or do they break down in complex, hot environments? Ideal gas assumptions are there to give a way to measure and investigate gasses that conform to certain assumptions, but when these gasses are put into the real-world scenarios, will they still hold up and how do we test this?
- What mechanisms are the main causes of afterburn, and can they be better understood? Though we attribute afterburn to the reflections and turbulent mixing of explosive products with additional oxygen, can we gain a better understanding of the timescales that these events occur at, and can the impact of afterburn on an explosive event be better understood?
- Can a better model be developed to predict pressures generated by a conventional explosive? Though complex modelling has been done and some simple predictors are available, is it possible to build a chemistry-based model that predicts pressures based on ideal gas laws and fundamentals of conventional explosives, not just the pure explosives such as PETN or RDX?

Chapter 3- Experimental Methodologies

3.1 The confined chamber

To measure the quasi-static pressure generated by an explosive event, a confined environment needs to be constructed in which pressure can be measured. To achieve this a basis was built around a 1 m long, 0.6 m internal diameter 10 mm thick S355 steel tube. This tube has flanges on either end which allows the attachment of end plates that can be bolted to either end, shown in Figure 22. Rubber gaskets were made to fit the pipe so that the end plates sealed on effectively and created a sealed chamber. To allow the insertion of a charge into the chamber, one of the end plates had a hole drilled, measuring 100 mm surrounded by 4 smaller threaded holes. This created a hole that a plug could be fitted into containing the explosive and detonator. This set up is shown below in Figure 23. On this plug there is a M10 bolt drilled and tapped with a hole drilled through allowing a steel rod to be inserted into it. This 3 or 4 mm rod is held in place using a screw that is screwed through the side of this bolt tightening onto the rod and keeping it held. This rod is bent back on itself at one end so that a small fibreglass cradle can be suspended from it, allowing the explosive to have a resting place whilst being as unobstructed as possible. This set up is shown in Figure 24.

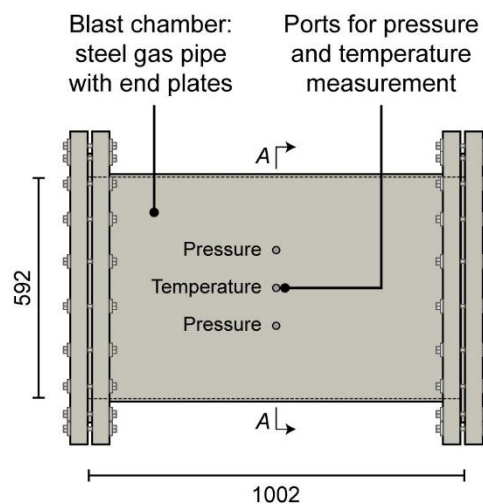


Figure 22 - QSP pipe schematic

This setup with chamber and singular gauge hole was created for a previous commercial project in which pressures of confined explosions were needed to be measured. The volume of the chamber was chosen so that for charges of the order of 10's of grams there would be sufficient oxygen to allow complete afterburn to occur in principle. Appendix 1 shows the thermochemical calculator for a 50 g PE4 charge with highlighted sections showing the oxygen

contained within the chamber before the test as well as the oxygen being used up by the reactions occurring. This then shows the total oxygen left in the chamber as 1.41 moles after the detonation and afterburn has occurred. Peak QSP's were estimated for UFC-340-02 for the charge types and masses that were expected to be used. A cylindrical shape was chosen as an efficient way of containing this confined pressure predominantly through the hoop tension in the chamber walls. Suitable types of flanged pressure pipe are commercially available and in this case were purchased from PT Pipe Fabrications Ltd of Basildon Essex.

To determine the safe working limit of the chamber, the hoop stress was calculated for the maximum internal pressure that can be contained by the steel tube. Using values for the planned dimensions having a diameter of 595 mm, a yield stress of the pipe wall of 355 MPa, a pipe wall thickness of 10 mm and a dynamic load factor for suddenly applied load of 2. The max pressure can be calculated using Equation 3.1.

$$P_{max} = \frac{2 \times t \times \sigma}{D \times DLF}$$

Equation 3.1

Where P_{max} is the max pressure possible, t is the pipe wall thickness, σ is the yield stress of the pipe wall, D is the diameter of the pipe and DLF is the dynamic load factor for suddenly applied load. When inputting the parameters into the equation, this gives a maximum pressure of 5.97 MPa and this is around 9 times the maximum pressures generated in this testing so has a large safety factor.

This thesis adds to the previous work the atmospheric variation ability to the previous set up which was the main experimental contribution. This allows the atmosphere to be altered from air to other constituents such as nitrogen or argon, changing the oxygen content of the chamber pre-test, making afterburn not able to occur as well as two different gasses to alter the specific heat capacities to see the effect of this also. These alterations included designing a gas flow system to purge the chamber of atmospheric oxygen and a high-pressure regulators and pipework to allow the flow of gas into and out of the chamber that could be controlled safely.

Some preliminary tests used a slightly different mechanism for holding the charge in place, this was done by having two rods bent round a screw held in place so that they provided two parallel beams for a piece of fibreglass mesh to be suspended between. This was altered so that less rods needed to be used to suspend a charge for each test.

This plug has a small hole through the centre of it Figure 24, this is to allow the detonation cord used to ignite the non-electric detonators to be passed through, which seals the hole and allows the detonator to be affixed to a charge before being inserted into the chamber. The plug is affixed to the chamber end plate using the 4 holes in the plug that line up with the holes in the end plate. These are lined up and screwed into place forcing the plug closed and sealing into place against the rubber seal that is placed around the plug. This keeps the chamber from having any venting and keeps it as a fully confined scenario. This was tested by the use of

a fine dust around any possible leak locations and recorded with high-speed video to assess any possible leaks as they would show movement of the dust, which did not occur.

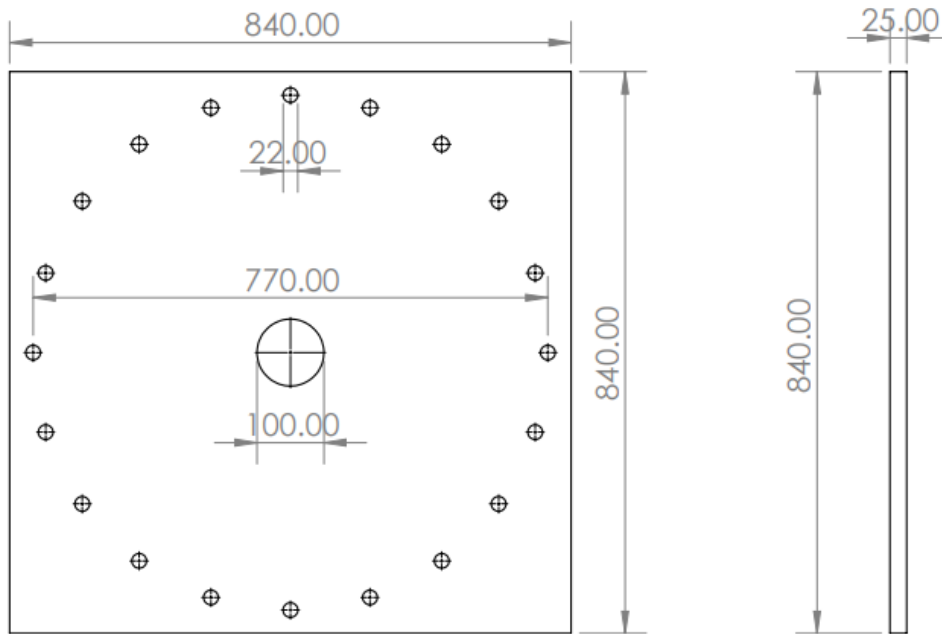


Figure 23 – 25 mm thickness end plate face on showing the holes and a plug next to it showing how they attach.

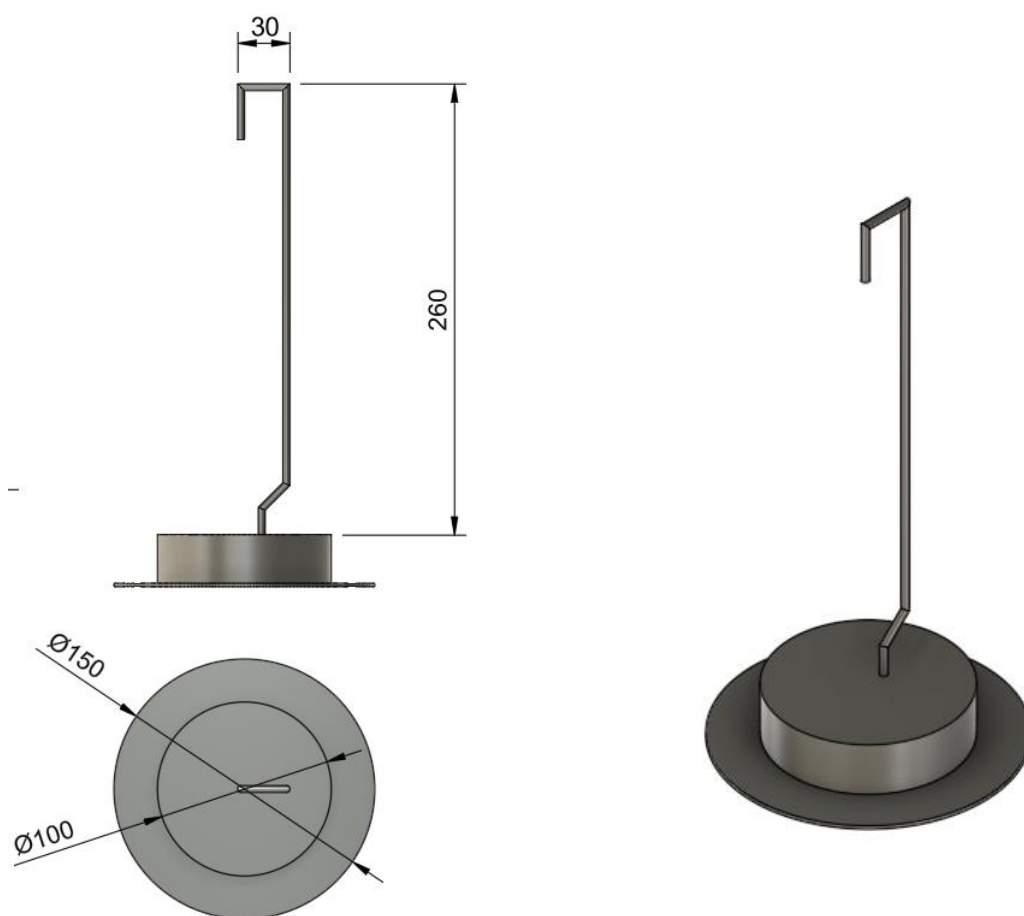


Figure 24 – diagram of the inner face of the end plate showing how a rod is held in place. (not to scale)

3.2 Data acquisition

To record the pressure time histories in the chamber, a Kulite piezo resistive pressure gauge was used. For the majority of tests, one gauge was a 17 bar Kulite HKM-375 and the other was a 35 bar HEM gauge. Two different rating gauges were used to establish data reliability across single tests when the peak shock pressure was uncertain so that two signal to noise ratios could be seen. This also gave the ability for the pressure traces to be compared to each other between tests to give an indication that the gauges were still performing correctly. The key issue was that while we expected QSP's in the range of 3-8 bar (hence suitable for the 17 bar gauge), there was a concern that the maximum shock pressures were not known before hand and if greater than 17 bar, could have affected the subsequent response of the 17 bar gauge so the 35 bar gauge was used as a back-up though preferentially not relied upon as it has a worse signal to noise ratio. The gauges available for this work were slightly different specification, with one being

rated for higher temperatures, though assessment of traces from both gauges for the same test indicate very close correlation which is shown in Figure 25.

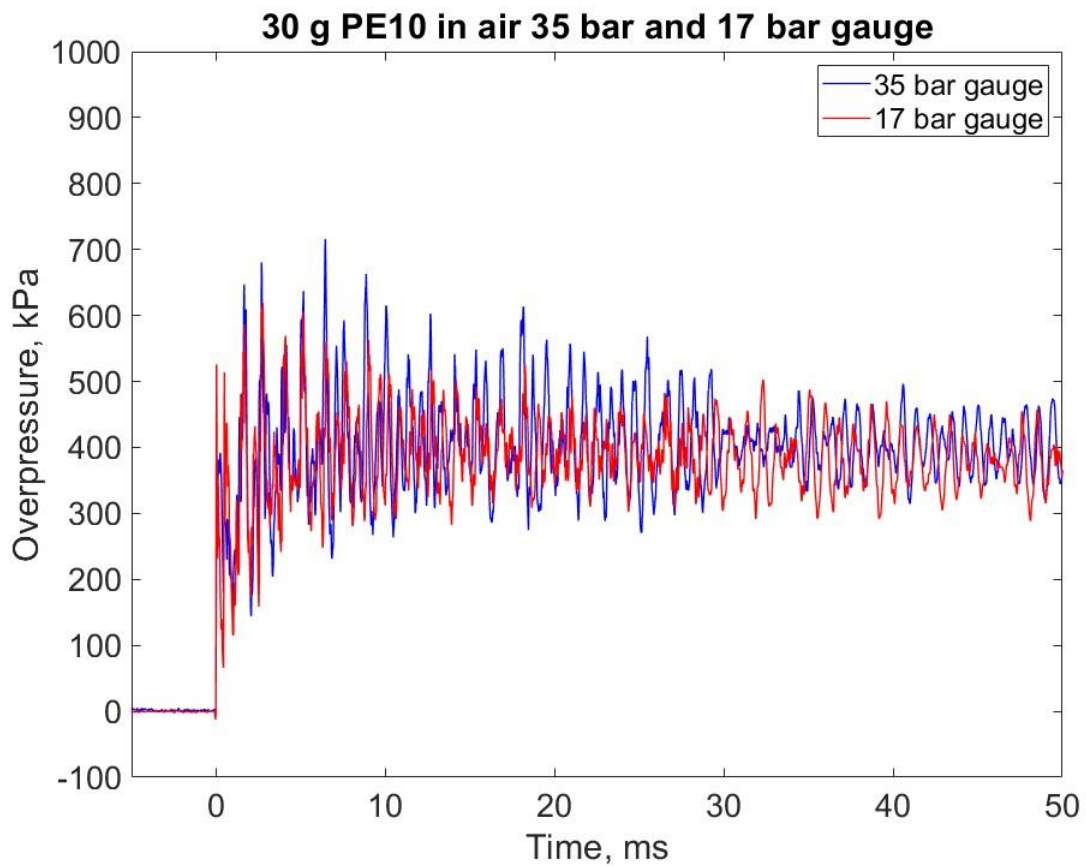


Figure 25 - Comparison of 17-bar gauge and 35 bar gauge for a 30 g PE10 detonation.

To record the data produced by the Kulite gauges, a Tie-Pie Handyscope HS4 digital recording device was used for some tests and for later tests a HS6 version was used. The HS4 scope was ran at 16-bit resolution, capturing 131,000 samples at a sample rate of 48.828 KHz (20.48 ms per sample). It was set with a 10 % pre trigger giving a recording window of 2.4 seconds. After upgrading to the HS6 scope, the data was set to capture at 16-bit resolution, capturing 131,000 samples at a sample rate of 78.25 KHz. The same pre-trigger was used in these tests as the HS4 tests.

The recording system was set to trigger by using a rising edge function of the scopes. This function starts the recording when the signal from the gauges causes the voltage to leave a set voltage window that is adjusted before the test so that it fits around the baseline of the gauge signal/noise. This was altered for each test so that it fitted as close as possible to the baseline signal as found through initial set up tests of the system. This system doesn't provide a time of

detonation, however this was deemed not necessary when looking at the QSP of the system as that is unrelated to initial time of arrival of the shock wave.

To evaluate the accuracy of the gauges before a test was conducted, they were tested using a static pressure pump. This was done by connecting the gauge through the same cabling and data acquisition equipment as would be used during the test and applying a known pressure to the gauge (35 bar for a 35-bar gauge and 17-bar to a 17-bar gauge) using the static pressure water pump. When this pressure is applied a voltage increase is observed, which corresponds to a pressure. This is checked by using the manufacturer's calibration factors which convert the voltage into a pressure. If the pressure gauges gave a value that was accurate to their designated bar rating, then they were considered acceptable to use for the testing. This pre-test calibration allows confidence that the pressure gauges are recording accurately. This testing set up can be seen in Figure 26 below.

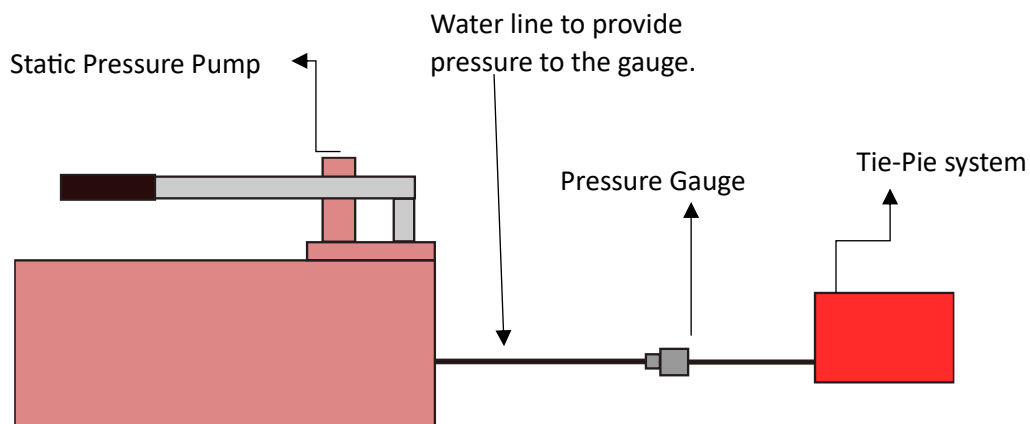


Figure 26- Diagram of the static pressure pump connected with a pressure gauge and tie-pie system.

The pressure gauges work through the use of a fully active, four arm Wheatstone bridge, where a series of resistors are balanced until a force is applied to one of the resistors and causes a change in resistance across one part of the circuit. This change is then translated into a voltage due to the balance of the resistors being affected. For the Kulite gauges used in this testing, the HKM gauges use a flush metal diaphragm as a force collector with a solid state piezoresistive sensing element immediately behind it protected by a metal screen. The transfer of the force inside the gauge is accomplished by using a non-compressible silicone oil that passes the force from the exterior of the gauge to its internals. This is housed in a stainless-steel body. These gauges run on a 10 V power supply which was provided by a benchtop power supply reading at 10 V, being checked by a multimeter before each test. A schematic of the gauges can be seen below in Figure 27.

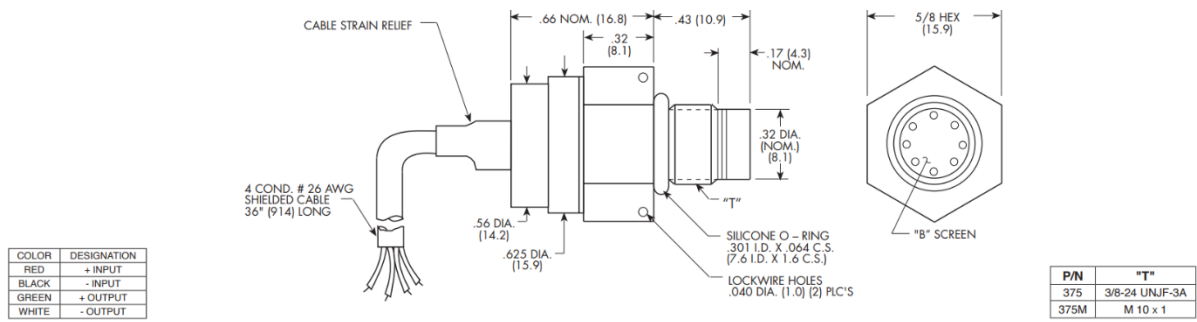


Figure 27- Schematic diagram for Kulite pressure gauge (KULITE SEMICONDUCTOR PRODUCTS, 2022)

A final schematic of the whole pipe system is shown below in Figure 28.

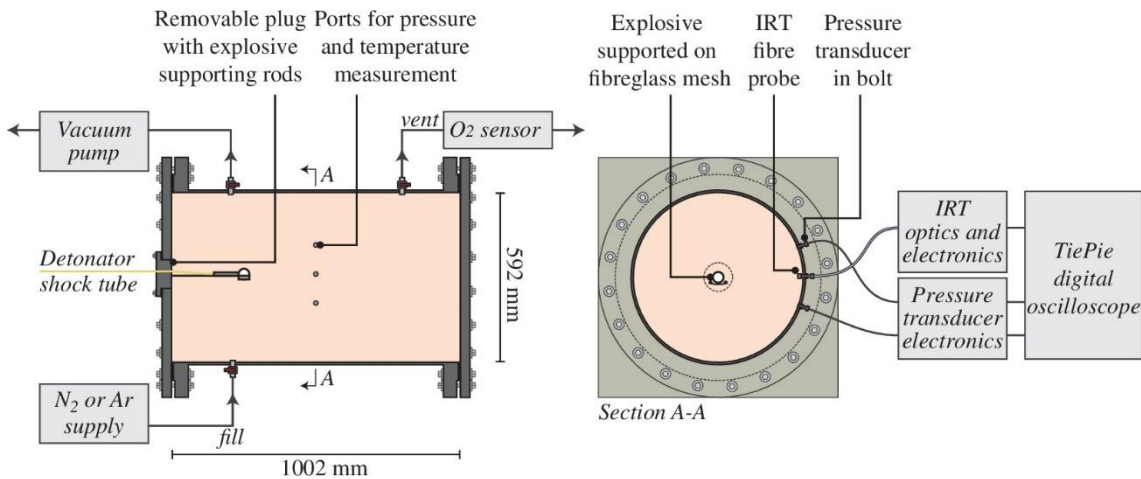


Figure 28 – Full schematic for the pipe system. (D. G. Farrimond, 2024)

3.3 Pressure gauge set up.

To include the pressure transducers to the chamber, two holes were drilled into the centre line of the chamber, 500 mm from either end to be as far from reflecting end walls as possible. These holes were tapped to fit M16 bolts. To allow the attachment of pressure transducers into these holes some special bolts were constructed so that the gauges would be shielded from direct contact with the fireball and out of direct line of sight of any explosive shock waves or shrapnel created in the chamber. These were created by taking some 70 mm long M16 bolts and coring out a 10 mm diameter hole 35 mm deep from the end of the bolt allowing a pressure gauge to be affixed into an air reservoir. A 3 mm hole was drilled into the opposite end

through the whole bolt to meet the reservoir. This provided a narrow passage for pressurised gas to pass through into the reservoir and interact with the pressure gauge. The bolt was then mounted into the chamber as seen in Figure 29 creating an airtight seal.

When using a coupling system to attach a pressure gauge to an environment, it degrades its ability to measure initial blast pressures accurately. In this situation, it can be justified the residual pressures in the chamber are being measured, rather than an exact description of any localised transients. An estimation of the degradation of the transducer's performance can be obtained by using acoustic theory (Walter, 2004). This works assuming that the wavelength of sound is much larger than the cavities or holes that the wave will travel over/through.

Keeping the gauges out of the fireball generated by the explosive is important due to the effects of high temperatures on the pressure gauges. If the gauge is exposed to high temperatures, they can experience some voltage drift as the temperature changes. Initial tests were performed to determine if filling the gauge bolt with grease to further protect it from high temperatures up to 2000 K (by adding grease to the gauge hole before adding the gauge into place so that it was a full seal of grease) would avert this. These tests showed a severe smoothing of the initial shock behaviours in the chamber and also had no change in signal in terms of any drift that could be caused by high temperatures on the gauges. A comparison of insulated and non-insulated gauge setups can be seen below in Figure 29.

The stated sensitivity to thermal effects is:

Thermal zero shift: $\pm 1\% \text{ FS}/100^\circ \text{ F}$ (Typ.)

Thermal sensitivity shift: $\pm 1\% /100^\circ \text{ F}$ (Typ.)

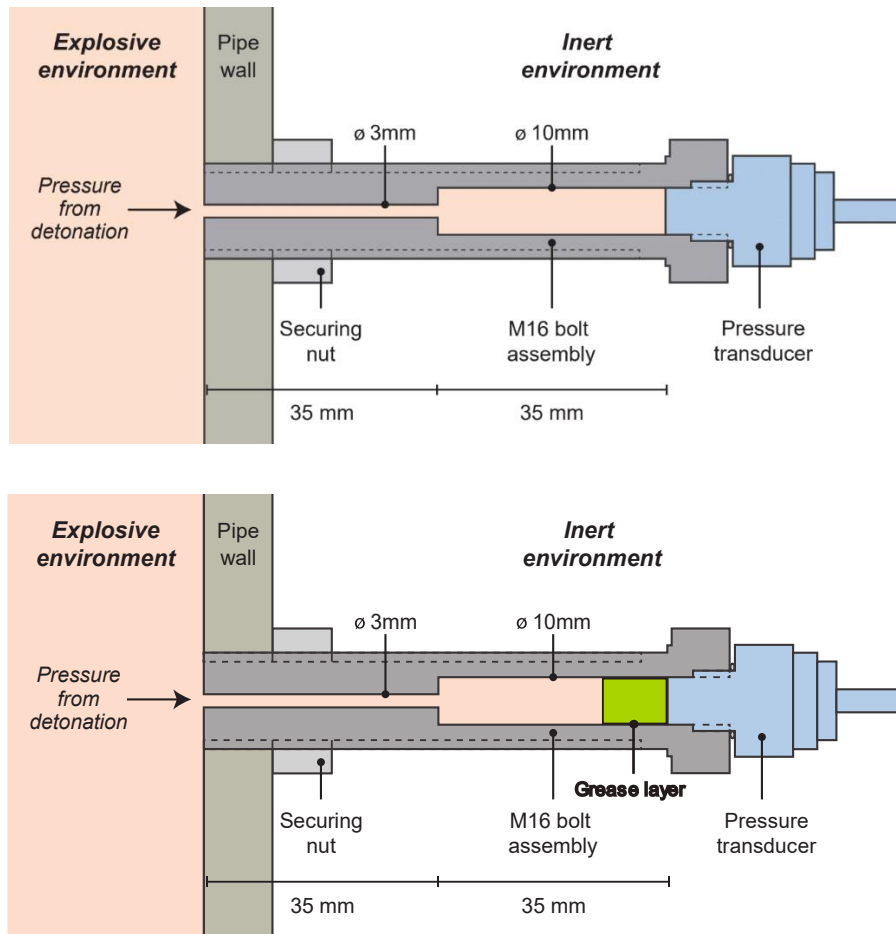


Figure 29 – Gauge bolt mounting system, greased and ungreased. (D. G. Farrimond, 2024)

Keeping the gauges out of direct line of the shock wave is also an important reason to use the shielding bolts. If the gauges were in direct line of sight or had a more reflected pressure wave coming into contact with them, this would cause a large pressure signal for this initial reflected pressure wave. It is thought that this initial peak would be the same as, or at least comparable in magnitude to, a free field reflected shock at the same scaled distance and though it could be useful in some circumstances, for these tests it is not the focus. Instead, it would provide a much smaller signal to noise ratio for the part that is being investigated. This would be due to the large initial peak caused by shock interactions followed by smaller peaks for the quasi-static pressures generated. By using this bolt to isolate the gauges from direct shocks, just the QSP is prominent in earlier stages under 50 ms and less initial shock peaks are evident. This means that the data will have a better signal to noise ratio in the sections under investigation as gauges with a smaller pressure rating can be used, meaning the signal will be a larger proportion of the total signal the gauge can take.

3.4 Capability to alter the atmosphere.

After initial trials were completed with a standard air atmosphere, it was decided to develop a way to change the atmosphere in the chamber to investigate its effects. To do this first a gas needed to be chosen to swap out the atmospheric oxygen for. In these trials, the decision was made to use nitrogen as a replacement gas. This was chosen as it has a very similar density to that of atmospheric air, as that is composed of 78% nitrogen. Keeping the density as close to the original as possible meant that as few variables were being altered as possible. Only changing the oxygen percentage in the chamber pre-test.

The nitrogen selected for this was 99.9% N₂ from BOC and was provided in 300-bar bottles. To allow this to be introduced to the system, a new set up was devised. First, a 300-bar nitrogen regulator (SWP brand) was attached to the bottle with a flow meter attached so that the flow of the gas out of the bottle could be controlled. This was then attached to some flexible hosing to provide distance between the chamber that the explosive event is taking place in and the bottle of compressed gas, allowing the bottle to be out of line of sight of the chamber. This flexible hosing was attached to the chamber by drilling and tapping a ¼ inch BSP hole in the top of the chamber at one end, as well as a ¼ inch BSP hole on the bottom of the chamber at the opposite end. The flexible hose was then connected using a high-pressure pipe and a high-pressure valve so that it could be separated from the chamber when the test was taking place. The holes were placed at the top and bottom because the nitrogen is less dense than air, which means it will rise to the top of the chamber and force the air atmosphere out the bottom of the chamber. Images of the alternate atmosphere set up can be seen in Figure 30. The locations of the holes were swapped around for using argon to alter the atmosphere so that the denser gas is pumped in from the bottom instead of the top.

On the exit valve for the chamber, an oxygen sensor was fitted to measure the percentage of oxygen present in the gas leaving the chamber. This was a Greisinger GOX100 oxygen meter which measures oxygen percentage with a precision of 1 decimal place and was used to measure the percentage of oxygen until it reached a stable 0.2% oxygen in the exiting gas before the test was conducted. The bottom also has a valve so that it can be sealed pre-test keeping the chamber fully sealed.

For some later tests a 230-bar bottle of nitrogen was used instead of 300 as well as a 230-bar regulator to allow a better control of the pressure and flow into the chamber as well as an argon bottle and regulator for tests including argon.

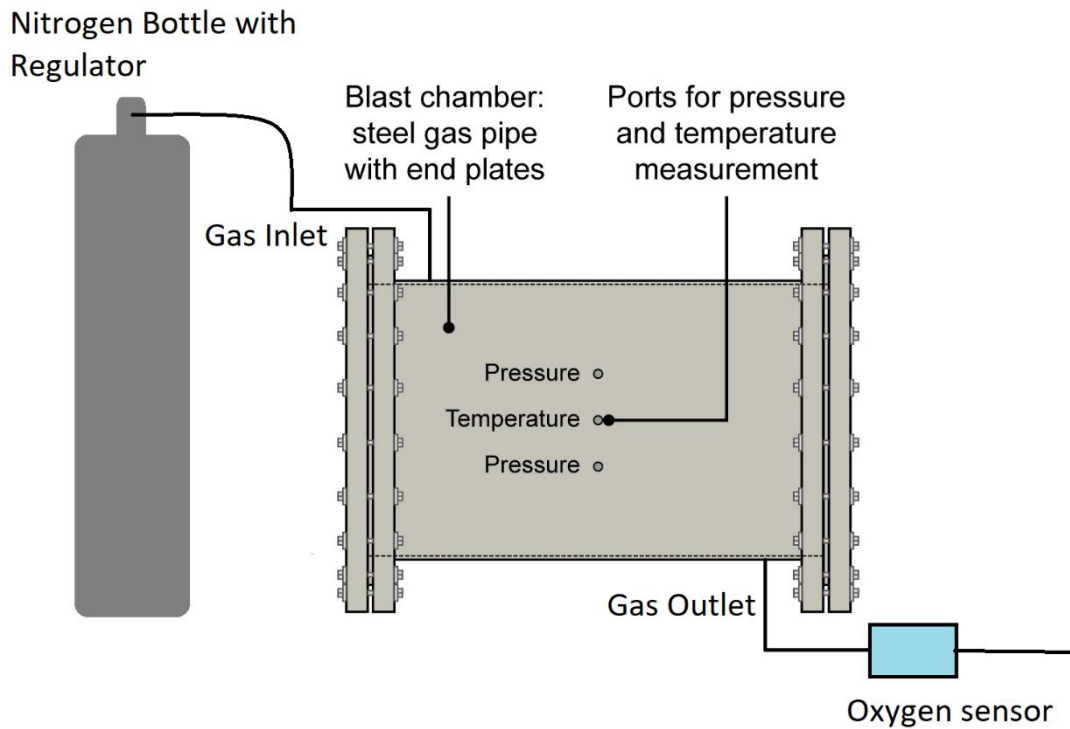


Figure 30- Alternate atmosphere chamber configuration.

When testing with a nitrogen or argon atmosphere, the purging took place once the charge was in position. After positioning the charge, the inlet and outlet on the chamber were opened and the nitrogen was flowed into the chamber at a pressure of around 1.5 to 2 bar. This slowly purged the chamber of air mixing and forcing the oxygen out of the chamber. Once the chamber reached an oxygen percentage of 0.2% the inlet valve was closed off and the flow of nitrogen/argon into the chamber stopped. The outlet was then placed into a water reservoir and allowed to bubble until it returned to atmospheric pressure. Once the bubbling of the air through the water had ceased the valve was closed off to seal the chamber and the test was initiated.

3.5 The explosive charge

For these tests, charges of PE4 and PE10 were used. These explosives were chosen due to the extensive research on them in the literature (Farrimond, 2023) that has been undertaken by the University of Sheffield. Many experiments have been completed looking at the consistency and repeatability of free field tests using these explosives. The purpose of then testing these explosives under a confined environment can be used to build a picture of how

consistent and repeatable these new experimental methods can be, since the underlying free field repeatability is known.

The charges used in these tests ranged from 10 g up to 50 g to provide a set of increasing masses up to near the maximum bounds for the oxygen consumption as explained previously and were mostly spherical charges but with a small number of 2:1 length to diameter end detonated cylinders used to test the influence of charge shape (Blastech Ltd, 2018). Charges were kept in 10 g increments for ease. Charges were hand rolled into spheres because less focus was on the initial shock pressures which would be affected by subtle inconsistencies in charge shape, but the overall pressure (QSP) would be the same as its dependant on the energy instead of the shape. These were still made to as accurate a dimension as possible while ensuring that the masses were always consistent with holes pressed in them the size of the detonator, so that the detonator could be pushed into the charge without deforming the shape, avoiding any lack of contact with the charge and making sure that the charge detonated more centrally. An example charge can be seen below in Figure 31.

Cylindrical charges were formed using a 3d printed charge mould printed on an Ultimaker 2 extended+. The filament used was 2.85 mm PLA with a layer height of 0.06 mm using the CURA slicing software. The explosive was then hand pressed into the two-part mould using a plastic rod. The two-part mould could then be separated to allow the charge removal with minimal disforming.

To detonate these charges, Euronel non-electric detonators were used. These detonators have a net explosive quantity of 0.8 g TNT equivalent mass, according to the manufacturer's specifications. These detonators are on the end of a length of shock tube that can vary in diameter. This meant that occasionally a very small gap was let around the shock tube through the hole in the end plate. This was discounted from the consideration of these tests being fully confined as it was not a large enough gap to allow a significant amount of pressure out of the system in the time frame over which measurements were taken. For nitrogen tests the charges were initiated as soon as possible after the pressure was reduced back to atmospheric pressure to avoid oxygen getting back into the chamber.

The shock tube was activated with Chemring mini shrike firing packs or Technical Concepts manual initiators. These firing packs work by charging a capacitor, which upon pressing the fire button, sends an electrical shock into the shock tube, which causes the explosive inside the tube to start a detonation down its length. Once this shock comes in contact with the detonator, it will transmit the shock wave to the explosives in the aluminium cased detonator, which causes its ignition.

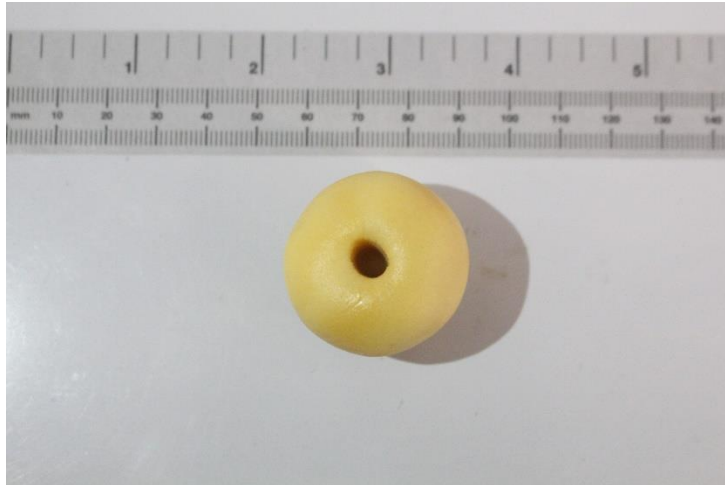


Figure 31 - A PE10 charge with detonator hole.

3.6 Infra-Red Thermometer set up.

To further investigate the process in a confined explosion, an Infra-red thermometer was designed by (Hobbs, 2021) to be used to directly measure the temperature of the chamber during the test. A fast-running Infra-red Thermometer (IRT) was developed that would be able to measure the temperature of the chamber at 250 kHz which is a faster rate than the pressure gauge oscilloscope can measure to facilitate direct comparison with high-rate pressure measurements.

To attach this IRT to the chamber, a 50 mm M16 bolt was cored through to allow the gold coated fibre probe to be inserted through fitting snugly after being screwed into place. On the end of this M16 bolt was a 4 mm thick sapphire window that was held in place by a cap with a rubber gasket to protect the end of the sensing probe. This was then connected to the electronics of the IRT through a silica fibre. This set up is shown below in Figure 32. The probe sticks into the chamber so that it can detect as much surface area as possible for the temperature measurements as it is protected by the sapphire glass window. This window was cleaned between tests so that it was as clean (as practically possible) as when the calibration was completed.

The IRT works by detecting emitted radiance from a target object, in this case the chamber or fireball, and can measure fast changes in transient temperature. This IRT measures the temperature over a large area in comparison to the pressure gauges which measure over a single point. The benefit of this is that it provides an “overall” temperature of the fireball instead of the temperature at a single point within the chamber compared to the gauge that measures pressure at a single location.

The IRT's are built around a two-colour Si/InGaAs photodiode which is a type of photodetector which signals light over two distinct wavelength bands and providing a photocurrent output for each. Each IRT can measure temperatures between 800 K and 5000 K. The IRT's are powered by a 12 V supply with 1 A of current and stabilised for a temperature of 40 degrees Celsius so are housed inside a temperature-controlled box. Each instrument was calibrated separately as though they are designed to be identical, calibration is needed separately to ensure accuracy.

The IRT's are set at a capture rate determined by the oscilloscope that records the data so was set to the same frequency as the pressure gauges, meaning the data was collected at the same time as the pressure gauges.

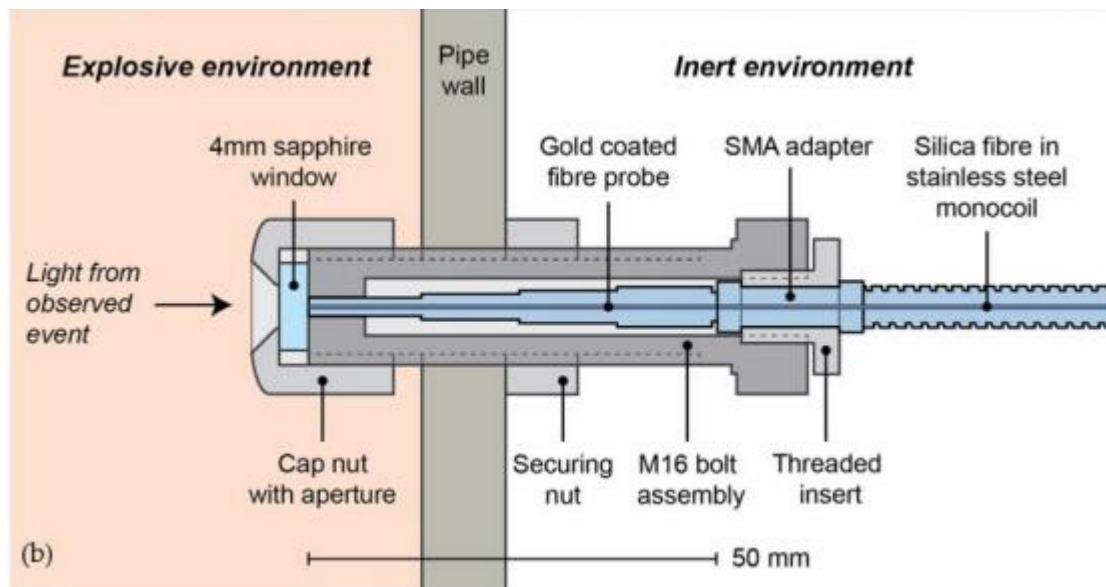


Figure 32 - Schematic drawing of IRT.

3.7 Step by Step Experimental Procedure

This next section provides a step-by-step procedure to perform one altered atmosphere quasi-static pressure test.

1. Cut a steel rod (3 mm) to length at 300 mm.
2. Bend the rod to shape, allowing charge placement at 240 mm up the rod.
3. Cut a small portion of fibreglass mesh to fit over the bent rod as well as a strip long enough to go around the charge and the cradle (dependant on charge size).
4. Glue the fibreglass mesh to the cradle at 240 mm so that the charge can be placed upon it later and leave to dry.
5. Using the static pressure pump system test the pressure gauges being used for the test, ensuring calibration certificates are available.
6. Insert the required pressure gauges into the chamber and plug them into the oscilloscope.
7. Hand mould a spherical charge of the desired mass making a hole for a detonator to be placed into.
8. Thread through a detonator shock tube through the hole in the end plate plug so that only a small amount and the detonator is left on the inside of the tube side.
9. Attach the steel rod to the plug using the tightening screw and ensure it is tight and the cradle is 240 mm from the end plate.
10. Insert the detonator into the charge and attach it to the cradle using a strip of fibreglass mesh.
11. Attach the detonator to the steel rod to avoid movement of the detonator during following set up using glue or small amounts of tape.
12. Place the plug into the chamber and tighten up the four bolts to ensure a tight seal with the rubber gasket.
13. Tape the shock tube to the outside of the plug or chamber to ensure it does not move.
14. Attach the hose between the gas cylinder and the chamber.
15. Ensure that the oxygen sensor is attached to the outflow pipe.
16. Open vents to the chamber and turn on the gas flow from the gas being used (around 1-2 bar).
17. Listen for any leaks at this stage to ensure no gas is escaping.
18. Monitor the gas oxygen percentage whilst the chamber is purging.
19. Ensure the oscilloscope has the correct settings and is getting readings from the gauges.
20. When the gas oxygen percentage of the out flow reaches 0.2 % turn off the gas flow and insert the out-flow pipe into a receptacle of water.
21. When the flow of bubbles through the water stops, close all vents from the chamber ensuring it is fully sealed.

22. After a final check that the system is working correctly and is stable, detonate the charge and record the pressures.
23. Ensure data is saved and backed up for analysis later.
24. After successful detonation, vent the gasses and leave to stand for 30 minutes.
25. Once the chamber is back to atmospheric pressure, open the sealed chamber using the plug and ensure full detonation and that it is safe.
26. Once safe, the chamber can be cleaned, and any steel left over or carbon dust can be removed using a pressure washer and vacuum.
27. Once clean, ensure that the chamber is dry before completing another test in the same chamber. (Ideally multiple chambers can be used to get multiple tests completed in a day.)

Data analysis Method

Once the data capture has occurred, it can be converted to a raw pressure signal and then smoothing can be applied. This process is detailed below.

1. To reduce noise in the baseline, obtain an average of the first 2000 voltage data points.
2. Take each voltage data point and minus the average from the previous step.
3. Multiply these values by 1000.
4. Divide the values by the calibration factor of the pressure gauge being used. This provides the pressure in Bar.
5. This data can then be plotted as the raw data.
6. To obtain the time dependant smoothed average, the data is loaded into a Matlab code which varies the amount of data points varied depending on the variation in the data points. This averages a smaller number of points when the variation is larger and more points when there is less variation.
7. Once inputted through the smoothing it can be plotted alongside the raw data.

Chapter 4 – Theoretical Thermochemical Modelling of Pressure

4.1- Introduction

To predict the effects that detonation of a high explosive will have in a confined space requires an accurate method to estimate the pressure that will be generated in the space. In this work it has been assumed that the chamber in question will be filled with air at standard conditions before detonation unless stated otherwise. Post initial detonation, the detonation products expanding from the charge location generate shock waves through the air which reflect off any barriers such as the confined chamber walls. These interactions become highly complex as multiple reflections rapidly occur at the same time, however as the process progresses these shocks decay, and in the absence of energy loss, reach an equilibrium where a uniform QSP above ambient pressure will exist in the space.

The defining factors of the QSP are the volume of the space, the volume of gas released in the explosion and the energy released by the explosion, which itself increases the temperature of the explosion and hence the pressure of the gas. The situation is made more complex due to most high explosives being manufactured to be fuel rich, which allows for the possibility of an afterburn reaction to take place, which also releases energy into the system as this excess fuel reacts with the oxygen present in the chamber's atmosphere. This already complex situation is made more so by the possibility of gasses venting from the chamber if it is not in a completely sealed environment, as well as thermal losses to non-gaseous elements of the chamber. In this work, venting is ignored as the chamber used was fully sealed, but the influence of thermal losses will be investigated later in this thesis.

The simplest type of prediction of QSP magnitudes comes from empirical predictive formulae, derived from experimental observations. Using dimensional analysis techniques for example, (Anderson Jr CE, 1983) showed that the peak QSP was a function of the charge mass to chamber volume ratio, while the decay of the QSP was a function of the peak QSP and vent area to chamber volume ratio (ignoring thermal energy loss). They then derived formulae that predicted these pressures from analysis of a large amount of experimental data. Here, the charge mass may be thought of as just a producer of gas and energy release due to the explosion. Anderson's experimental data were primarily from detonations of TNT and it should readily be appreciated that this may have a limited use if interested in other explosives which may release different quantities of gas and energy per unit mass.

On the other end of the spectrum, the most complex way to estimate the QSP is by a detailed numerical model of a detonation, subsequent propagation of the air shocks and the mixing of the detonation products and air caused by these air shocks. The accuracy of these approaches is dependent on the method used to obtain energy release values and the modelling

of the afterburn reactions. Even if these models worked perfectly, they are typically very computationally expensive to run, and the level of detail of the output, which includes the propagating shocks may not be required if we are solely interested in the average QSP.

Another approach for this prediction is the use of simplified thermochemical analysis aimed to predict the release of gas energy and the effect on the QSP. Codes such as CHEETAH (Fried, et al., 1998) perform detailed calculations of the chemical reactions at various thermal states and these calculations can be used to predict the mixtures that result from the complex resulting gas mixture. However, these codes aren't always available to the general researcher/designer, and the level of detail needed as the real-world conditions aren't always well defined so are hard to predict every possible situation when they are not fast running.

Ideally, we would like a third option that retains the strengths of each of these approaches and doesn't have the negatives of them. Frequently, especially for first order analysis, we would only want to know the peak QSP value, but for a range of explosive types. Such a model would be more physically based than the Baer empirical approach but computationally far less demanding than a fully computational physics-based model. There is therefore a need to develop a fast running and computationally simple modelling approach, which captures the key mechanisms which define the peak QSP. This allows the inclusion of explosives that haven't been experimentally tested in detail as it uses chemistry-based solutions to provide a maximum QSP value instead of complex numerical models. (Edri, et al., 2019) presented a model that does just that, based on simple assumptions for the chemical reactions and energy release considering the detonation and afterburn of four common high explosives (TNT, RDX, PETN and ANFO). They derived predictions for the energy release, the chemical species in post detonation gaseous mixture, and the ratio of specific heats (γ) of the mix assuming a complete reaction up to the consumption of all available oxygen in the chamber. They were then able to use ideal gas assumptions to predict the associated temperature and pressure of the gas. It should be noted that time is not considered here and the reactions are assumed to occur instantaneously and there is no allowance for thermal loss of energy or loss of pressure through venting.

The next section describes the model proposed by Edri. A key feature of the model published by Edri is that it only includes pure explosives without the binders and plasticizers included. Although the binders and plasticisers in typical plastic explosives comprise a small percentage of the mass, they have a very high heat of combustion, typically about 3-4 times the heat of combustion of RDX or PETN. We therefore might expect large differences between predictions based on the pure explosive and the composition of the plasticized explosive. In this model however, there may be differing energy releases due to these additional factors. The description of the Edri method will then be followed by an updated version to further increase its use in real-world applications and include the missing components to make it more realistic and accurate.

In a later section, the validation of the model will be completed in the discussion section by comparing it to experimental results.

4.2 The Edri model

The first stage of the Edri model is to determine the limits of the explosive weight to chamber volume ratio (W/V) of the explosive that allows the detonation products from the explosion to react with the atmospheric oxygen and the amount of excess oxygen in the chamber needed to allow this reaction. From this it can be known the amount of afterburn that can occur from the detonation products. This is done by investigating the detonation reaction of the explosive and determining the amount of fuel in the detonation products that could react further with oxygen. In cases where the ratio of oxygen available to detonation product fuels is not high enough to allow full afterburn, this is taken into account when determining the energy released.

Assuming the atmosphere is made of 21% oxygen and 79% nitrogen, the following Equation 4.1 shows the volume of air per 1 kg of explosive needed for the full combustion of the fuel in the detonation products (Γ_{exp}).

$$\Gamma_{exp} = \frac{MW(O_2) \cdot \beta_{exp} + MW(N_2) \cdot \frac{79}{21} \beta_{exp}}{\rho_{air}} \cdot \frac{1}{MW(exp)}$$

Equation 4.1

Where, β_{exp} is the total number of moles of O_2 required for full combustion of the fuels from a specific explosive, $MW_{(exp)}$ is the molecular weight of the molecule in the brackets next to it in g/mole, ρ_{air} is the ambient air density in kg/m³. The value of the charge weight divided by the chamber volume (W/V) representing the transition point between full and partial combustion is given in Equation 4.2.

$$\left(\frac{W}{V}\right)_{lim} = \frac{1}{\Gamma_{exp}}$$

Equation 4.2

The amount of afterburn energy is then calculated per mole of explosive, as well as the heat of reaction released in the chemical reaction. The heat of reaction and the energy are taken from known values available in the literature and are given below in Table 3 and Table 4 respectively.

Table 3- Heat of reaction of fuel

Fuel	Reaction	Moles of fuel produced per mole of explosive				$\Delta H_r(i)$ [kJ/mole]
		TNT	RDX	PETN	ANFO	
C	$C + O_2 \rightarrow CO_2$	3.5	0	0	0	393.60
CO	$CO + 0.5O_2 \rightarrow CO_2$	3.5	3.0	2.0	0	282.80

Table 4- Detonation reactions and detonation energy

Explosive	Molecular weight g/mole	Chemical reaction	Detonation energy kJ/kg
TNT	227.13	$C_7H_5N_3O_6 \rightarrow 1.5N_2 + 2.5H_2O + 3.5CO + 3.5C$	4560
RDX	222.12	$C_3H_6N_6O_6 \rightarrow 3N_2 + 3H_2O + 3CO$	6178
PETN	316.13	$C_5H_8N_4O_{12} \rightarrow 2N_2 + 4H_2O + 2CO + 3CO_2$	5706
ANFO	84.72	$3NH_4NO_3 + CH_2 \rightarrow 3N_2 + 7H_2O + CO$	2668

From these values, the total energy released by the reaction can be calculated depending on whether the reaction is occurring in a chamber with enough oxygen for full combustion or only partial combustion of the detonation products. If there is a full afterburn, the afterburn energy can be given by Equation 4.3 and if there is partial afterburn, it can be calculated using Equation 4.4.

$$\Delta H_{ab} = \sum_i \frac{n(i) \cdot \Delta H_r(i)}{MW(exp)} \quad , \quad \left(\frac{W}{V}\right) \leq \left(\frac{W}{V}\right)_{lim}$$

Equation 4.3

$$\Delta H_{ab} = \sum_i \frac{n(i) \cdot \Delta H_r(i)}{\left(\frac{W}{V}\right) \cdot \Gamma_{exp} \cdot MW(exp)} \quad , \quad \left(\frac{W}{V}\right) > \left(\frac{W}{V}\right)_{lim}$$

Equation 4.4

Where ΔH_{ab} is the afterburn energy, $n(i)$ is the number of moles per one mole of explosive of each combustible component (Table 4), $\Delta H_r(i)$ is the energy released in the full chemical combustion of each component. Once the afterburn energy has been calculated, the total energy of the reaction is the detonation energy, plus the afterburn energy.

$$\Delta H_{tot} = \Delta H_{det} + \Delta H_{ab}$$

Equation 4.5

The next step is to calculate the number of moles of gas in the chamber post detonation. Assuming full afterburn can take place, the number of moles of gas is equal to the number of moles pre-detonation, plus the number of moles created by the explosion, minus the number of

moles of oxygen used by the detonation products during afterburn. In the case of a partial afterburn, the number of moles post detonation will be the same, but the number of moles used up will be different depending on the extent of the afterburn available. This can be calculated by comparing the moles of fuel left over from the chemical detonation compared to the amount of oxygen available in the chamber atmosphere. If there is enough oxygen to fully react with the remaining fuel, this will allow full afterburn, but if there is less oxygen than needed there will only be partial and the amount of afterburn will rely on the amount of available oxygen.

Next, the temperature needs to be calculated, to do this, the adiabatic flame temperature is calculated using Equation 4.6, which uses specific heat capacity at constant pressure (C_p) of the number of moles and works backwards to calculate what temperature would be achieved from the amount of energy input into the system.

$$\Delta Q = n \int_{T_i}^{T_f} C_p dT$$

Equation 4.6

Where n is the number of moles of gas, T_i is the standard temperature 298K and T_f is the adiabatic flame temperature at constant pressure. C_p is the heat capacity at constant pressure which is a function of temperature. C_p values can be taken from literature. ΔQ is the total heat that is generated by the chemical reaction.

4.3 The Modified Edri Model

The Edri model is based on analytical considerations, assuming that the ideal gas equation of state can properly represent the relation of the volume, pressure, quantity and temperature of the gas mixture in a given state.

The new modified model, developed in this thesis, is based on the model proposed by Edri but also includes the high energy binder/plasticiser. To Calculate the energy from in the system, equation 4.8 uses the specific heat ratios of the gases to calculate energy. This process follows the following steps. (The inclusion of the binder/plasticiser means the inclusion of new processes in steps 2-4 compared to the Edri version.)

Assumptions

- 1) For a given initial volume, temperature and pressure, determine the initial energy of the gas (E_0) from equation 4.7.
- 2) Determine the volumes of each chemical constituent in the post-explosion atmosphere, using standard chemical reaction pathways (Cooper, 2018) as to the reactions occurring at detonation and afterburn stages, shown in Table 5. (This includes binders and plasticizer volume release as the inclusion of this modifies the gasses and volumes produced.)
- 3) From standard relations between γ and T for each molar fraction of the gas, determine the mol-weighted average relation between γ and T for the post-explosion atmosphere. (This is also altered due to the inclusion of the binders and plasticizer as they alter the final atmosphere composition and hence the mol weighted gamma.)
- 4) Determine the energy released by detonation (Equation 4.7) and afterburn (Equation 4.8) from standard values given in the literature. (This is altered from the Edri version as the inclusion of the plasticizer creates a large difference in the energy production due to its large deflagration energy.)
- 5) Iteratively determine values of γ and T from step 3 that satisfy equation 4.8, with $E=E_0+E_1+E_2$
- 6) Determine the absolute pressure P from equation 4.7 and deduct the ambient pressure to find the predicted peak QSP.

$$PV = nRT$$

Equation 2.1

$$E = \frac{1}{\gamma-1}PV = \frac{1}{\gamma-1}nRT$$

Equation 4.7

Where P =Gas pressure (Pa), V =chamber volume (m^3), n =mols of gas in the chamber, R is the gas constant 8.314 J/(mol.K), T =gas temperature (K), E is the thermodynamic energy of the gas (Joules) and γ is the ratio of specific heats or adiabatic constant of the gas mixture.

The chemical process of detonation releases a certain amount of energy, known as detonation energy in units of kJ/kg. Below in Table 5 is a list of the explosives used in this work and their molecular weight, detonation reaction and their detonation energy. (Data for explosives not used in this thesis has been removed for ease of use.)

Table 5 - molecular weight, detonation reaction and detonation energy, adapted from (Edri, 2019).

Explosive	Molecular weight (MW) g/mole	Detonation chemical reaction	Detonation energy kJ/kg
RDX	222.12	$C_3H_6N_6O_6 \rightarrow 3CO + 3H_2O + 3N_2$	6178
PETN	316.13	$C_5H_8N_4O_{12} \rightarrow 2C + 3CO_2 + 4H_2O + 2N_2$	5706

Determining the amount of available oxygen in a confined chamber needs to be known so that the products can be predicted. To do this, the volume of the chamber, V , is multiplied by the percentage of the atmosphere that is oxygen. In this case there is 21% O_2 in the atmosphere. With a volume of 275 L used in these tests that would make a volume of oxygen of 57.75 L of oxygen. Using the ideal gas equation, $PV = nRT$, the number of moles can be determined that would be contained in that volume of air at standard temperature and pressure.

$$PV/RT = n$$

Equation 4.8

$$101300 \times 0.05775 / 8.314 \times 273 = n$$

$$5850 / 2269.722 = 2.577 \text{ mols}$$

This provides an estimate of the amount of free oxygen present to react with the detonation products post detonation. When determining if an explosion will undergo a full reaction over the course of the explosive event depends on the amount of products left over at the end of the detonation and the further reactions that are then possible from the remaining products and the atmospheric components.

To calculate if the oxygen present is enough for a full detonation, the mass and type of explosive must be considered as different explosives provide different products as well as different masses providing different volumes of these products.

For example, if a 1 mole (222.12 g) charge of RDX was to detonate in a sealed chamber, it would generate 3 moles of CO through its reaction process (Cooper, 2018). This carbon monoxide would then be free to react with atmospheric components, namely oxygen to form further products and reactions. In terms of the one mole of RDX detonating it would require an atmospheric oxygen level of 1.5 moles to fully react with the 3 moles of CO, creating 3 moles of CO_2 which is the more stable compound. For there to be enough oxygen in the environment to allow this full reaction to occur, a volume of 171.4 L is required, as each L provides 0.875 moles of O_2 .

This is the case for when there is a pure explosive being considered, however when explosives are manufactured for use, they are often mixed with binders and plasticizers to create a more favorable explosive for its applications. In this work the explosives used are PE4 and PE10 which are made up of a majority of RDX and PETN respectively, but also contain a mineral oil as a plasticizer/binder. This mineral oil also contributes during the reaction process and releases products. The reaction and contribution of this mineral oil is compared to those of the explosive components in Table 6.

Table 6 - Explosives and corresponding heat of detonation, heat of afterburn and afterburn reaction.

Material	Detonation reaction	Heat of detonation (kJ/kg)	Afterburn reaction	Heat of afterburn (kJ/kg)
RDX	$C_3H_6N_6O_6 \rightarrow 3CO + 3H_2O + 3N_2$	6178	$3CO + 1.5O_2 \rightarrow 3CO_2$	3820
PETN	$C_5H_8N_4O_{12} \rightarrow 2C + 3CO_2 + 4H_2O + 2N_2$	5706	$2CO + O_2 \rightarrow 2CO_2$	1790
Mineral Oil (EURENCO, 2014)	N/A	N/A	$C_{25}H_{52} + 38O_2 \rightarrow 25CO_2 + 26H_2O$	42000

The composition of the two explosives used in this study differ from each other and so the composition of each is given below in Table 7.

Table 7 - Explosive compositions.

Component	Quantity	
	PE4	PE10
RDX	87%	N/A
PETN	N/A	86%
Mineral Oil	13%	14%
Taggants	Trace	Trace

4.4 Degrees of Freedom and Internal Energy of Gases

In ideal gas theory, the pressure exerted by a gas on the walls of a confining chamber is related to the momentum imparted to the walls by the elastic collision of the particles with the walls. A gas with a higher average particle translational velocity will impart more momentum onto the walls, and hence produce a higher pressure. However, the higher translational velocity also manifests itself as a higher temperature, and hence there is a direct relationship between pressure and temperature, given by the Ideal gas Law as in Equation 2.1. It is assumed that the collision of particles into the chamber walls is an adiabatic process, and so the collisions are perfectly elastic, in practice this may not be strictly correct, and this issue will be addressed in later sections.

The degrees of freedom of a molecule are a descriptor of the space that molecule can move in. This is important in gas thermodynamics because of the principle of equipartition of energy which states that the total kinetic energy of a gas is equally split between all the available degrees of freedom (Rayleigh, 1900). With each degree of freedom having a kinetic energy equal to $\frac{1}{2}PV = \frac{1}{2}nRT$.

Simple monatomic gases, such as argon which have one atom of the same species, have three translational degrees of freedom (parallel to three axes). The atoms are of such small physical scale that any energy they may have through rotation is assumed to be negligible, that is, the atoms are assumed to occupy one dimensional points in space. The total energy of a monatomic gas is therefore $\frac{3}{2}PV = \frac{3}{2}nRT$.

For gas molecules with diatomic structure, the situation is different, as there are rotational degrees of freedom to be considered. For example, a simple diatomic gas such as O_2 or N_2 has two rotational degrees of freedom, associated with the rotation of the molecules about axes perpendicular to the intramolecular bond. There is no rotational degree of freedom with an axis along the intramolecular bond as there is no second moment of mass about this axis as the atoms are assumed to be infinitesimal points. Therefore, as a first approximation, diatomic gases have total energy of $\frac{5}{2}PV = \frac{5}{2}nRT$. For still more structurally complex gas molecules, such as CO_2 or gaseous H_2O , there are more rotational degrees of freedom and generally, the energy of a gas is $\frac{f}{2}PV = \frac{f}{2}nRT$, where f is the number of degrees of freedom.

For any specific gas, the ratio C_p/C_v , is defined as the heat capacity ratio γ as described in the literature review (Waples, 2004). This is related to the degrees of freedom of the gas f , by $\gamma = 1 + 2/f$. Thus, the energy of a gas can be stated as $E = PV/(\gamma - 1) = nRT/(\gamma - 1)$.

The above description holds reasonably well for gases at room temperature: γ for monatomic gasses is $1 + 2/3 = 1.6666$, whilst that for diatomic gases is $1 + 2/5 = 1.4$. For gases which are not monatomic, another effect becomes important at higher temperatures. Here, the effect of vibration of the atoms along the axis of each intramolecular bond becomes

significant. The energy contained in this vibration is small at low temperatures but becomes higher at higher temperatures. The effect of this is to introduce a temperature-dependent partial degree of freedom, which generally means that f increases with temperature and hence γ decreases. At very high temperatures, this vibration may be sufficiently energetic to break the intramolecular bonds – this is generally at several thousand kelvin and will be ignored here. However, the effect of the temperature dependence of γ is important to the analysis in this thesis and must be taken into account for some calculations in the thermochemical model. Fortunately, this is well understood and definitive empirical data exists for most common gases and is referenced where used.

In an atmosphere comprising a mixture of gases at a given temperature, a weighted average of the value of γ can be defined by determining the value of γ for each constituent gas, then weighting by the number of moles of that gas compared to the total number of moles of gas. If, say, a volume V of air at pressure P and temperature T , with n total mols of air, given by $n = PV/RT$. Assuming the air comprises 78.08% N_2 , 20.95% O_2 , 0.93% Ar and 0.04% CO_2 , it can therefore calculate the total moles of each constituent gas and determine the mol-weighted γ_{MW0} as:

$$\gamma_{MW0} = 0.7808\gamma_{N_2} + 0.2095\gamma_{O_2} + 0.0093\gamma_{Ar} + 0.0004\gamma_{CO_2}$$

The energy of that gas can then be calculated using:

$$E_0 = PV/(\gamma_{MW0} - 1) = nRT/(\gamma_{MW0} - 1)$$

Equation 4.9

After a confined detonation in this atmosphere, assuming it's a known chemical reaction which has occurred, the moles of gas can be recalculated for each gas. There are also standard book figures for the energy released by the different chemical reactions associated with detonation and secondary deflagration of standard explosives and binders, and we assume the total post-event energy of the gas is $E_1 = E_0 + \Delta E$, where ΔE is the energy added to the confined atmosphere by the explosion. Hence now, the energy equation becomes:

$$E_1 = PV/(\gamma_{MW1} - 1) = nRT/(\gamma_{MW1} - 1)$$

Equation 4.10

Where γ_{MW1} is the mol-weighted heat capacity ratio of the new gas mixture at the post-explosion temperature.

Again, the value of γ_{MW1} can be determined for any value of T , but in the absence of direct measurement, this value is an unknown. However, by an iterative approach, a value of T can be found, and hence a value of γ_{MW1} that satisfies the energy equation. $E_1 = nRT/(\gamma_{MW1} - 1)$. It can then be determined that the absolute pressure, P from either. $E_1 = PV/(\gamma_{MW1} - 1)$ or equivalently, $PV = nRT$. This is further explained in the worked examples later in this section.

Note that this model is time independent, so there is no manner in which to alter time dependant phenomena such as energy loss of the system to the chamber walls or through venting. In principle having calculated the peak QSP this way, venting could be predicted by using this as an input parameter in the Anderson/baker method of prediction through empirical equations.

4.5 Worked Examples

The following section provides example calculations for the generation of pressure and temperature values for the confined explosion of PE10. It goes through a standard experiment in a nitrogen atmosphere, followed by an example in an air atmosphere.

Before the results including additional fuel oils are considered, Figure 33 and Figure 34 shows a plot from (Edri I.E., 2019) where the data from the thermochemical model used in this work without binder/plasticiser has been plotted over the top. This shows that the resulting values match well as they are the same method before the additional energy is added for the fuel oils.

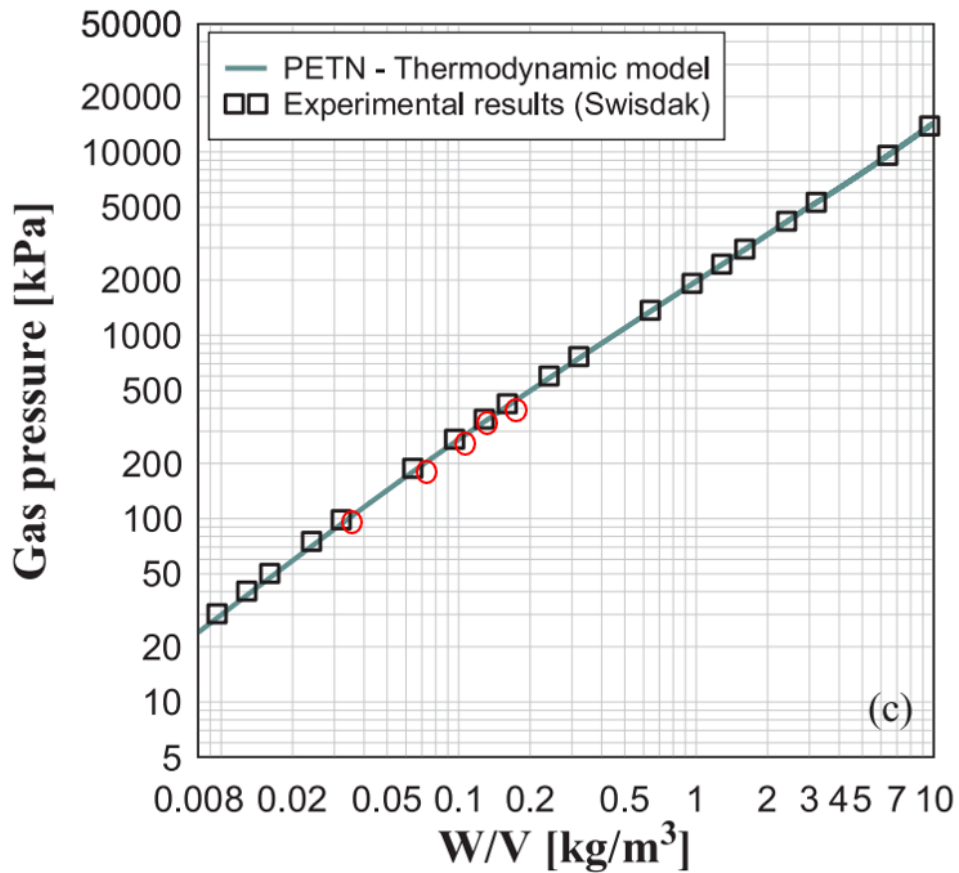


Figure 33 - PETN thermodynamic model comparison of (Edri I.E., 2019) and the thermochemical model used in this work.

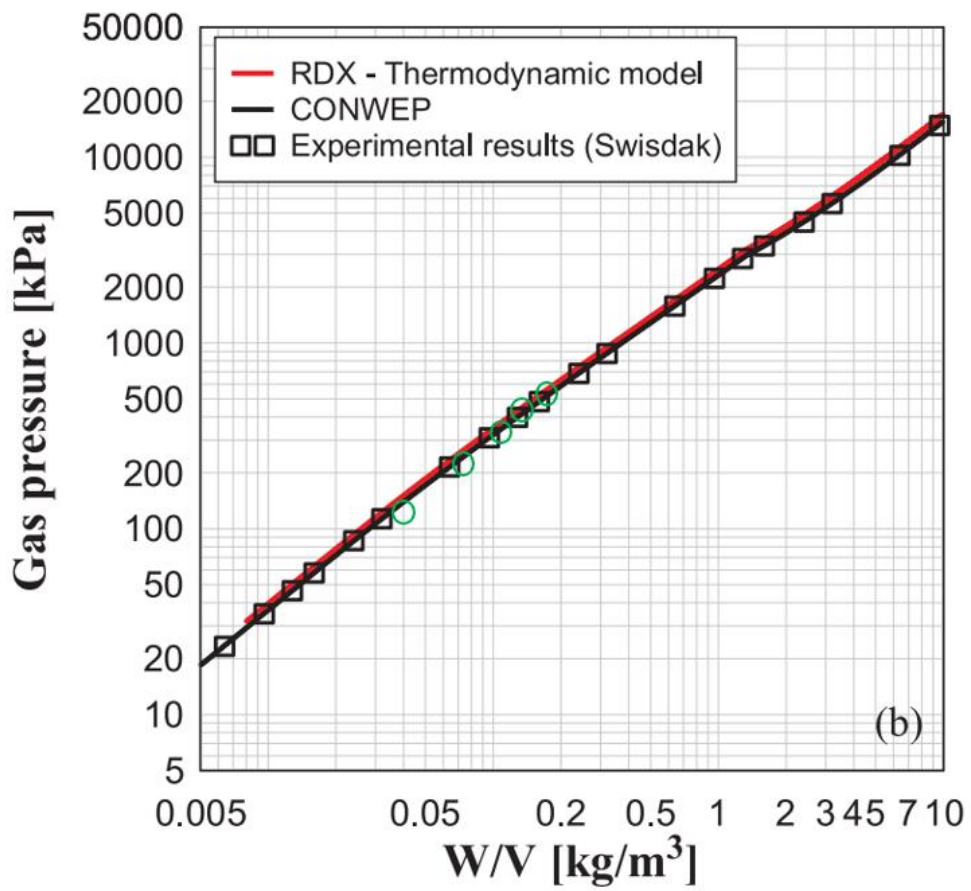


Figure 34 -RDX thermodynamic model comparison of (Edri I.E., 2019) and the thermochemical model used in this work.

4.5.1 Nitrogen Atmosphere Example

This method ignores the effect of afterburn on the system as there is no atmospheric oxygen for the excess fuels to react with and so is a simpler calculation and hence is given as the first example. A charge of 30 g PE4 in a 275 L chamber in dry air and initial conditions of $T = 288$ K and $P = 100$ kPa, $\gamma = 1.401$. Assuming the constituents of air are 78.08% N_2 , 20.95% O_2 , 0.93% Ar and 0.04% CO_2 . Values for these examples were taken from average temperature and atmospheric pressure of the testing location during testing.

Step 1

Using Equation 2.1, calculate the initial moles of gas in the chamber. For this example, this provides the following calculation.

$$n = 100000 * \frac{0.275}{(288 * 8.314)} = 11.48 \text{ mols}$$

Next calculate the initial energy of the chamber by using the specific heat capacity tables and Equation 4.9. For this example, the equation would become:

$$E_0 = \frac{100 * 0.275}{(1.444 - 1)} = 61.9 \text{ kJ}$$

Step 2

Using the molecular mass of RDX (222.1 g/mol) and mineral oil (352.7 g/mol) calculated from the periodic table, calculate the mass of each constituent in the explosive. In this case for the 30 g of PE4 in equates to:

$$30 \times 0.87 = 26.1$$

$$30 \times 0.13 = 3.9$$

Once the masses have been calculated, the number of moles of each substance can also be calculated using the molecular weights as shown below.

$$n = \frac{26.1}{222.1} = 0.1175$$

$$n = \frac{3.9}{352.7} = 0.0111$$

Using these initial moles and the reaction equations, calculate the number of moles of the products in the gas post detonation assuming no afterburn reaction occurs. Calculate the constituent moles of each substance this way so that a mole fraction can be determined for each

constituent by dividing the number of moles of constituent by the total moles in the system and multiplying by 100.



This provides the values given in Table 8.

Table 8 - Chamber atmosphere pre and post detonation with a nitrogen atmosphere

	N ₂	O ₂	Ar	CO	H ₂ O	C ₂ H ₂	Total
Pre-explosion (mols)	11.48	0	0	0	0	0	11.48
Post-explosion (mols)	11.8325	0	0	0.3525	0.3525	0.011	12.55
Post-explosion (mol fraction - %)	94.28	0	0	2.81	2.81	0.08	100

Step 3

To calculate the molar weighted specific heat capacity of the gas, the values from Table 8 can be used with the specific heat capacity values at different temperatures provided by online sources (The Engineering Toolbox, 2024). This is temperature dependant and changes as the temperature increases or decreases. An example of a specific heat capacity table is given in Table 9. These tables were then used to generate a curve fit so that the ratios can be calculated for any temperature within that range.

Table 9 - Heat capacity ratios and gamma values for different temperatures of H₂O between 750 K and 2000 K. (The Engineering Toolbox, 2024))

T(K)	Cp(kJ/(kg.K))	Cv(kJ/(kg.K))	Gamma
750	2.113	1.651496	1.279446
800	2.147	1.685496	1.273809
850	2.182	1.720496	1.268239
900	2.217	1.755496	1.262891
950	2.252	1.790496	1.257752
1000	2.288	1.826496	1.252672
1050	2.323	1.861496	1.247921
1100	2.358	1.896496	1.243346
1150	2.392	1.930496	1.23906
1200	2.425	1.963496	1.235042
1250	2.458	1.996496	1.231157
1300	2.49	2.028496	1.227511
1350	2.521	2.059496	1.224086
1400	2.552	2.090496	1.220763
1500	2.609	2.147496	1.214903
1600	2.662	2.200496	1.209727
1700	2.711	2.249496	1.205159
1800	2.756	2.294496	1.201135
1900	2.798	2.336496	1.19752
2000	2.836	2.374496	1.194359

These values are used in a later step when solving to determine the temperature of the gas post detonation.

Step 4

To calculate the detonation energy of the constituent parts of the explosive, the energy per kilogram is multiplied by the mass of the explosive in kg.

$$E = E_{kg} \times M$$

Where E is the energy in kJ, E_{kg} is the energy per kg of substance and M is the mass of the substance.

When determining the detonation energy, the only aspect is from the explosive in the case of PE4 and can be calculated with Equation 4.13. In the case of this example the following values are determined.

$$E_{det} = \frac{26.1}{1000} \times 6178 = 161.25 \text{ kJ}$$

This gives the total energy in the system post detonation when added to the initial energy (61.9 kJ), giving a total energy of 223.15 kJ.

Step 5

Now that the energy of the system post detonation has been calculated, this can be used along with Equation 4.7 to determine the temperature that this process would cause. This is done through inputting a temperature into the equation, calculating the mol weighted gamma value at that temperature and then checking to determine what energy output this provides. This is done iteratively from a chosen value until the energy value is correct. For this example, an initial value of 1000 K is chosen and the mol weighted gamma values are provided in Table 10.

$$E = \frac{1}{\gamma - 1} \times n \times R \times T$$

Equation 4.7

Table 10 – Iterative solving of temperature values.

Temperature Choice / K	Weighted γ	Resulting energy / kJ
1000	1.34	306.9
750	1.36	217.4
800	1.36	231.9
769.6	1.36	223.1

This results in a weighted gamma of 1.36 and an energy value of 223.1 kJ. (This could be iterated further to find the exact value but for simplicity, it has been left as a close value.)

Step 6

Using the temperature value found in step 5 and the ideal gas equation (Equation 2.1), the pressure of the system can then be calculated. For this example, it is shown below.

$$P = \frac{12.55 \times 8.314 \times 769.6}{0.275} = 292 \text{ kPa}$$

This is the total pressure of the system, so the initial pressure needs to be subtracted to find the quasi-static pressure. This provides a total of 192 kPa QSP for a 30 g PE4 charge in a 275 L chamber full of nitrogen.

4.5.2 Air Atmosphere Adjustment Example

This method includes the afterburn energy generated by the oxygen present in the chamber external to the charge. Similar to the first example, a charge of 30 g PE4 in a 275 L chamber in dry air and initial conditions of $T = 288 \text{ K}$ and $P = 100 \text{ kPa}$, $\gamma = 1.401$. Assuming the constituents of air are 78.08% N_2 , 20.95% O_2 , 0.93% Ar and 0.04% CO_2 .

Step 1

Using Equation 2.1, calculate the initial moles of gas in the chamber. For this example, this provides the following calculation.

$$n = \frac{100000 \times 0.275}{(288 * 8.314)} = 11.48 \text{ mols}$$

Next calculate the initial energy of the chamber by using the specific heat capacity tables and Equation 4.9. For this example, the equation would become:

$$E_0 = \frac{100 \times 0.275}{(1.401 - 1)} = 68.58 \text{ kJ}$$

Step 2

Using the molecular mass of RDX (222.1 g/mol) and mineral oil (352.7 g/mol) calculated from the periodic table, calculate the mass of each constituent in the explosive. In this case for the 30 g of PE4 in equates to:

$$30 \times 0.87 = 26.1$$

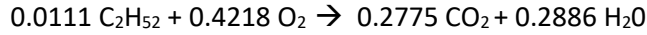
$$30 \times 0.13 = 3.9$$

Once the masses have been calculated, the number of moles of each substance can also be calculated using the molecular weights as shown below.

$$n = \frac{26.1}{222.1} = 0.1175$$

$$n = \frac{3.9}{352.7} = 0.0111$$

Using these initial moles and the reaction equations, calculate the number of moles of the products in the gas post detonation.



The amount of oxygen extracted from the atmosphere can then be calculated using these equations by fully oxidising the constituents that need further oxidation such as CO. Since 0.3525 moles of CO are left over, half as many moles of oxygen will be needed to fully oxidise it, taking out 0.17625 moles of O₂. The binder takes in oxygen in its process also from the atmosphere as noted by the 0.4218 moles on the left side of the arrow. This means that the total oxygen taken out of the atmosphere would equate to the sum of those values, 0.59805 moles.

Calculate the constituent moles of each substance this way so that a mole fraction can be determined for each constituent by dividing the number of moles of constituent by the total moles in the system and multiplying by 100. The values of these are shown in Table 11.

Table 11 – Chamber atmosphere pre and post detonation in air.

	N ₂	O ₂	Ar	CO ₂	H ₂ O	Total
Pre-explosion (mols)	8.964	2.405	0.1067	0.0046	0	11.48
Post-explosion (mols)	9.3165	1.81	0.1067	0.6346	0.6411	12.51
Post-explosion (mol fraction - %)	74.47	14.47	0.85	5.07	5.12	100

Step 3

To calculate the molar weighted specific heat capacity of the gas, the values from Table 11 can be used with the specific heat capacity values at different temperatures provided by online sources ((The Engineering Toolbox, 2024)). This is temperature dependant and changes as the temperature increases or decreases. An example of a specific heat capacity table is given in Table 9. These tables were then used to generate a curve fit so that the ratios can be calculated for any temperature within that range.

These values are used in a later step when solving to determine the temperature of the gas post detonation.

Step 4

To calculate the detonation energy and the afterburn energy of the constituent parts of the explosive, the energy per kilogram is multiplied by the mass of the explosive in kg.

$$E = E_{kg} \times M$$

Where E is the energy in kJ, E_{kg} is the energy per kg of substance and M is the mass of the substance.

When determining the detonation energy, the only aspect is from the explosive in the case of PE4, but when considering the deflagration energy there is a constituent from both the explosive and the binder/plasticiser so both need to be added together. In the case of this example, the following values are determined.

$$E_{det} = \frac{26.1}{1000} \times 6178 = 161.25 \text{ kJ}$$

$$E_{def} = \left(\frac{3.9}{1000} \times 42000 \right) + \left(\frac{26.1}{1000} \times 3820 \right) = 263.50 \text{ kJ}$$

This allows the total energy in the system to be determined by adding these values together, as well as the initial energy in the system (68.58 kJ), giving a value of 493.33 kJ.

Step 5

Now that the energy of the system post detonation has been calculated, this can be used along with Equation 4.7 to determine the temperature that this process would cause. This is done through inputting a temperature into the equation, calculating the mol weighted gamma value at that temperature and then checking to determine what energy output this provides. This is done iteratively from a chosen value until the energy value is correct. For this example, an initial value of 1000 K is chosen and the mol weighted gamma values are provided in Table 12.

$$E = \frac{1}{\gamma - 1} \times n \times R \times T$$

Equation 4.7

Table 12- Chamber atmosphere pre and post detonation in nitrogen.

Component	N ₂	O ₂	CO ₂	H ₂ O
γ at 1000 K	1.341	1.31	1.18	1.25
Molar ratio of gas	0.7467	0.1464	0.0489	0.0494
Weighted γ	1.001325	0.191784	0.172752	0.06175

The sum of these weighted gamma values is equal to 1.4276. inputting these values into Equation 4.7 gives:

$$E = \frac{1}{1.4276 - 1} \times 12.51 \times 8.314 \times 1000 = 243 \text{ kJ}$$

This value is lower than the target energy, which means the temperature chosen is too low. Therefore, a higher temperature is chosen to increase the energy and the equation is solved again for the new temperature and mole weighted gamma. A small series of chosen temperatures and output energies are given in Table 13 to show this iterative solving.

Table 13 – Iteration of temperature values for air test.

Temperature / K	Choice	Weighted γ	Resulting energy / kJ
1000		1.4276	242
1500		1.2869	544
1300		1.2953	458
1438		1.303	494

This results in a weighted gamma of 1.303 and an energy value of 494 kJ. (This could be iterated further to find the exact value but for simplicity, it has been left as a close value.)

Step 6

Using the temperature value found in step 5 and the ideal gas equation (Equation 2.1), the pressure of the system can then be calculated. For this example, it is shown below.

$$P = \frac{12.51 \times 8.314 \times 1446}{0.275} = 547 \text{ kPa}$$

This is the total pressure of the system so the initial pressure needs to be subtracted to find the quasi-static pressure. This provides a total of 447 kPa QSP for a 30 g PE4 charge in a 275 L chamber full of air.

This method provides a computationally simple way to predict the maximum QSP pressures from an explosive charge which can be automated to provide data dependant on inputs of explosive type, charge mass, chamber volume and atmospheric conditions.

4.5.4 Comparisons of pure explosive to including a binder/plasticiser.

With results now established for plasticised explosives, the effect of the reaction of the fuel-rich plasticiser can be appraised by comparing the predicted peak QSP and temperature from the plasticised explosive with the prediction of the values for the same masses of pure explosive. This shows the difference between the new method to the (Edri I.E., 2019) model that does not include the plasticisers and binders.

Shown in Table 14 below is the results of this comparison for temperature and pressures of PETN compared to PE10. This shows an increase in pressure of around 50-60 % broadly speaking and an increase in temperature of 20-35 % in terms of temperature. This shows that including these additional components into the model, provides much higher pressures and temperatures than without, which is why it is important to have this capability for prediction of pressures from explosives.

This comparison is a view into a comparison between this new method and the one proposed in the Edri paper that this work was based on. Though it was a good starting point, the difference of the inclusion of the binder and plasticiser shows a large pressure ratio difference, showing the importance of the ability to include this binder/plasticiser in the calculator.

Table 14 - Pressure and Temperature ratios comparison at different charge mass to volume ratios for pure explosives and those including binders and plasticisers.

W/V ratio	Pressure ratio	Temperature ratio
0.02	1.59	1.19
0.05	1.53	1.29
0.1	1.53	1.35
0.2	1.53	1.35

In summary of this section so far, a thermochemical model was created that builds upon an existing model to include the effects of binders and plasticisers on the quasi-static pressure generated by an explosive. In this work PE4 and PE10 have been modelled to show two explosives made from different explosive compounds, RDX and PETN. The difference between the model without these additional plasticisers and binders are notable due to the large increase in pressure due to these additives.

4.5.5 Sensitivity Analysis

To understand the sensitivity of the model to alterations of input parameters, a series of percentage changes were made to each of the inputs, charge mass, chamber volume and initial temperature. These were changed in increments of 1%, 2%, 4% and 8%. To make these alterations, the thermochemical model inputs were changed by the desired percentage for each input separately. The predicted QSP was then taken as the output of these changes and recorded in a spreadsheet. Once this had been done for each percentage change, the predicted QSP was compared to the original QSP prediction, giving a percentage difference in output using Equation 4.14.

$$P_{QSP} - 0_{QSP}$$

Equation 4.14

Where P_{QSP} is the predicted QSP and 0_{QSP} is the QSP at 0% change.

Once these percentage difference values had been obtained for each percentage change, this value was divided by the percentage change to give a normalised change in value. This was again done for each percentage change shown in Equation 4.15. One set of these results are then shown in Table 15, Table 16 and Table 17 below for a 40 g PE4 charge.

$$\frac{P_{QSP}}{\%C}$$

Equation 4.15

Where P_{QSP} is the predicted QSP and %C is the percentage change.

Table 15 – Percentage change of mass and normalised change for 40 g of PE4.

% Mass change	Mass	QSP	% change	Normalised	Gamma
0	40	574.13	0	0	1.29
1	40.4	579.12	0.87	0.87	1.29
2	40.8	584.1	1.74	0.87	1.29
4	41.6	594.03	3.47	0.87	1.29
8	43.2	613.83	6.91	0.86	1.29

Table 16 – Percentage change of volume and normalised change for 40 g of PE4.

% volume change	Volume	QSP	% change	Normalised	Gamma
0	275	574.13	0	0	1.29
1	277.75	569.19	0.86	0.86	1.29
2	280.5	564.33	1.71	0.85	1.29
4	286	554.87	3.35	0.84	1.29
8	297	536.92	6.48	0.81	1.3

Table 17 – Percentage change of temperature and normalised change for 40 g of PE4.

% Temp change	Initial Temperature	QSP	% change	Normalised	Gamma
0	280	574.13	0	0	1.29
1	282.8	573.01	0.2	0.195	1.29
2	285.6	571.90	0.39	0.194	1.29
4	291.2	569.72	0.77	0.192	1.29
8	302.4	565.53	1.5	0.187	1.29

Also noted in the table is the mol weighted gamma of the system during these calculations. This is taken from the calculations done in the model to provide an understanding of the effect the small changes are having on the system in terms of the ratio of specific heats in the system.

As can be seen from Table 15, Table 16 and Table 17, the normalised percentage change is relatively constant, with a slow decrease with the increase in percentage change. This shows that as the percentage change increases, the influence of the changes in input becomes lessened. This means that the influence a change in mass a linear response in the output.

This process was completed for each variable (mass, volume and temperature) for each mass of explosive, type of explosive and atmosphere. The tables for these results can be found in Appendix 2. From these additional values, it can be seen that the normalised change in the temperature gives the lowest value around 0.19 compared to the mass and volume which are closer to 0.8-0.9. This shows that the least sensitive variable is the initial temperature of the chamber and the mass and chamber volume are very similar in terms of influence.

These normalised changes were then plotted against the percentage change to give a visual representation of the sensitivity of each process. The graphs for PE4 are shown in Figure 35 Figure 35 - Percentage change vs normalised change for mass of PE4, Figure 36 and Figure 37.

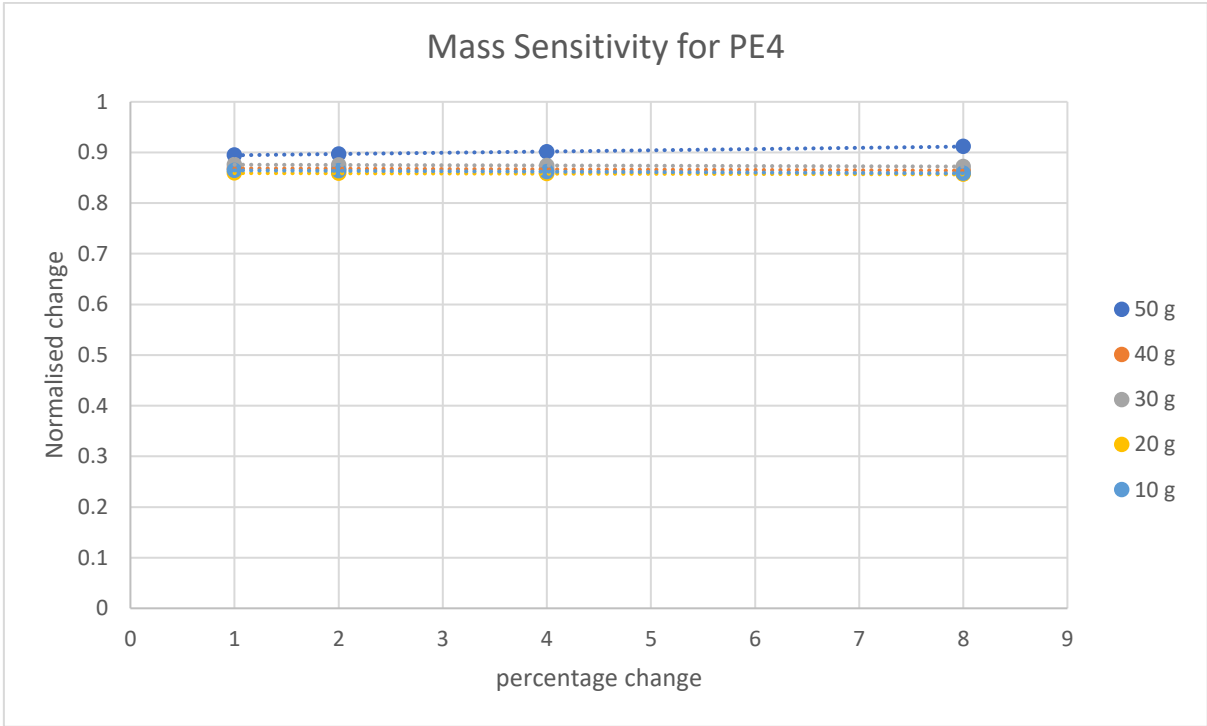


Figure 35 - Percentage change vs normalised change for mass of PE4

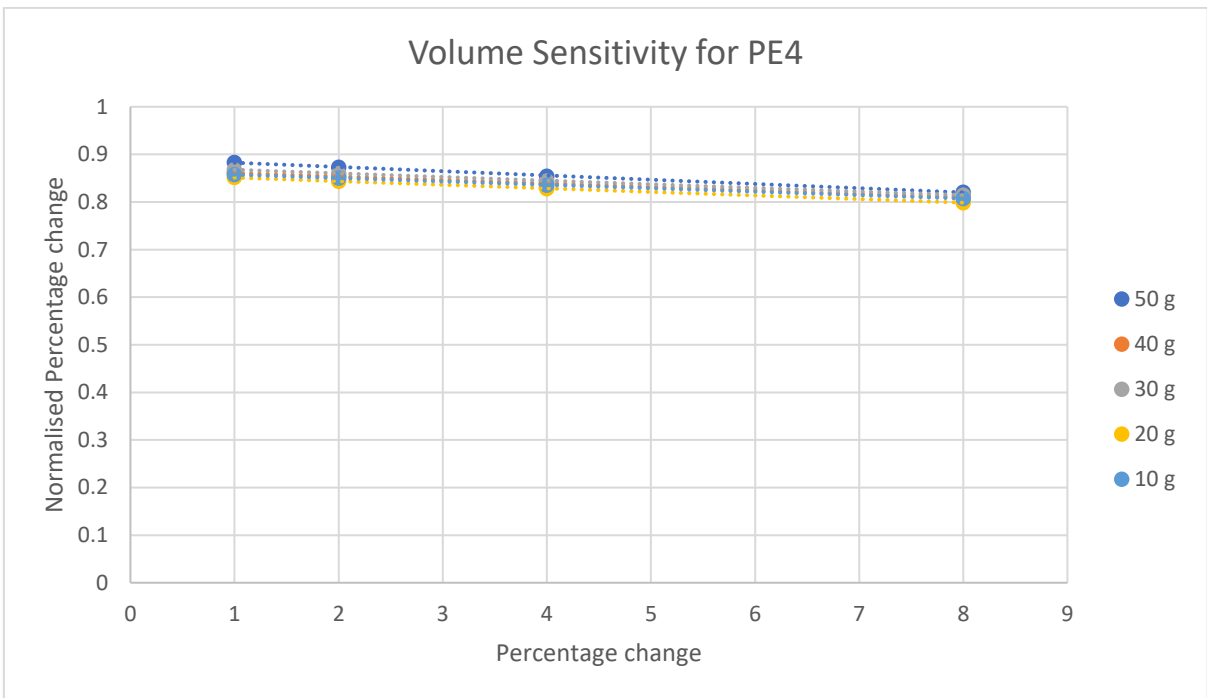


Figure 36 - Percentage change vs normalised change for Volume of PE4.

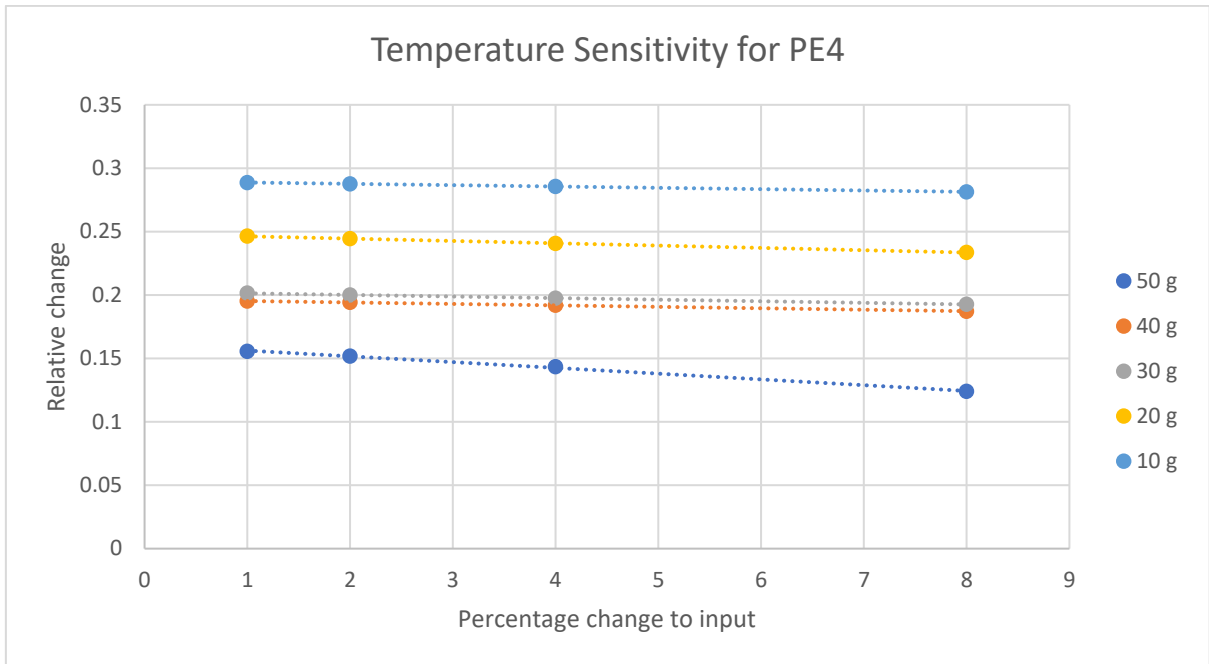


Figure 37 - Percentage change vs normalised change for Temperature of PE4

From these graphs it can be shown that the initial temperature has the smallest overall impact on the predicted QSP as the relative change is much lower than for mass and volume. This could be due to difference in initial and final temperature being high, causing a small change in initial temperature to not cause a significant change in the overall temperature post-test, causing values to be close to the unmodified QSP.

Also notable for the initial temperature, the sensitivity increases the smaller the charge gets, however for the mass and volume it is not the case. When looking at the mass and volume though the sensitivity is similar for each change, they do not follow an order from smallest charge to largest, they are instead “random”. This shows that a slight variation in initial temperature would not cause a significant effect on the quasi-static pressure of the system unless the change was of a very large magnitude that would not occur from weather changes at the test site.

This increases the confidence in the model’s accuracy, since the changes in the model don’t cause a percentage change of the output higher than the percentage change to the input. It also shows that the increase in the predicted QSP is impacted by the changes in the gamma of the system. As the mass and initial temperature are increased, the gamma also increases due to the increase in energy of the system, however because increasing the volume of the chamber would cause a reduction in the energy of the system, the gamma also reduces.

Chapter 5- Experimental Results

5.1 Test Plan

This chapter presents experimental data of confined explosions to investigate the consistency of the test method that has been developed as well as probing the mechanisms of afterburn that occur during a confined explosion. First, the preliminary tests were carried out investigating the effects of thermal stability of the gauges as well as the bolt mounting system as well as the effect of charge shape. The main series of tests then covers the investigation into the effect of afterburn on the QSP. This series of tests includes test alterations such as explosive type, charge size and atmosphere. The full list of tests can be found in Table 18.

A total of 26 tests plus 3 preliminary tests were conducted for this thesis, these tests consist of a mixture of explosives, PE4 and PE10 as well as a mixture of charge masses from 10 g to 50 g, a mixture of atmospheres including air, nitrogen and argon. Two of the preliminary tests were conducted with explosives not available for publishing so have been given a composition of X and a mass of Y for this thesis.

Table 18 - Test summary (Tests P1 and P2 were part of a different study so details on charge type and mass cannot be included so have been denoted as X and Y.)

Test number	Explosive Type	Shape	Mass(g)	Atmosphere	Additions
1	PE4	sphere	50	Air	n/a
2	PE4	sphere	50	Air	n/a
3	PE4	sphere	50	Air	n/a
4	PE4	sphere	50	Air	n/a
5	PE4	sphere	50	Nitrogen	n/a
6	PE4	cylinder 2:1	50	Nitrogen	n/a
7	PE4	cylinder 2:1	50	Air	n/a
8	PE4	sphere	30	Air	n/a
9	PE10	sphere	30	Air	n/a
10	PE10	sphere	30	Nitrogen	n/a
11	PE4	sphere	50	Argon	n/a
12	PE4	sphere	30	Argon	n/a
13	PE4	sphere	50	Air	n/a
14	PE10	sphere	10	Air	n/a
15	PE10	sphere	20	Air	n/a
16	PE10	sphere	30	Air	n/a
17	PE10	sphere	40	Air	n/a
18	PE10	sphere	40	Air	n/a
19	PE10	sphere	30	Air	n/a
20	PE10	sphere	30	Air	n/a
21	PE10	sphere	30	Air	n/a
22	PE10	sphere	30	Argon	n/a
23	PE10	sphere	30	Argon	n/a
24	PE10	sphere	30	Argon	n/a
25	PE10	sphere	30	Nitrogen	n/a
26	PE10	sphere	30	Nitrogen	n/a
P1	X	sphere	Y	Air	Greased bolt
P2	X	sphere	Y	Air	Greased bolt
P3	PE4	sphere	50	Air	Gauge directly mounted

5.2 Thermal Stability

To make sure that these tests would be reliable, the method for recording data must be consistent and reliable. The pressure gauges used for this testing are noted to have some possible temperature drift when they experience high temperatures, and this can be seen when a gauge is kept under constant heat for some time. To make sure this would not affect the results for this testing the following was done.

When designing the mounting mechanism to ensure peak QSP pressures are obtained whilst protecting the gauges from becoming damaged over time, it was important to undertake some initial trials to ensure the test set up would allow the collection of the data necessary. To do this a short series of tests was conducted with pressure gauges protected by a grease and those that were unprotected. The grease provides a layer of insulation from the high temperatures of the explosion but still passes the pressure on to the pressure gauge as it is a compressible medium. A diagram of the grease location in a test is shown in Figure 29 alongside the non-greased bolt for comparison.

Two of the tests in this section were part of an external project so the specifics of the charge details cannot be used as they are not sanctioned for release, but the data from the tests can be used as a comparison in this case as a qualitative method of discussion and they have been labelled as Test P1 and Test P2.

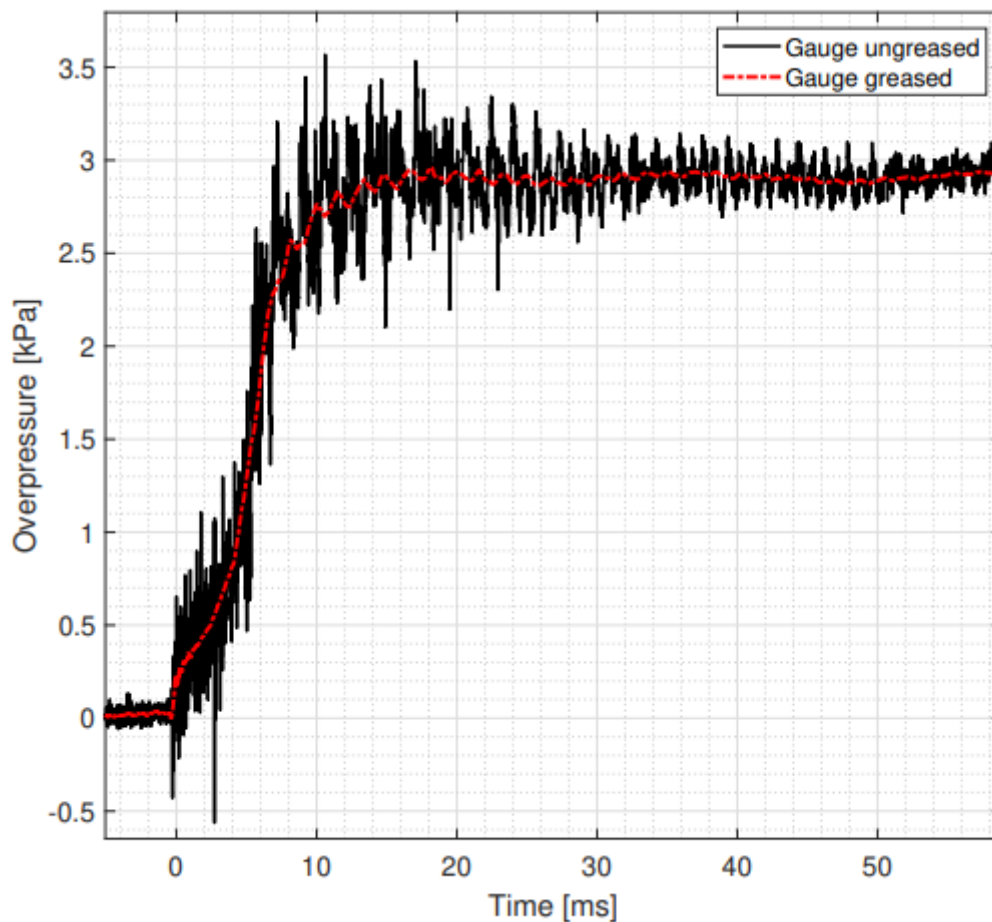


Figure 38 - Raw pressure-time history plot for test P1. The 35-bar gauge was mounted with a lithium grease filled reservoir and a 17-bar, with a standard air-filled reservoir.

Shown in Figure 38, are two raw pressure-time histories recorded using a 17-bar and a 35-bar gauge taken from the same test, in a confined chamber of volume 275 L. In this test the 35-bar gauge was filled with lithium grease near the end of the bolt as the environmental protection for the gauge.

When considering the difference in the signal from the 17-bar gauge compared to the 35-bar gauge it should be noted that generally a 35-bar gauge experiencing the same pressure as a 17-bar gauge would have lower magnitudes of voltage rise since it has a higher range and hence a larger signal to noise ratio. However, this wouldn't be the cause of the relatively large difference in the signals. In these tests the large difference in the shock structure of the signals is due to the reduction in sharp peaks produced by the insulation of the grease. Despite this dampening of the peak shocks, the results show that the grease protection does not make a difference to the overall QSP of the system, meaning it is not necessary to use in further testing as it only reduces signal and the gauge being in the bolt doesn't experience thermal drift.

Because the pressure traces are at a same magnitude throughout the signal that shows that there is no downside to not using the lithium grease as it allows better resolution of the shocks and still shows the same QSP measurements as when it is insulated.

Another trial was conducted to investigate the difference between having a gauge directly in the side of the chamber, unshielded from detonation products and pressure waves, compared to a gauge in the bolt to provide shielding Figure 39. This was to test the theory in the work of (Walter, 2004) where the use of a chamber to separate the pressure gauge from the fireball interfering with pressure measurements was used. The results from this test are shown in Figure 40. By comparing the pressure traces from the two gauges it shows that the gauge in direct line of the fireball and shock wave shows a higher increase over the first peak or two, but the following peaks follow a similar pattern and the long term QSP is consistent between the two gauges. This allows confidence in the recording method used for these tests to ensure accurate data and allows a robust testing regime without risking equipment in the process.

Since the gauges are not orthogonal to the shock wave it will not be a reflected pressure, or an incident pressure because it has a boundary to the edge of the pressure gauge since it fits into a pre-made hole, this means that the clearing and angle of incidence will not be the same as on a true reflected surface or a free field shock. Once the initial shock has passed however, and the pressure becomes QSP, meaning there will be solely outwards force acting on the pipe so it will be more like a reflected pressure.

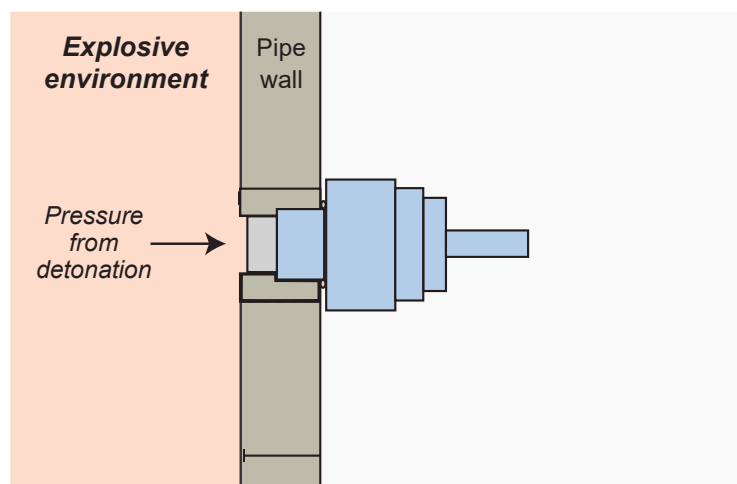


Figure 39 - Gauge bolt located inside of the chamber with no separating chamber.

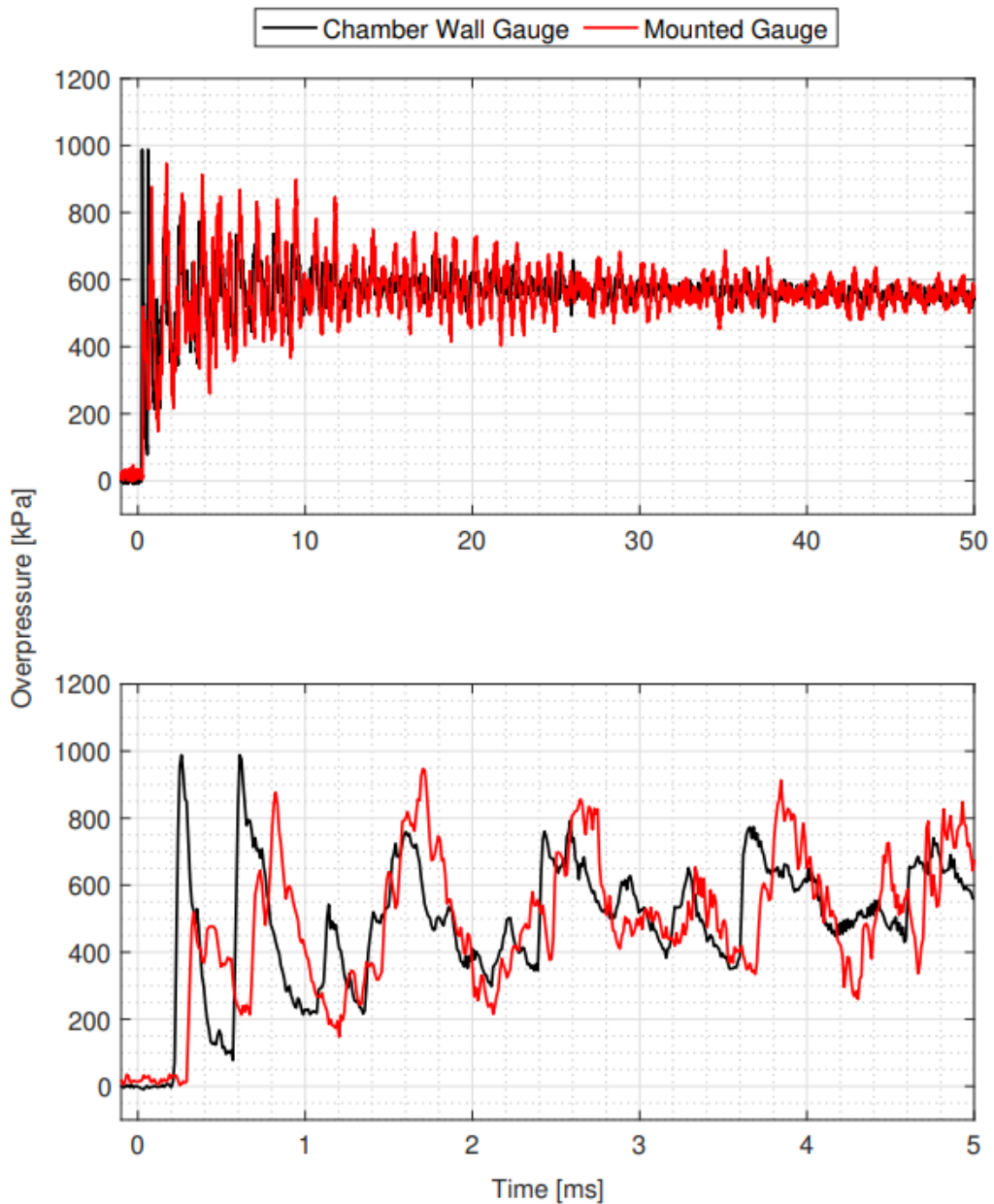


Figure 40- Raw pressure-time history plot for 50 g sphere of PE4 detonated within an air atmosphere with pressure gauges taking measurements from direct line of sight to the fireball, installed on the chamber wall, and a gauge mounted in the protective bolt.

These two pressure traces show some differences in the early time steps in terms of peaks and troughs. A break wire was used for these tests instead of the normal rising edge system so that a time zero for initiation is known, meaning they did not need to be time shifted and the difference in times is a feature. Where the value of the initial peak or two is different from each other before they start to be much more consistent with each other is likely due to being in the near field and close enough to the charge that there is an effect from the fireball

instabilities on the pressure experienced with the initial shocks having different arrival times. This has been investigated in previous work by (Tyas A. , 2018) which showed that differences from fireball jet instabilities changed the localised pressure but not the overall (area-integrated) impulse of an explosion.

This could also be caused partially due to the reflected pressures inside the bolt system requiring the shock wave to compress the air inside the chamber before the gauge, causing a more complex environment than that outside the gauge bolt. This does mean it's not possible to effectively measure reflected pressures with this configuration, due to the obstruction of the protective bolt interrupting the shock wave path from the point of detonation. However, that is not the aim for this work but should be considered for future studies.

5.3 Consistency of Trial Data

Once it was established that the testing methods were not affected by thermal drift or deviations due to instabilities in the early shock wave expansion. It was then on to determine the consistency of nominally identical trials using this test set up. Shown in Figure 41 is the raw pressure-time histories from four nominally identical detonations of 50 g spheres of PE4 in a standard air atmosphere (Test 1, 2, 3 and 4). Each plot in the series zooms in on the time base of the previous test to show the details of the traces. When looking at all the tests together, it can be seen that there is significant agreement between all the tests across all the time scales. Taking a close look at the raw data from the earliest stage of the event, between 0 and 5 ms, the shocks are almost identical in magnitude, duration and arrival which provides confidence that when the same test set up is used the consistency of the data is very good in the early-stage development of the fireball and the initial propagation of the shocks through the chamber. After the 5 ms point, the individual shock structures get slightly out of sync due to the chaotic mixing of the detonation products and possible human-induced variations in charge placement causing different distances for the shocks to transfer. However, when considering the QSP of the system these slight changes in the shock profiles ultimately do not significantly affect the developed pressure.

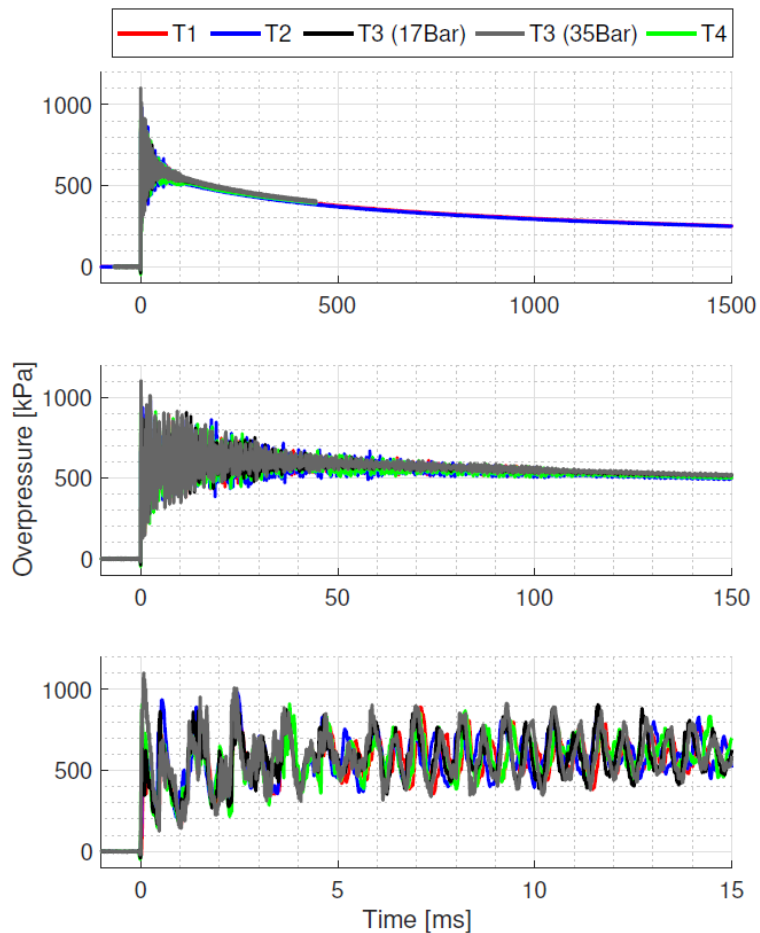


Figure 41 - Raw pressure-time history plots for nominally identical 50 g PE4 spherical detonations within the described confined chamber, within an air atmosphere across three different timescales of interest.

The larger timescale graph shows the overall trends of the pressure, it starts with an almost immediate rise up to a high pressure, before slowly reducing back down as time increases. This decrease in pressure as the time increases throughout the test is due to energy being lost from the system. The main factors that would take energy from the system are thermal losses to the steel pipe as it gets heated by the high temperature gasses produced. There were no losses through venting of the chamber as post-test when there was a pressure held in the chamber, no leaks could be heard emanating from the chamber, meaning the chamber was fully sealed so pressure could not vent into the environment around the chamber. This was also checked when doing tests where the chamber was filled with nitrogen as the chamber held pressure whilst being pumped if the exit valves were closed off, increasing the pressure pre-test before venting back down. This thermal loss phenomenon is further being investigated in the wider scope of this MaCE project but is not considered further in this thesis as it is only a prominent feature after the maximum QSP has been reached in the system.

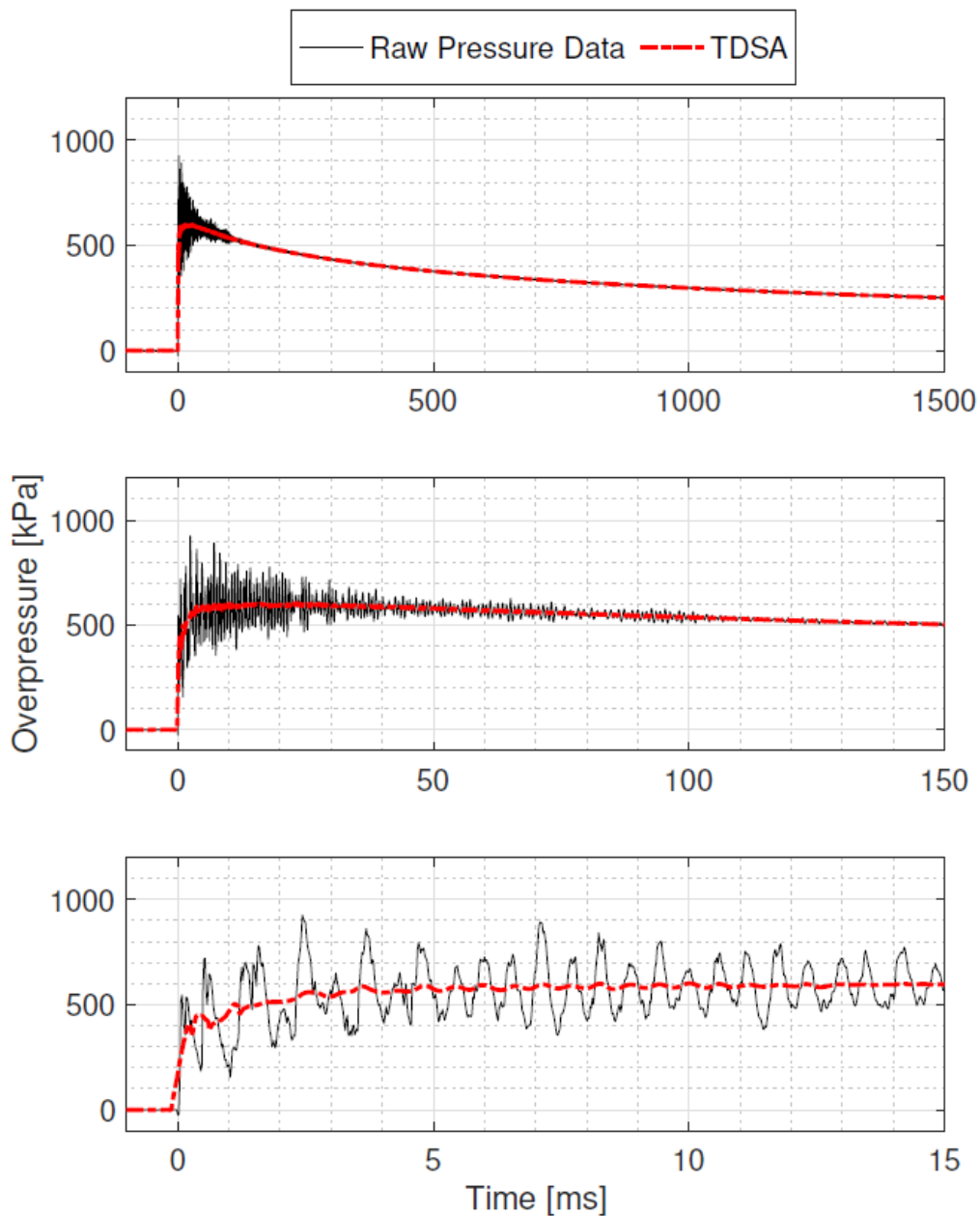


Figure 42- Raw pressure-time history plots and time dependant smoothed average for 50 g PE4 spherical detonations for Test 1.

Displayed in Figure 42 are three similar plots to Figure 41, showing an increasingly shortened timescale of the same test (Test 1). The complex shock interactions and chaotic mixing of the detonation products as they reflect off the chamber walls can make it difficult to determine a maximum QSP peak pressure. To remedy this issue a time dependant smooth average (TDSA) was developed to provide an easier to read peak pressure. A TDSA is a commonly used method to determine the maximum QSP value within a confined pipe (Kuhl A. L., 1998). The method proposed here was coded into MATLAB which automates the fitting process to the

raw data. This method works by varying the number of data points averaged against depending on the change in overall pressure, taking more points of average the larger the difference in pressure is. The early stages have a large difference in the maximum and minimum pressures seen so this uses a small number of points to average to maintain as accurate a curve as possible, but when the changes in pressure are smaller such as in the late time of the process the more points are used for the averaging process, giving a smoother curve and eliminating signal noise (from both successive shocks and from genuine signal noise). This method of averaging will be used throughout this work and will be used when determining the maximum QSP values for all trials that are part of this research.

After the averaging was done, a maximum QSP value was obtained by taking an average of the time frame in which the peak occurred, determined by eye for each set of data. These values for peak QSP for each test are given below in Table 19.

Table 19 – Maximum QSP values determined from experimental data

Test	Max QSP
1	596.67
2	598.32
3	605.71
4	596.65
5	253.15
6	633.61
7	603.16
8	412.61
9	409.47
10	174.92
11	369.49
12	244.38
13	633.08
14	155.07
15	292.83
16	393.92
17	497.34
18	411.05
19	392.85
20	431.24
21	244.05
22	258.68
23	261.01
24	178.42
25	173.4
26	173.4

5.4 Effects of charge shape

Preliminary studies were undertaken to investigate the effect of charge shape of the overall QSP within a confined chamber. For these tests, charges of 50 g PE4 were moulded into cylinders of 2:1 ratio length to width respectively (Blastech Ltd, 2018) with the detonator inserted into one end. These were then compared to tests using 50 g PE4 spheres in air. To form the charges for this work 3D printed moulds were used to ensure the correct ratio of length to width was achieved, removing any variability from the cylinder charge shapes.

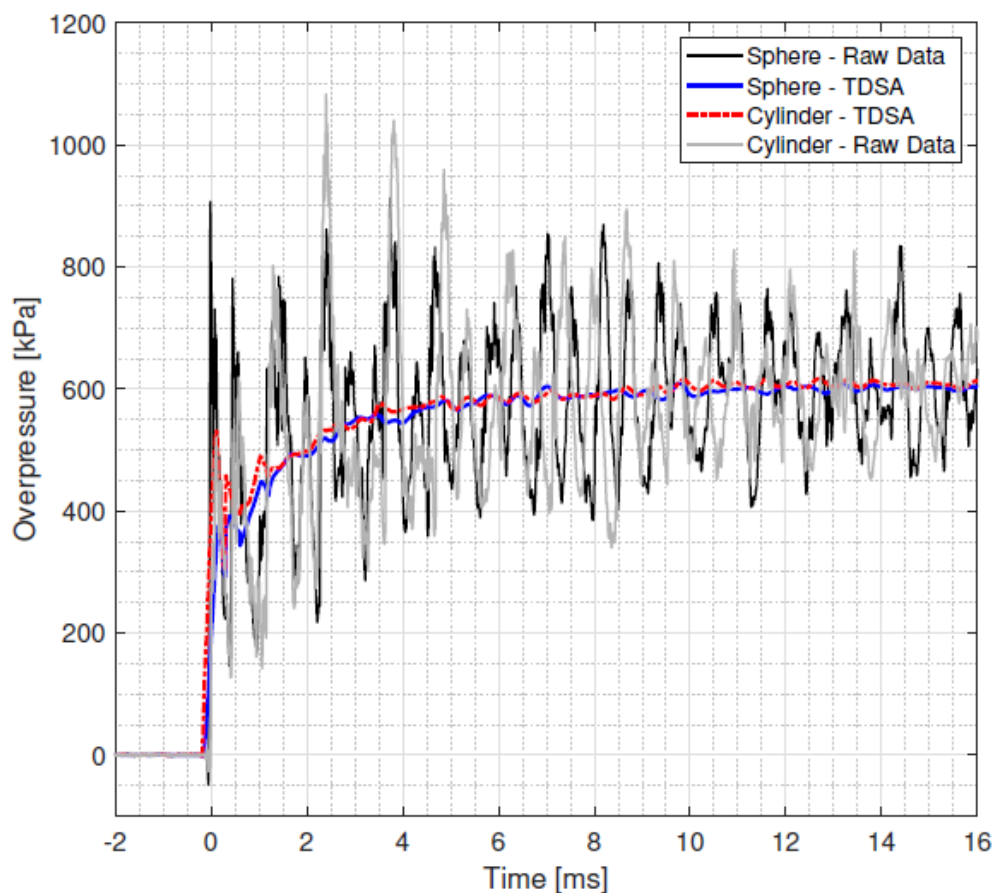


Figure 43-Raw pressure-time history plots for both 50 g sphere and cylinder PE4 detonations within the described confined chamber, denoted by red and blue lines are the TDSA for each test evaluating a peak QSP pressure.

Figure 43 displays the pressure development with respect to time of the confined chamber for spherical and cylindrical charges (Test 4 and 7). When looking at the raw traces, it emphasises the individual shock propagation through the chamber which show the difference

in the early time in terms of magnitude and arrival times. One aspect to note is the difference in the opening few shocks, as the cylindrical charge gives lower pressures, compared to the spherical charge. This is linked to the directionality of the blast wave produced by the charge. A cylindrical charge will form a shock wave that propagates longitudinally more than radially (Langran-Wheeler, 2021). This results in a lower proportion of the energy being in the part of the shock wave that passes over the pressure gauge in those initial few passes until the atmosphere has been chaotically mixed, and the pressure equalises around the chamber in the later time-period. This occurs in these tests as the gauges are located centrally to the pipe, this effect would differ depending on the gauge locations used but would still equalise out over the longer time-period.

Once the signal passes 6 ms for both charges, the behaviour becomes similar due to the shock wave propagation becoming more coalesced into a much more complicated shock interaction with no influence coming from the initial breakout of the shape. At this stage it is assumed that the explosive has reacted as much as it can, given the available oxygen in the environment.

The TDSA are also shown on the plot over the raw traces, these smoothed traces react almost identically, making it evident that despite the raw data having different peaks and troughs within the magnitude of pressure, and the overall QSP inside the system is effectively identical, due to the energy generated by the system being the driving factor for the QSP over the initial shock wave. This shows that the QSP is not charge shape dependant for this mass and composition of explosive, so spheres were the only charge shape discussed further in this work. Future work could look at more extreme charge shapes to see if large changes would cause different energy release of the explosive.

Further insight into the influence of geometry of charges is provided in the discussion section.

5.5 Atmospheric variation and its effects on QSP

Further tests have been conducted with differing atmospheric conditions contained within the chamber. For one of the tests the chamber was left filled with standard air and the other the chamber was purged of air and filled with nitrogen. These tests were conducted in an effort to gain a fundamental understanding of the afterburn phenomenon, including the physical mechanisms that cause it to occur and the time scale at which these mechanisms act over. To attempt to reduce the number of variables being altered when performing these tests, nitrogen was chosen due to its density being close to that of air, as air is made up of 78% nitrogen. The most important difference between the two gasses is the lack of oxygen present within the

nitrogen atmosphere as oxygen is the driving force for the afterburn reaction with these plastic explosives.

Figure 44 displays the pressure traces for the two tests discussed above, this shows the relationship between the first shock interacting with the pressure gauge and that they share almost identical magnitude shocks initially. (Balakrishnan, 2010) presented a comparison of 1-dimensional and 3-dimensional modelling of free-air TNT explosions attempting to establish afterburn mechanisms. This work in an open environment showed that considering the event in 3 dimensions allowing turbulent mixing, the secondary shock wave arrived sooner than compared to a 1-dimensional model. This is an important finding from those models that the magnitude of the peak pressures were identical but overall impulse and secondary shock arrival times were different, suggesting that the effects of afterburn can be seen as soon as there is interaction between the shock and a boundary that causes turbulent mixing of the detonation products with the atmospheric oxygen.

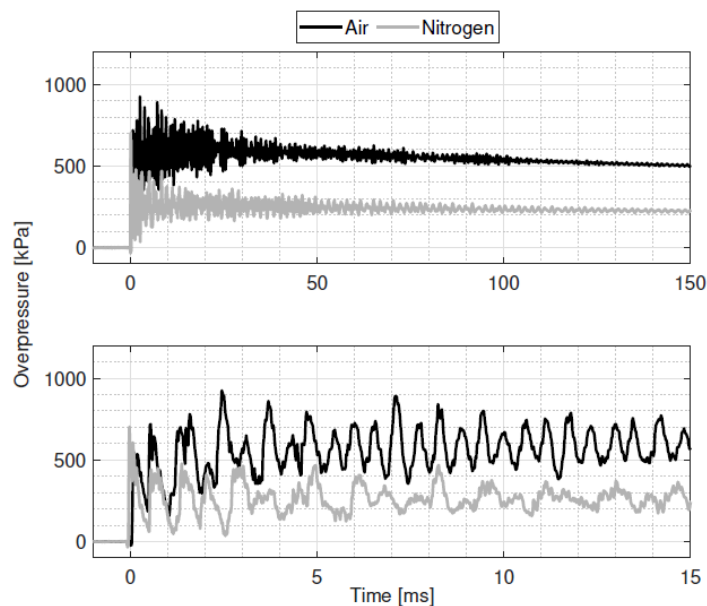


Figure 44 - Raw pressure-time histories of 50 g PE4 spherical detonations within a confined chamber with air and nitrogen atmospheres.

Upon the arrival of the second shock that reaches the pressure gauge, the magnitude of the pressure recorded is much larger in the air test compared to the one conducted in nitrogen. The nitrogen starving the fuel-rich detonation products of oxygen means that no additional energy release occurs from those fuels, stopping the afterburn phenomenon from occurring (Kuhl A. I., 2000) (Edri I.E., 2019). The proposed theory for why this happens is that by the time the secondary shock interacts with the pressure gauge, it has been involved in the turbulent mixing of the detonation products and the oxygen which releases additional energy and hence

increases the magnitude of the shock wave before it reaches the gauge. This means that mechanisms that allow afterburn to occur will be directly related to the ability of the detonation products to be forcefully mixed into a surrounding oxygen atmosphere.

Now that the mechanism of afterburn is linked to the mixing of detonation products with the atmospheric oxygen, it can be tested against other gasses that provide an atmosphere devoid of oxygen to check that this holds for other atmospheres. The next gas used to investigate this was chosen to be argon so that more knowledge could be gained about the fundamental pressure development in confined spaces. Argon's density is much higher than that of nitrogen and air, with argon's density being 1.603 g/L and air and nitrogen being 1.184 g/L and 1.126 g/L at 26.9°C respectively. Theoretically this increase in density would result in an increase in kinetic energy of the shock waves and thus an increase in QSP compared to a nitrogen atmosphere. This theory was investigated through experimental means and results from those tests are shown in Figure 45 and Figure 46.

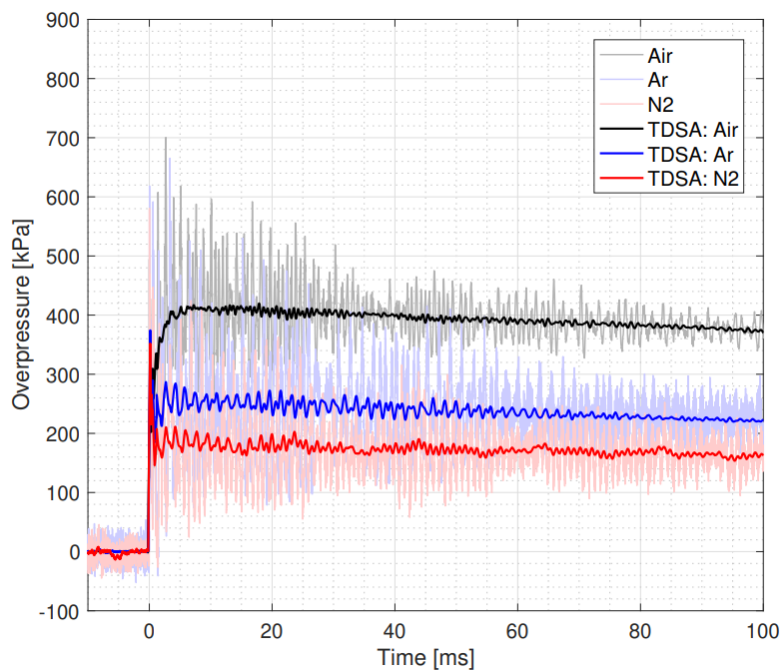


Figure 45 - Raw Pressure-Time history of 30 g PE10 spherical charges detonated with air, nitrogen and argon atmospheres with a TDSA fit for each plot.

Clearly seen in Figure 46 is the difference between the argon atmosphere and the nitrogen atmosphere, where the argon atmosphere has a higher QSP compared to the nitrogen atmosphere. This difference in QSP is due to the difference in specific heat capacities of the two gasses. For a nitrogen atmosphere, the ratio of specific heats is 1.40 whereas the ratio for argon is 1.66. This means that when iteratively determining the temperature of the system, since the

energy is dependant on the explosive in question and is independant of the atmosphere, the temperature for an argon test would need to be higher to achieve the same value of energy. This increase in temperature means that the pressure in the system would also be increased, hence the difference between the argon and nitrogen atmosphere tests.

$$E = \frac{1}{\gamma - 1} \times n \times R \times T$$

Equation 4.7

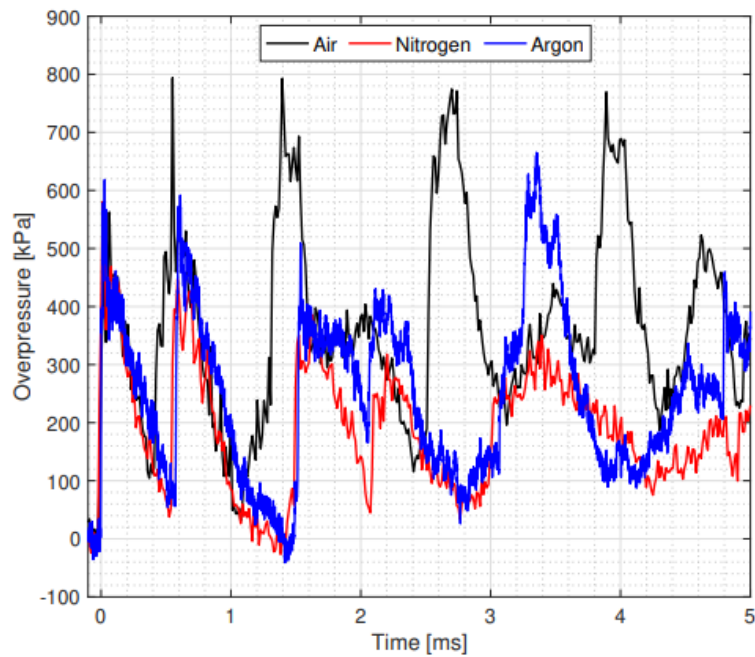


Figure 46 – Raw Pressure-Time History of 30 g PE10 over the first few shocks in differing atmospheres.

Figure 47 shows the compiled data from each test, using the ratio of mass to chamber volume expressed as the reduced mass, kg/cm^3 . Plotting the data this way shows that there is a clear trend dependant on atmosphere and mass of explosive. It is clear that as the charge size to volume ratio increases, the higher the pressure generated by its detonation. This is expected as there is more explosive to release energy compared to chamber volume, but seems to follow a relatively linear trend. It also shows that the argon atmosphere may also follow a similar trend but two data clusters is not enough to confirm this for definite as the trend could taper off outside of the bounds tested. The same is true for nitrogen atmospheres, however it clearly shows that the nitrogen atmosphere provides a lower maximum QSP pressure compared to that of argon in the bounds of this work.

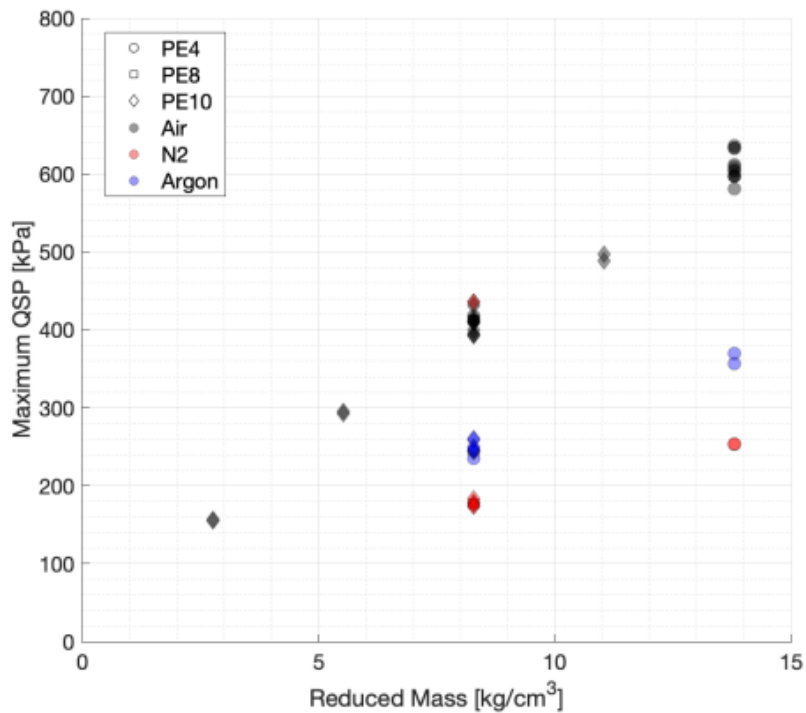


Figure 47 – Compiled processed maximum QSP data from three explosives, with different atmospheres and different mass to chamber volume ratios.

When looking at the data for PE10 in air, a line of best fit can be put through the data to provide an idea of the trend as the mass to chamber volume ratio changes. This was initially done as a linear line of best fit, which provided an equation of $11.144x + 62.505$. This did not provide an intersect very close to the point 0,0 which is where you would expect a trend to go through for this data so it was redone with a cubic polynomial best fit line which provides the equation $Y = -0.0009x^2 - 0.064x^2 + 16.31x - 0.755$. This provides a data point very close to zero which is much more in line with where that value should be. These are shown in Figure 48 with an R^2 value of 0.9885 according to the automatic calculations done by Excell.

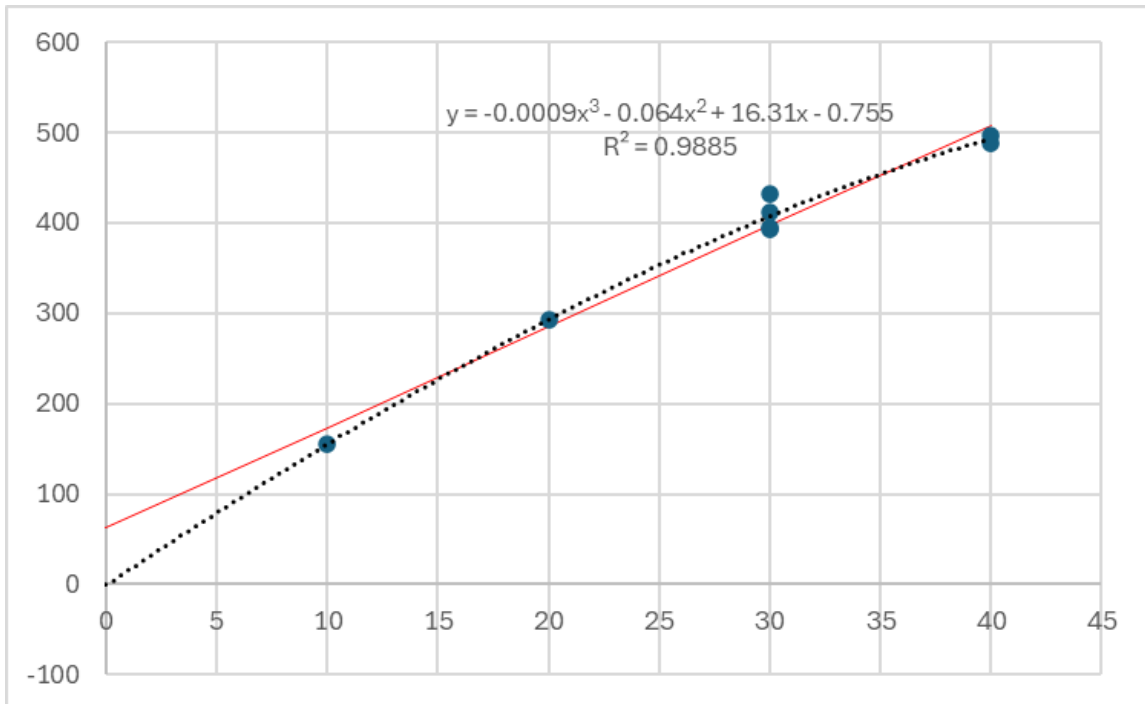


Figure 48 - PE10 trendline and equation through use of a cubic polynomial line of best fit.

5.6 Infrared Thermometry

To directly measure the temperature of an explosion, a series of tests were conducted using a bespoke, high-speed infrared thermometer alongside pressure gauges. These tests were used to measure temperature and pressure directly from the same explosive event ensuring that they can be compared without issues of repeatability into differing test set ups. This was required to determine if the assumption that the ideal gas equation can be used for high temperature events such as this, that was used in the thermochemical model.

The tests conducted involved different atmospheres, air, nitrogen and argon to investigate the effect of changing atmospheres on the temperature of the detonation and hence the pressure. The results from these tests can be seen in Figure 49 where they show the differences in pressure caused by the use of altering atmosphere. The measured temperature from these tests was converted to pressure using the ideal gas equation before plotting so that they could be compared. This shows good agreement between the temperature inferred pressure and measured pressure when looking at the QSP of the system except in the early stages of the air trial.

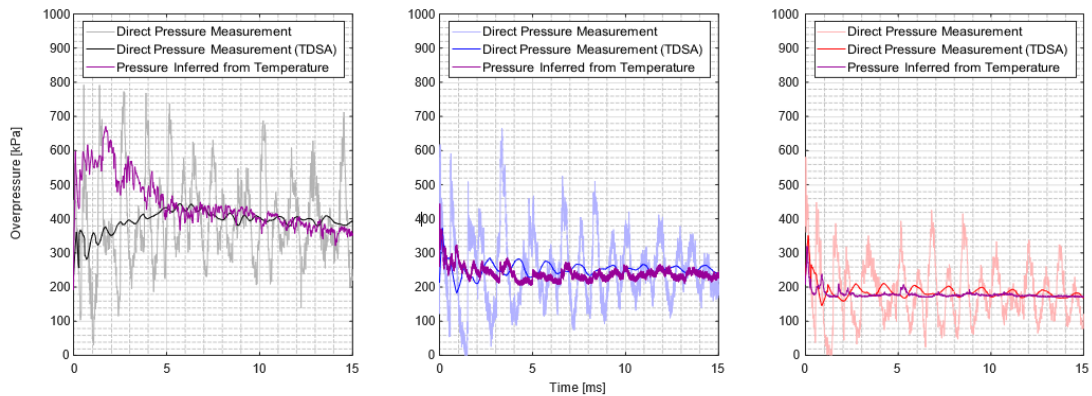


Figure 49 - Infrared Thermometry of an explosive event in air, argon and nitrogen respectively.

Though there is a discrepancy between the pressure gauge measurement and IRT measurement in the first 5 ms of the air test, after this point, the two signals coalesce and become much more similar. In the case of the nitrogen and argon tests as others, where the argon tests show a higher pressure than those of the nitrogen ones, due to the increase in specific heat capacity ratio of the atmosphere.

A possible mechanism for the difference seen in the first 5 ms of the air test may be due to the IRT picking up the afterburn flame temperature, instead of the overall temperature of the chamber. This is due to the process by which the IRT works where it measures wavelengths of radiation over a fixed area, and where the fireball passes into that area, the temperature of that fireball will be picked up, even if the whole chamber is not at the temperature of the still reacting fireball. This mechanism would explain why the 5 ms discrepancy is not seen in the oxygen deficient atmospheres and is only seen over the first fraction of a millisecond, where there is an initial flash of the detonation occurring.

A further investigation into this is given in section 6.3.

Section 6- Discussion

In this chapter, a further discussion of the results section will be undertaken to explain how these results have built upon the main issues in the field that were noted in the literature review. This includes problems such as consistency of blast testing, verification of the Edri model and ideal gas equation assumptions holding for blast testing, starting with the consistency of QSP testing.

6.1 The Consistency of QSP Explosions

Though in the literature there are many examples of high variability in explosive testing as shown in the literature review, the data presented in this thesis will prove that this inherent variation in explosives, at least in confined testing, is considerably lower. In fact, the data presented in Figure 50 shows the results from multiple well-controlled identical QSP tests. These tests show that the variation occurring between each experiment is minimal if any. This consistency shows that when performing an experiment, as long as it is well-controlled and the variables are kept the same each time, the explosive will behave in generally the same way.

This lends additional weight to the work completed by (Farrimond, 2023) to show the repeatability of free field explosive testing. As well as this work, well conducted experimental small scale testing by (Rickman, 2007) provided comparable results to those of (Kingery & Bulmash, 1984) predictions when investigating normally reflected conditions in far-field scaled distances. The conclusions drawn from this work shows that there is an increase in understanding of repeatability in explosives and that there should now be more of an effort made to ensure that experimental work is well controlled and should provide more consistent data, where in places this is not the case, explanations should be given for why this repeatability is not seen.

The ability to have consistency in data capture for even complex environments such as a confined explosion should be noted as an important development in the field of blast parameter measurement and is more similar to the consistency shown by work such as (Kingery & Bulmash, 1984) which many of today's modelling and understanding is based on.

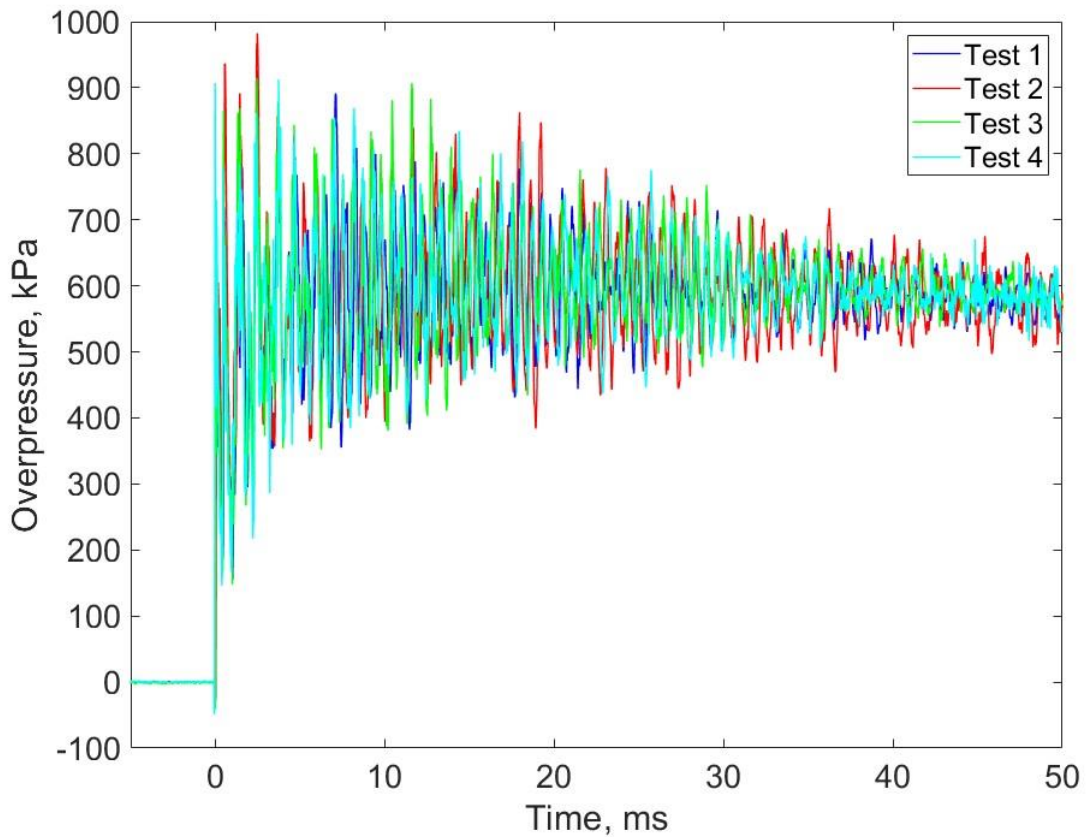


Figure 50 – A comparison of 4 50 g PE4 experimental tests showing the consistency of data.

This is an important development, which together with the work of (Farrimond, 2023), offers evidence to question the assumption that large variations should be expected in explosive testing. More accurate and consistent data like that presented here will allow for better validation of theoretical models. With more consistent and controlled experimental data that is more consistent and therefore more reliable for comparisons. This increased consistency is due to the well-controlled experimental procedures used when conducting the tests. When the experiment is performed to a high degree of accuracy each time, the expansion of the detonation product cloud also becomes more consistent. A further analysis of the averages and standard deviations of this data when compared to the theoretical thermochemical predictor is provided later in this section.

6.2 Charge and Chamber Shape Discussion

When investigating the effect of charge shape on the QSP generated by the explosive, it is generally considered that the shape of a charge or chamber doesn't have an impact on the QSP (Baker, 1983) (Anderson Jr CE, 1983). In terms of a first order investigation, this would be a correct way to interpret it because the QSP is based on the charge weight to chamber volume ratio. When considering this same effect more in depth however, we know that the pressure generation of afterburn in a confined explosion is due to the turbulent mixing of detonation products and atmospheric oxygen. If the chamber to charge ratio is very small and the time it takes for the shock to travel to the chamber walls and back through the fireball is long enough, this may cause the temperature of the fireball may be lower than the temperature needed to continue afterburn, hence not producing as much energy into the system. Also, if the chamber has a complex structure, this could cause a larger surface area internally than a standard chamber, which could increase the energy that can be taken out of the system through loss to the walls and this could affect the pressure build up generated from the detonation.

Though it is shown in Figure 51 (which is a duplicate of a previous figure) that in the case of this work, the shape of the charge had little effect on the pressures generated, it could have a different process to reach maximum QSP, taking longer and reaching a lower QSP if the energy being taken out of the system is increased due to more surface area of a complex shaped chamber.

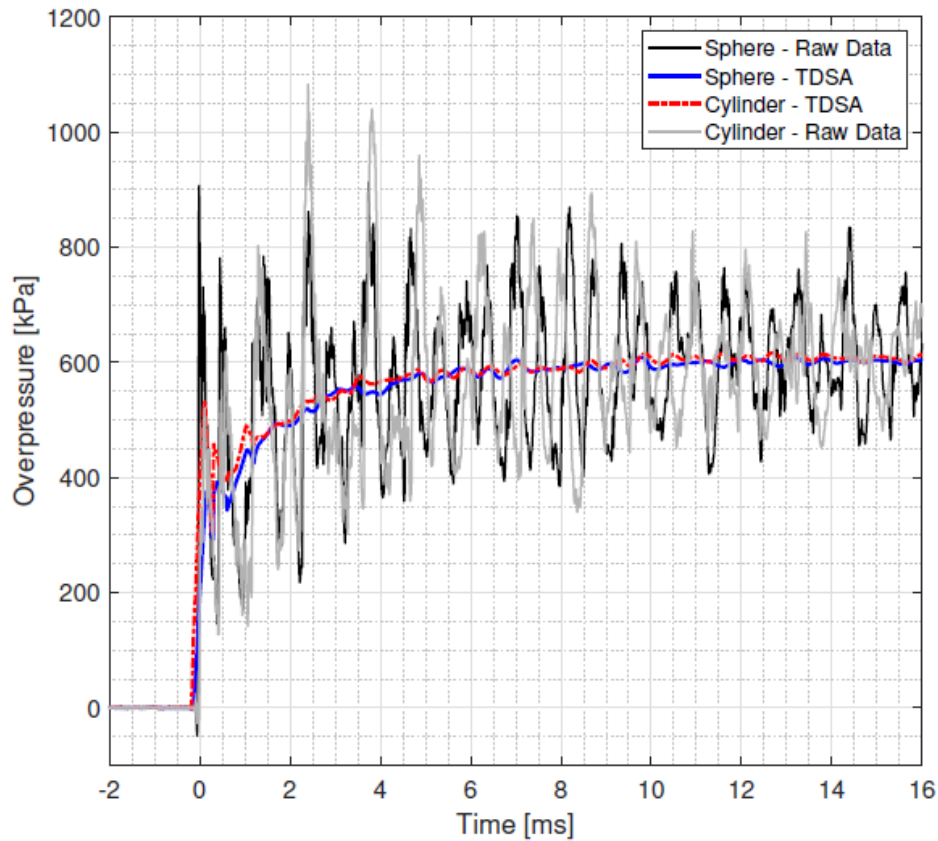


Figure 51 - Raw pressure-time history plots for both 50 g sphere and cylinder PE4 detonations within the described confined chamber.

This could be an additional area of research to gain understanding of the processes involved in the energy loss to the chamber walls since currently the process by which the energy is dissipated is unknown and needs to be further understood for modelling of energy losses to the chamber and how this effects the generation and loss of pressure.

6.3 Ideal Gas Assumptions

In this work, the Ideal gas equation was assumed to be valid in the use of the thermochemical model. To prove that the ideal gas equation was valid, a series of tests where the direct temperature of the chamber was measured using an infra-red thermometer as well as measuring the pressure from the same test. This means that the temperature of the chamber and the pressure were independently measured for the same test, and therefore the temperature from the direct measurement can be compared to the temperature generated by

using the ideal gas equation and the directly measured pressure (from the same test). To do this the pressure value from the gauges was converted to temperature using $PV = nRT$ and rearranging into $PV/nR = T$. This allows the temperature to be calculated since the number of moles in the chamber is known, pre- and post-explosion, as are the chamber volume and gas constant.

Through performing this analysis on the data from these tests, Figure 52 is created where the direct pressure measurement is compared to the experimental ideal gas equation pressure calculated from the temperature measured by the infra-red thermometer. This figure shows that other than in the initial phase of the explosion (first 5 ms), all of these pressure traces are in good agreement with one another, showing that the ideal gas equation does hold in these environments and so can be used when developing the model created in this thesis.

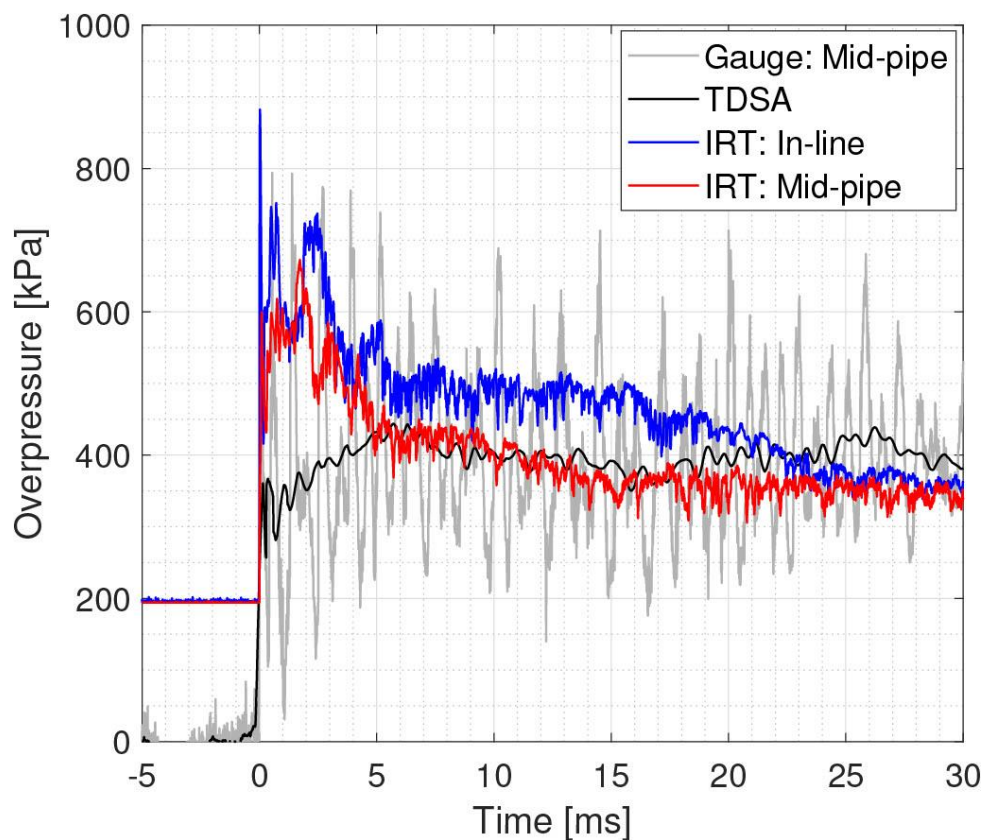


Figure 52 – A comparison of Infra-red thermometry inferred pressure against pressure gauge direct measurements.

Work presented by (Xiangshao Kong, 2019) also looks at the energy release of an explosive in a confined environment of 1800 mm x 800 mm x 800 mm chamber, which has a length scale similar to that of the testing in this work being under double the length. This work displayed the time history of total energy release and energy-release rates for a typical fuel-rich

explosive over the course of a confined explosion. This is shown in Figure 53 and when investigating the time scales seen match well with the experimental results in this work. Where you have an initial pressure release through detonation within the first nanoseconds of the detonation occurring which raises the energy of the system, followed by an energy release due to afterburn in the microsecond time frames up to millisecond time frames and causing a further increase in total energy in the system. These two distinct processes cause a joint effect on the energy of the system, not two separate energy changes and hence both effect the pressure in the system. This increase in energy due to afterburn is shown in Figure 52 (black line) where the initial spike in pressure is followed by a gentle rise until it hits a maximum value before dropping off.

If this work was performed at a different set of scale with a much longer chamber, this would cause a change in the mass of explosive needed to maintain the W/V ratio. This increase would rely on the scaling proposed by (Hopkinson B. , 1915) and (Cranz, 1926) where an increase of 10 times in length would incur an increase of 1000 in volume, leading to a charge mass increase of 1000 times. This increase would then cause a change in time scales of 10 times according to these scaling laws and hence the energy process of detonation and afterburn would therefore also be 10 times different. So, if the chamber increased in length by 10 times, the energy release rates would also reduce by 10 times becoming slower.

This leads to the possibility of adding this feature to the thermochemical model in the future so can be considered for future works on this topic to allow the understanding of these scaling laws to be introduced to the model. This would provide an increase in usability for the model if these changes can be made for a scaling factor for the charge size and the time frame that the maximum QSP would take to occur.

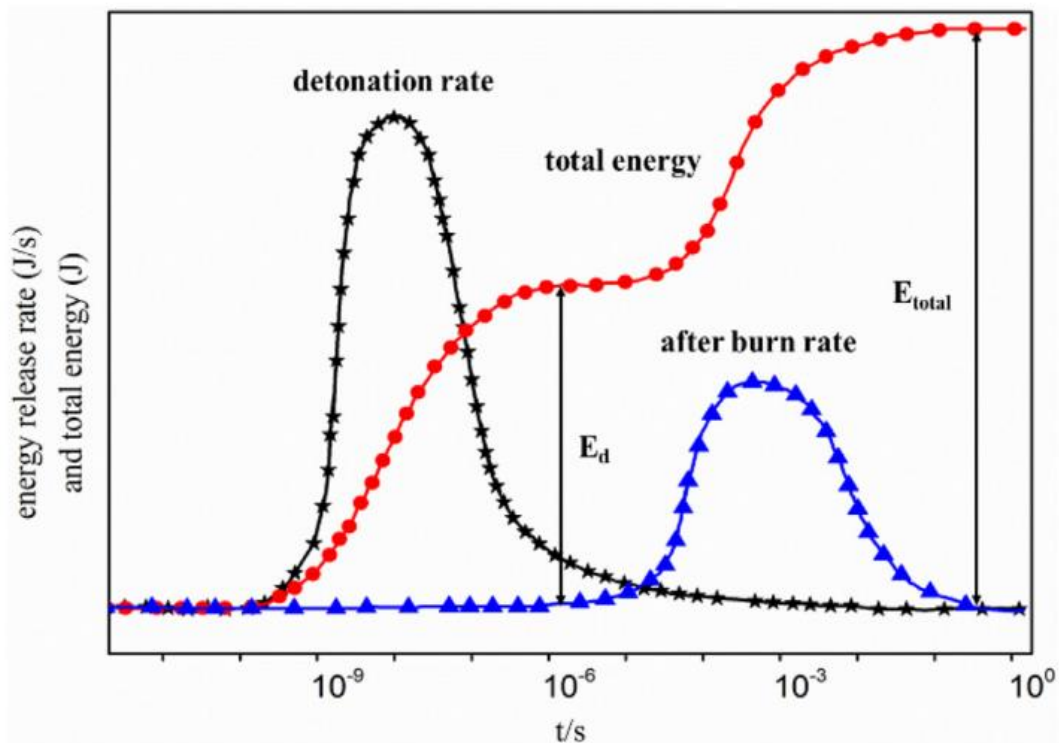


Figure 53 - Time history of total energy release against energy-release rates of fuel rich explosive (Xiangshao Kong, 2019).

A working hypothesis on why the early time pressures are not identical, is that the directly-measured temperature is that of the fireball flame temperature. This would be different to the global (average) temperature of the chamber itself as the former is much more localised. This would explain the early time deviation as the pressure measurements do not pick up localised temperature changes; they are only picking up pressure measurements in the chamber.

Further work was undertaken by (Xiangshao Kong, 2019) looking at the pressure and temperature inside a confined experiment, and a temperature graph from that work is shown in Figure 54. The temperature in this graph rises slowly to its maximum temperature over the first 0.25 seconds. When comparing this to the pressure signals from the same test of 120 g of TNT FIG, the pressure develops to its maximum within 1 ms. This difference between time frame of the rise to maximum doesn't fit with the theory of the ideal gas equation, as for the pressure to increase in the chamber, the temperature should also increase over the same time frame. This shows that the temperature measurement using a thermocouple is not the most effective way to measure the temperature at a rate that matches that of the pressure measurements.

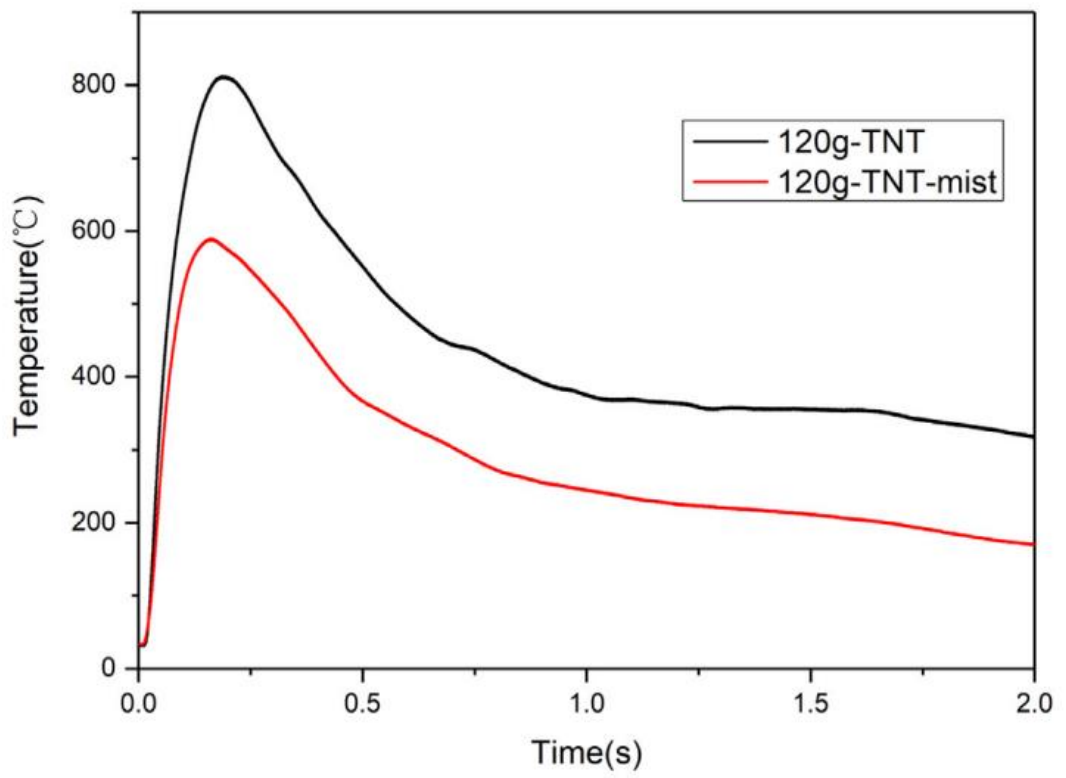


Figure 54 – Temperature history for 120 g TNT charge with and without water mist.

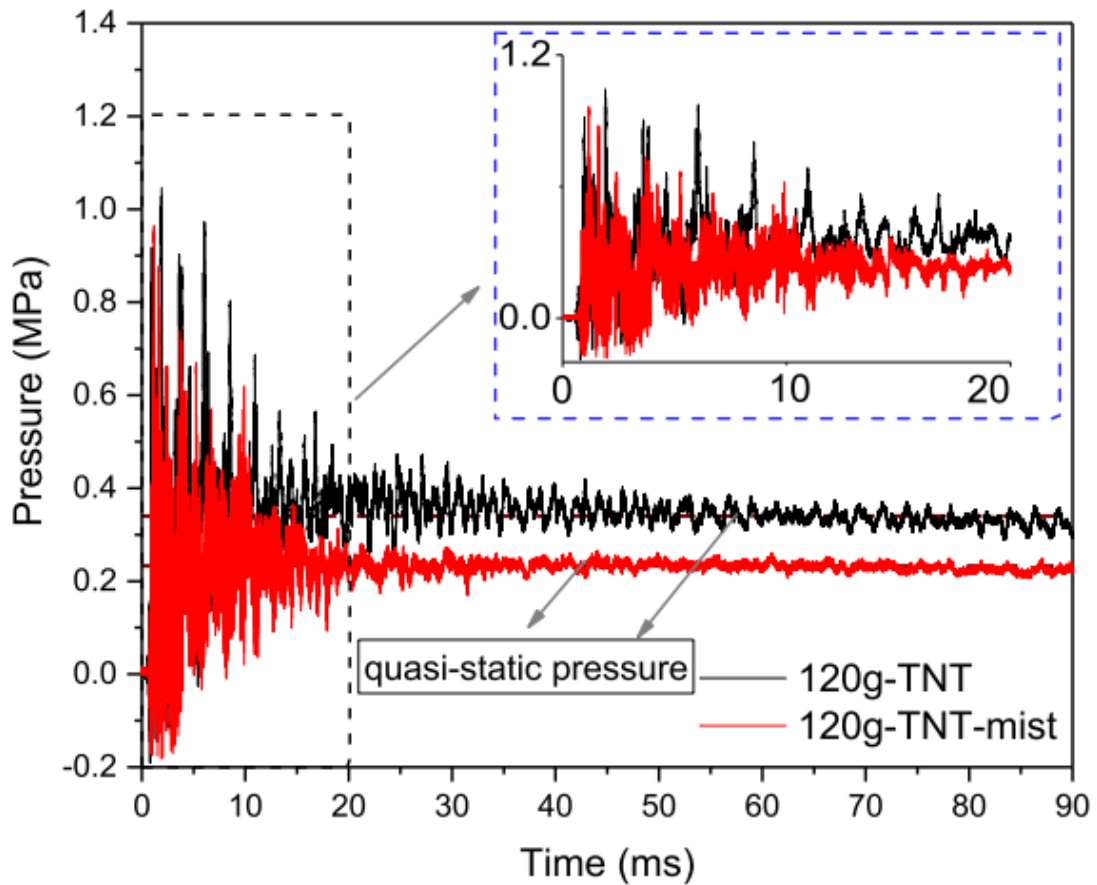


Figure 55 - Pressure-time history of 120 g TNT with and without mist.

Tests in nitrogen were performed to investigate the influence of afterburn on the temperatures recorded. This test shown in Figure 56, Figure 57 and Figure 58 shows that the amount of deviation in the early stage is still apparent, however it is generally lower and considerably shorter in duration, suggesting that the difference is indeed due to the initial fireball breakout. However, when the initial fireball has passed, because there are no afterburn flames occurring from interactions with oxygen in the chamber, there is no continued flame temperature as it has burned out at this point and the temperature being measured is the temperature of the chamber itself. The rate that the temperatures are measured over, using this method is much faster than the work by (Xiangshao Kong, 2019) and it can be seen that the temperature increase occurs at the same timescales as the pressures. This indicates that little useful quantitative data can be extracted from the use of conventional thermocouples.

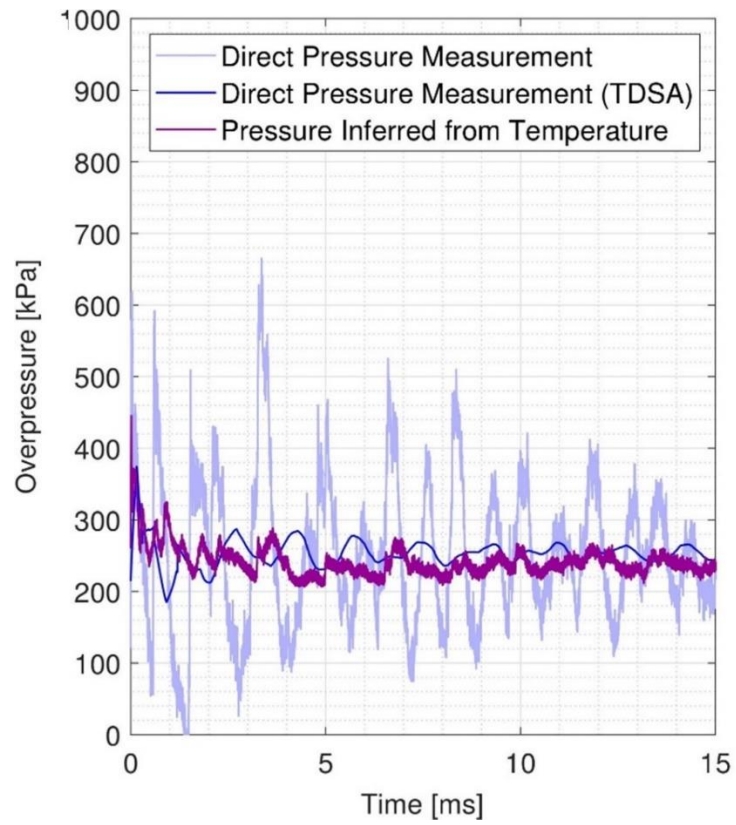


Figure 56 - Pressure measurements generated from IRT data compared to direct pressure measurements from a 30 g PE10 charge in an argon atmosphere (D. G Farrimond, 2024).

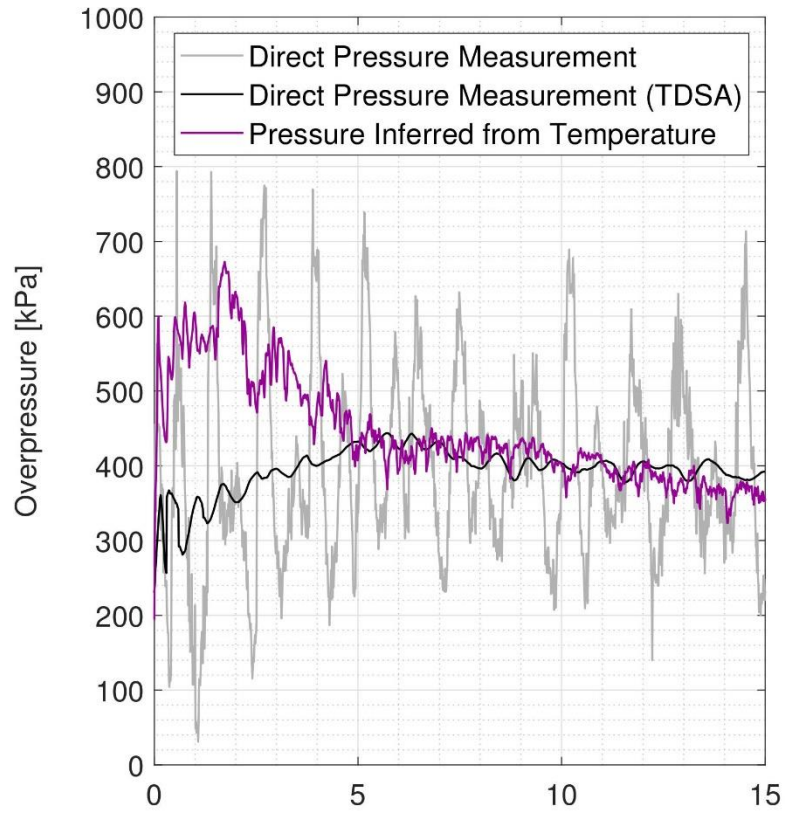


Figure 57 - Pressure measurements derived from IRT temperature data Vs Direct pressure measurements of a 30 g PE10 charge in air (D. G Farrimond, 2024).

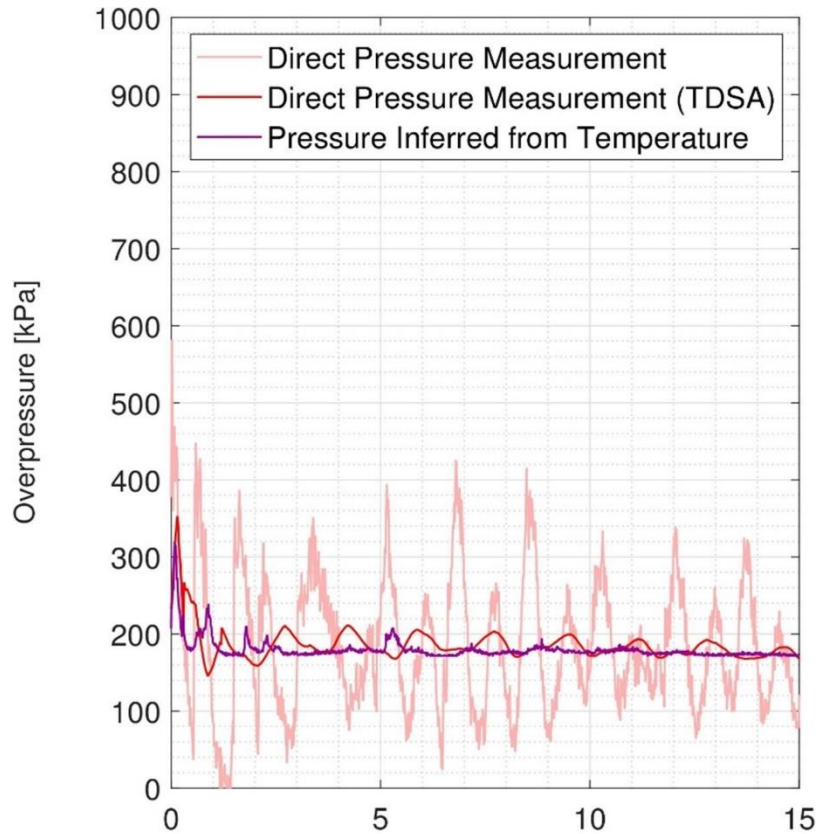


Figure 58 - Pressure inferred from temperature measurements Vs Direct pressure measurements of a 30 g PE10 charge in a nitrogen atmosphere (D. G Farrimond, 2024).

This knowledge of the ideal gas equation holding during these experiments does more than just show that the pressure given by the thermochemical calculator is not using invalid assumptions. A big development of this is also showing that since the ideal gas equation is holding, we know that the pressure/temperature loss in the chamber is not due to the loss of gas through venting, since we know the moles of gas in the chamber. Because of this, we know that the decreasing pressure as time increases in the QSP test is due to something else. It is theorised here that this loss of pressure is due to energy transfer to the outer walls of the chamber. Though this has been identified as a principle, the mechanism through which the energy is transferred through to the chamber walls is unknown, whether that process is conduction, radiation etc it is likely that there is no equilibrium in the temperatures between internal chamber temperature, wall temperature and outside temperature due to the short time frames that this process is occurring over. This is an important development as many modelling software's do not include the energy loss through heat transfer in their development, instead they use the idea of venting to account for this energy loss. This inclusion of energy loss through the walls of the chamber could be performed using alternative wall structures in these complex

models that allow energy transfer through the medium instead of being just a rigid boundary allowing reflection of the shock wave.

Definitive confirmation of the precise mechanism of the loss of thermal energy and therefore pressure, is beyond the scope of this thesis. Nevertheless simple calculations suggest that this may be due to localised flash heating of the chamber walls, rather than a steady flow of heat from the inside of the walls to the external atmosphere as follows.

We assume as an example, the heating of a 1 mm thickness of steel on the inside face of the chamber (surface area of 2.451 m²). This equates to a mass of steel of approximately 19 kg. Using a specific heat capacity of 490 J/kg C° (Toolbox, 2024) this would result in an energy loss to the pipe wall of approximately 9000 J for every degree kelvin increase in the steel temperature. Given that for even the most energetic charges investigated in this work, the total energy released by the detonation and afterburn is of the order of 700 kJ, it is clear that even a small rise in temperature of this 1 mm thick inside layer could account for a high proportion of the energy released.

This experimental procedure can also be used to prove that there is no venting in the chamber during the test. This is because using the ideal gas equation, Equation 2.1, we assume that the number of moles in the system remains constant due to no losses through venting in the system. If this is the case, any increase in pressure or temperature in the system would directly result in changes to the other. Thus, if venting did occur, since the number of moles in the chamber would be lower than assumed, the pressure inferred from a given measured temperature assuming the original number of moles of gas, would be higher than the pressure directly measured. In the long-term plot for the temperature inferred pressure against experimentally measured pressure shown in Figure 59 it can be seen that both measurements follow very similar trends over the long term decay, indicating that the assumption of no venting is correct.

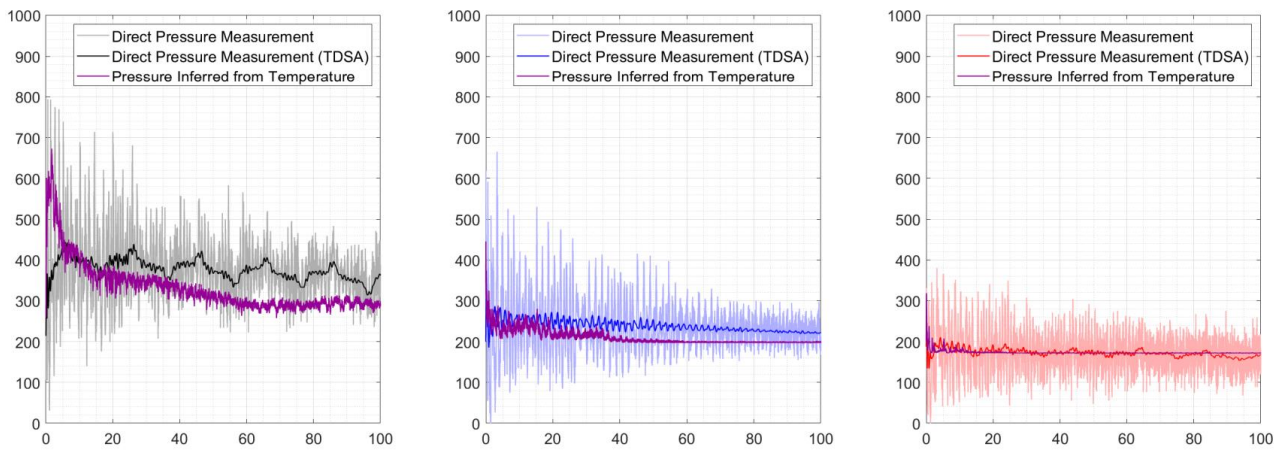


Figure 59 - Long term behaviour of IRT inferred pressure and gauge pressure.

6.4 Thermochemical model

With the ideal gas equation demonstrated to apply in the conditions of the tests we are considering, this means that the model for predicting max QSP pressure can be further used and validated. To validate a model such as this, it needs to be compared to experimental data. To do this the model was used to predict a pressure from the inputs that are identical to the inputs for the experimental tests that have been performed. Figure 60 shows a PE4 experimental pressure trace, overlaid with a line that corresponds to the predicted max QSP pressure generated using the thermochemical model.

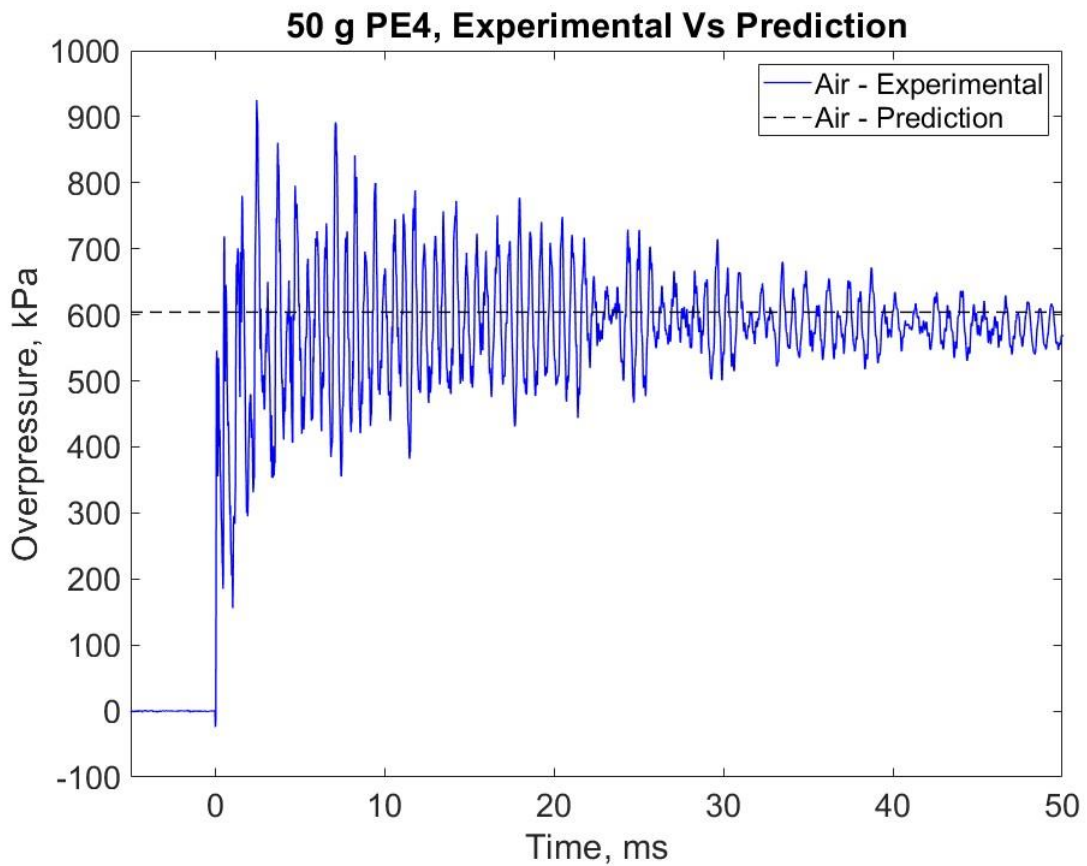


Figure 60 – Comparison of 50 g PE4 in air against the thermochemical model prediction.

This graph shows that the thermochemical model is predicting to a good degree the maximum QSP being generated from a given explosive and chamber volume. This prediction, based on ideal gas equations, shows good accuracy for this prediction of maximum QSP scenario with 50 g of PE4. When comparing this same experimental data to the thermochemical model without plasticiser/binder, such as the method proposed by (Edri I.E., 2019), the prediction shows a large difference going from over 600 down to below 500. This is shown below in Figure 61 and shows the importance of the inclusion of the plasticiser and binder.

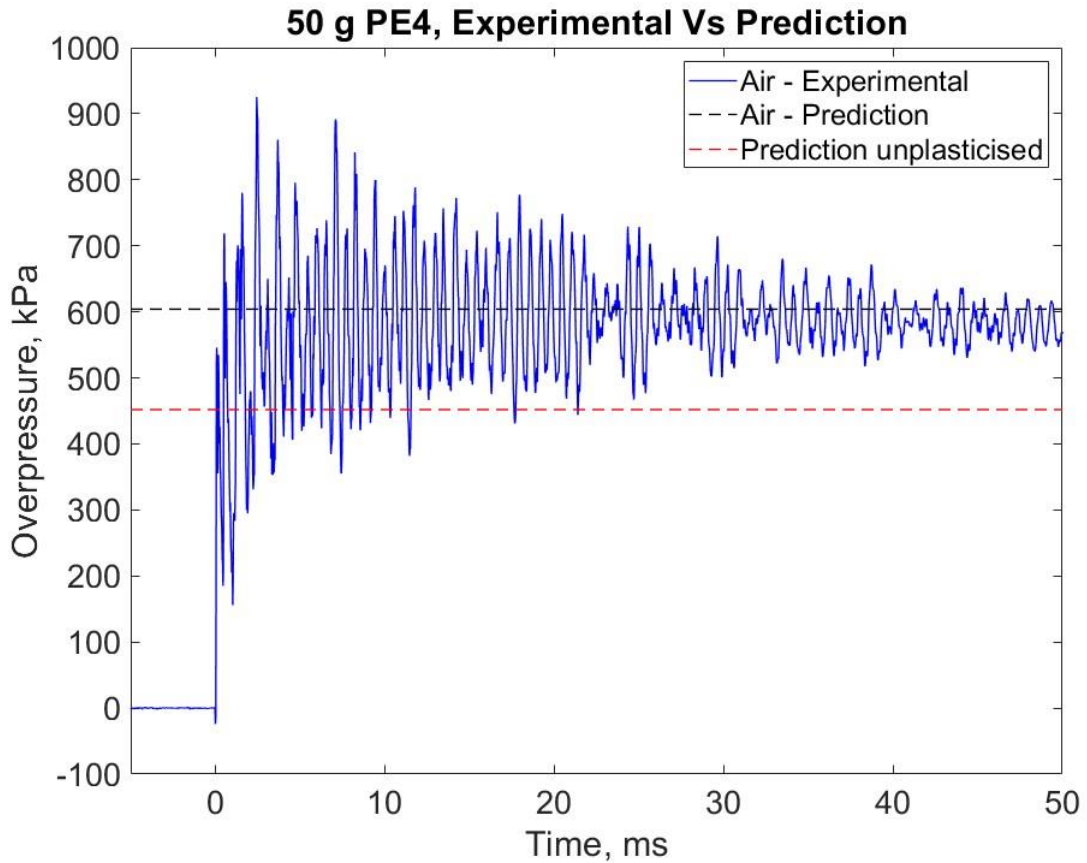


Figure 61 – Comparison of thermochemical model with and without plasticiser of a 50 g PE4/pure RDX charge and experimental data.

This shows a large difference between the thermochemical model that was available previously in (Edri, 2019) compared to the addition of plasticisers and binders that release energy in the afterburn of the explosive.

Since the thermochemical model has been validated against the PE4 explosive, it is important to validate it against different explosives. This is shown Figure 62 where a PE10 charge was used in an experiment and the thermochemical model was altered to account for the different explosive compositions. As is evident by Figure 62, the different explosives are also very well matched with the thermochemical model for this test.

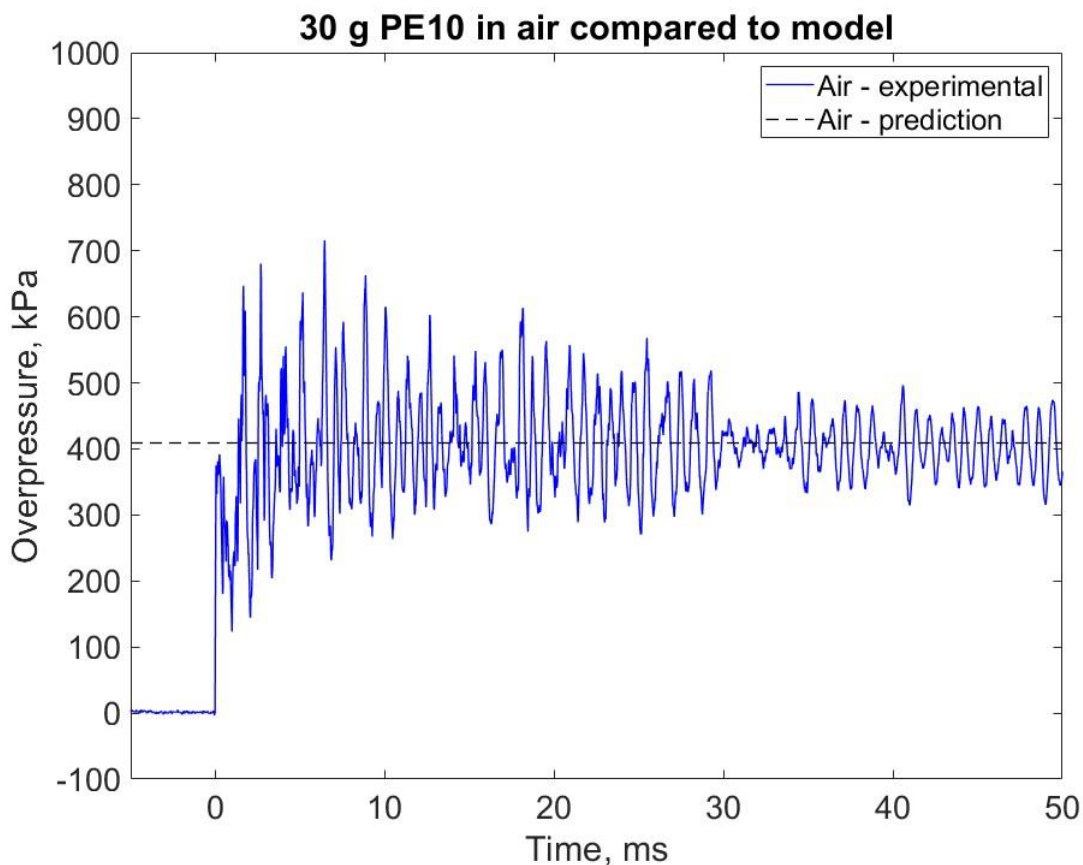


Figure 62 – Comparison of a 30 g PE10 experimental pressure vs predicted pressure.

To determine if this method can be adaptable to this other scenario, it needs to be tested against other mass to volume ratios to ensure consistency between changing parameters. Figure 63 shows the results of pressure traces from 10, 20, 30 and 40 g PE10 charges, each overlaid with a line of max QSP predictions made by the thermochemical model. These different pressures generated by the altering masses of explosive are all matched by the predictor to an acceptable degree. This allows the validation of the model for PE4 explosives and PE10 at least up to a charge mass volume ration of 50 g in 275 L.

A series of the experimental tests from this work have also been compared in terms of maximum quasi-static pressure seen experimentally, against the thermochemical model value and have been given in Table 20. This data shows the majority of the deviations from experimental to model between 1-4% for detonations of ideal explosives in air. This is another indicator that the experimental work shows a good consistency as the percentage differences to the model are all small in value. For the PE4 tests conducted in an air atmosphere, the average value of experimental maximum QSP error against the thermochemical model is 2.074 % with a standard deviation of 1.03.

Table 20 - Max QSP from experimental vs theoretical for a PE4 in air tests.

Test	Explosive	Atmosphere	Mass / g	Max QSP	Predicted Max QSP	% Error vs model
1	PE4	Air	50	596.67	622.8	4.20
2	PE4	Air	50	598.32	622.8	3.93
3	PE4	Air	50	605.71	622.8	2.74
4	PE4	Air	50	596.65	622.8	4.20
7	PE4	Air	50	603.16	622.8	3.15
8	PE4	Air	30	412.61	404.3	2.06
13	PE4	Air	50	633.08	622.8	1.65

When looking at the tests conducted with PE10 explosive, the average absolute percentage difference between the experimental value and the thermochemical model is 2.96% with a standard deviation of 2.38 and these results are given in Table 21.

Table 21 - Max QSP from experimental vs theoretical for a PE10 in air tests.

Test	Explosive	Atmosphere	Mass / g	Experimental Max QSP	Predicted Max QSP	% Error vs model
9	PE10	Air	30	409.47	397	3.14
14	PE10	Air	10	155.07	157.7	1.67
15	PE10	Air	20	292.83	283.2	3.40
16	PE10	Air	30	393.92	397	0.78
17	PE10	Air	40	497.34	504.3	1.38
18	PE10	Air	40	488.89	504.3	3.06
19	PE10	Air	30	411.05	397	3.54
20	PE10	Air	30	392.85	397	1.05
21	PE10	Air	30	431.24	397	8.62

This shows that the error between the thermochemical model and the experimental data is very small. When comparing that percentage difference to the percentage error reported by those such as (Formby & Wharton, 1996) of 15-30% error between their experimental data, this shows a much more consistent spread of results for a more complex system.

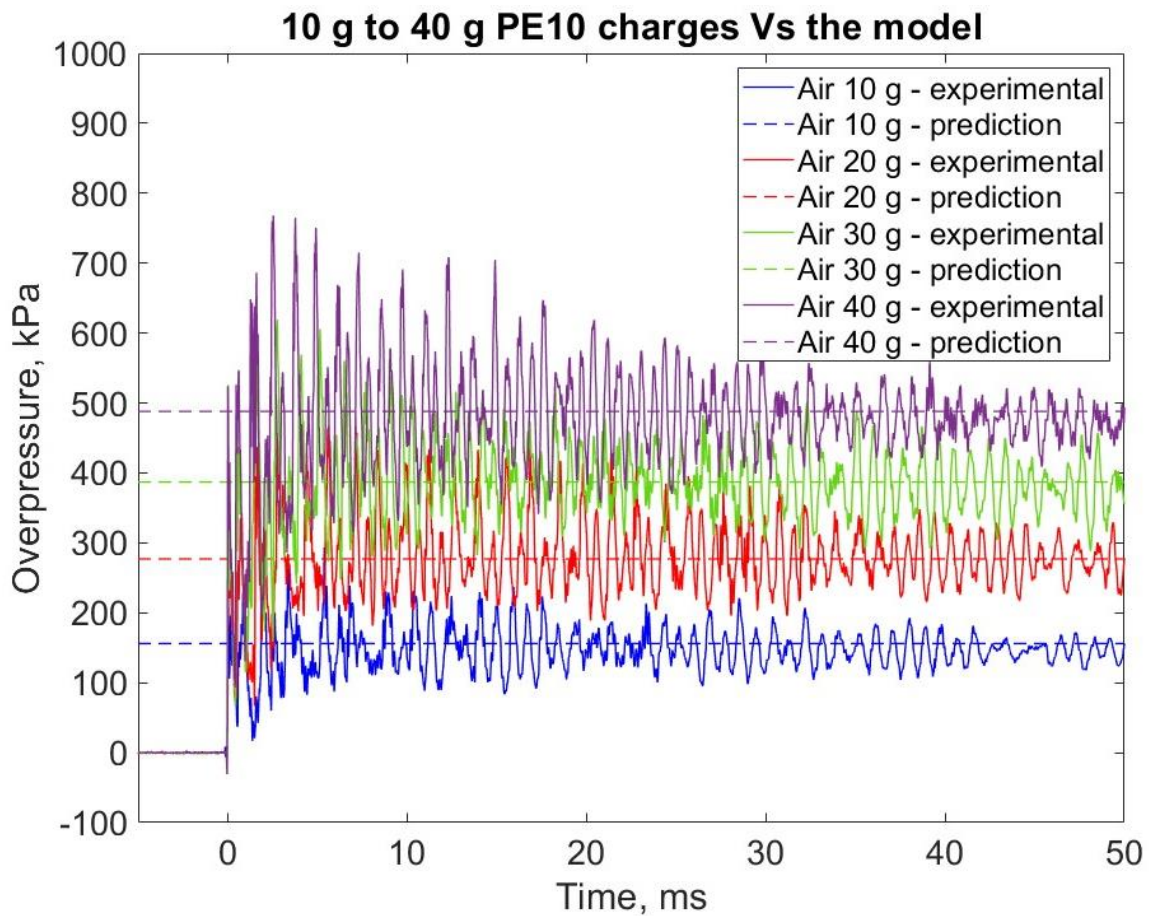


Figure 63 - A comparison of 10 g up to 40 g PE10 charges with comparisons to the thermochemical model.

This is now a very useful tool for evaluating the pressures generated by multiple explosives in a confined, unvented environment. This allows the prediction of pressures within these charge mass to volume ratios in a much faster fashion than using complex modelling to arrive at this prediction. To further the usefulness of this model, it can again be altered to ensure that it works when considering the use of different atmospheres that the explosive could detonate in. Previous validation data was generated by performing tests in nitrogen atmosphere and argon atmosphere. This allows the prediction of the pressures generated post initial shocks and afterburn when there are not standard conditions taking place.

Figure 64 and Figure 65 show the predictions of PE4 charges in nitrogen and argon atmospheres respectively, where they are compared to the thermochemical model results for these atmospheres. This shows that even when changing atmospheric conditions, the model holds well and can adapt and still accurately predict the pressures generated in those scenarios. This would not be the case if the ideal gas assumptions were not valid in these experiments as the model would be predicting away from the actual values.

With the ability to predict pressures when no afterburn is occurring accurately, this further reinforces the idea that the early stage increases in pressure seen in the pressure traces comparing a nitrogen test and a standard test, is due to the afterburn effect in the early stages as this difference is accounted for in the model which then maps accurately over the pressure traces.

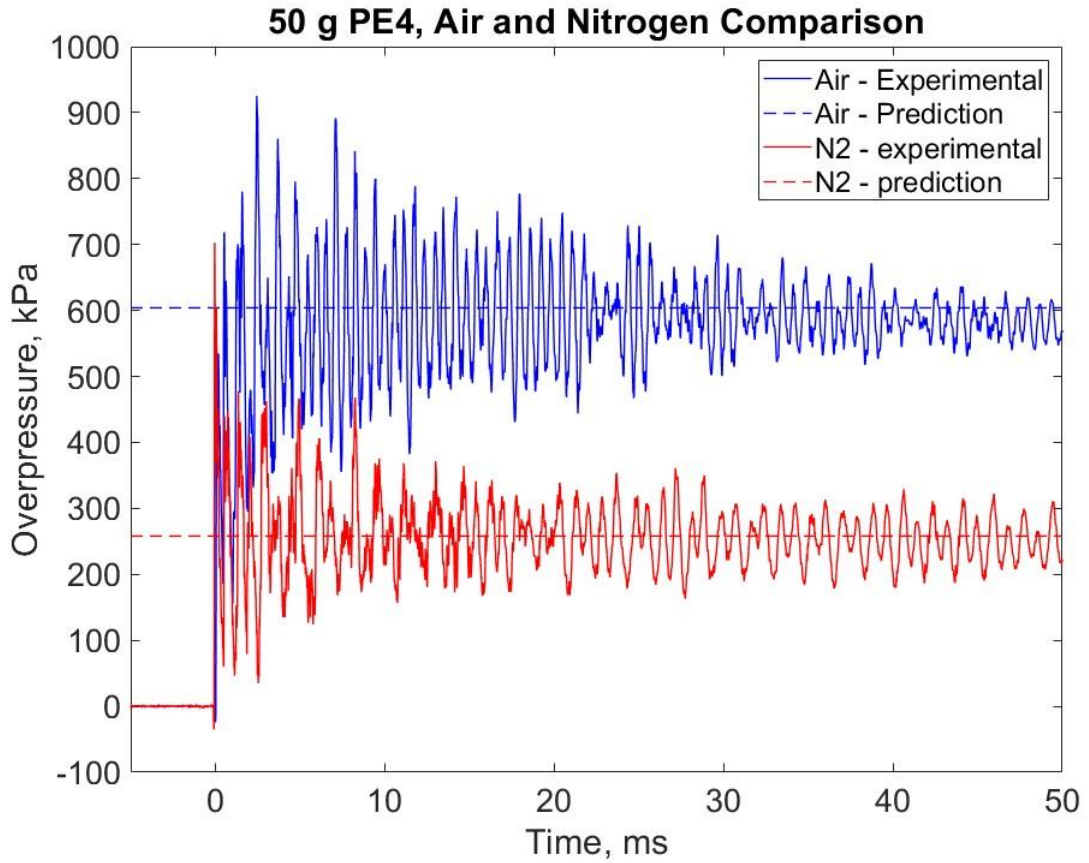


Figure 64 – Comparison of a 50 g PE4 charge detonating in nitrogen and air with thermochemical model prediction lines.

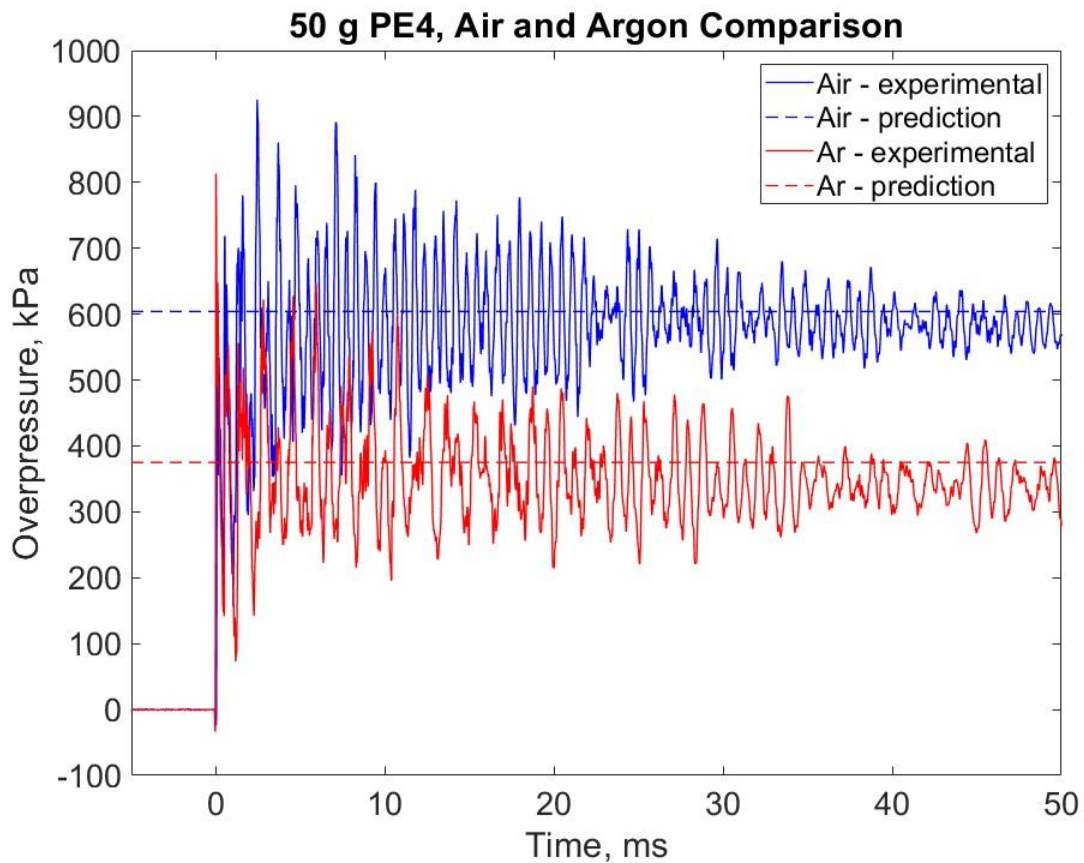


Figure 65 - Comparison of a 50 g PE4 charge detonating in argon and air with thermochemical model prediction lines.

Now that the thermochemical model has been evaluated across multiple charge sizes, multiple atmospheres, and multiple explosive types, it can be said that this model shows good promise for use as a fast-running thermochemical model able to predict maximum QSP values for explosive events. This is a significant contribution towards the understanding of the explosive process as it shows that energy loss to container or barriers is influential on the pressure loss over time. Therefore, if this can be implemented into a modelling software, it would make that model much more accurate and representative of real-world scenarios. It does however bring up issues with current modelling software that doesn't include these thermal losses into their design and uses venting to account for energy losses where values could end up lower or higher than predicted due to changes in the energy loss mechanisms.

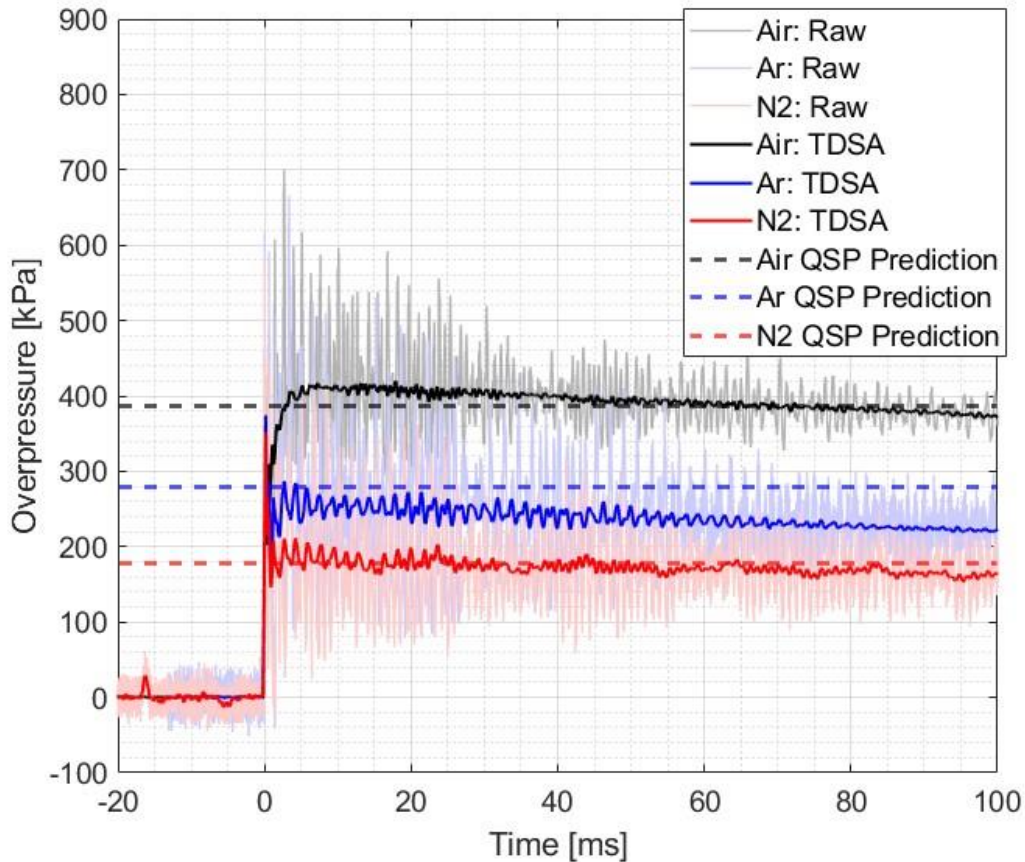


Figure 66 - QSP prediction comparisons of PE10 to smoothed data sets for air, argon and nitrogen.

Now the predictor has been compared to the raw data, we can compare it also to the smoothed data. This shows that for the nitrogen test there is the most overlap between the prediction line and the smoothed pressure trace, followed by the air atmosphere in which it underpredicts slightly at early stages before it converges to the line after 40 ms. Argon overpredicts slightly when compared to the smoothed data, though early stages are still close to the prediction line as shown before by around 10%. This may be a reason to investigate the thermochemical model and the way it calculates the pressure generation of argon and work out a more accurate version to become in line with the other predictors.

A table of the experimental maximum QSP values against thermochemical model values for PE4 and PE10 in nitrogen and argon is given in Table 22 and shows that the absolute percentage error for tests in nitrogen is 3.36 % and a standard deviation of 1.39, which is low, just as the average error of the tests conducted in air. The average error for the tests conducted in argon is 21.8 % and a standard deviation of 0.12 and is higher than the average error for nitrogen. The cause of this discrepancy is currently unknown, especially with the larger difference with PE4, but is still under investigation by the research group. This shows that the atmosphere does make a difference to the ability of the thermochemical model to predict the maximum QSP and that there is a need to further investigate the argon model to achieve the same level of confidence as the nitrogen and air tests.

Table 22 - Max QSP from experimental vs theoretical for PE4 and PE10 in nitrogen and argon.

Test	Explosive	Mass / g	Atmosphere	Experimental Max QSP	Predictor Max QSP	Error vs model
5	PE4	50	Nitrogen	253.15	264.6	4.33
6	PE4	50	Nitrogen	633.61	264.6	1.74
10	PE10	30	Nitrogen	174.92	182.1	3.94
11	PE4	50	Argon	369.49	585.8	36.93
12	PE4	30	Argon	244.38	363.8	32.83
22	PE10	30	Argon	244.05	292.8	16.65
23	PE10	30	Argon	258.68	292.8	11.65
24	PE10	30	Argon	261.01	292.8	10.86
25	PE10	30	Nitrogen	178.42	182.1	2.02
26	PE10	30	Nitrogen	173.4	182.1	4.78

Overall, this shows that there is a good consistency between the thermochemical model and the experimental data and hence it can be used in these situations to predict the QSP occurring in confined scenarios.

Chapter 7 – Conclusions and Future Work

7.1 Conclusions

This section will be a summary of the main findings from this thesis with respect to the questions generated from the literature review. The focus of the thesis was to gain an understanding of the nature of confined explosions and if they could be measured in a repeatable way. This work proves that not only can they be measured in a reliable way, but also that the events occurring in a confined explosion are consistent and repeatable when the experimental methodology is well controlled. This understanding provided the groundwork to investigate the influence of afterburn on an explosive charge and the time frames in which that affects the pressures in the system as well as helping to develop a fast-running thermochemical model based off first principles and ideal gas laws that predicts the maximum QSP generation. Further explanation of the different aspects are given in this chapter.

7.1.1 Repeatability of Confined Explosions

- Following confined testing of multiple identical tests of 50 g PE4 explosive in a confined chamber of 275 L volume, pressure traces showed consistent measurement of pressure where consistency of the explosive event was shown to be of a high level.
- Continuing this testing using other explosive types, namely PE10, the consistency was seen to maintain and pressure readings from alternate explosives also seemed to be consistent between tests.
- Though initial peaks between the explosive events varied, the maximum quasi-static pressures between the tests were seen to be consistent, which is the main focus of this section of the thesis.

7.1.2 Afterburn Effects

- To determine the effects of afterburn in a confined explosion, testing was done where the explosive charge was surrounded by a medium that contains no air, such as nitrogen or argon. These tests eliminated the possibility of afterburning with external oxygen to the explosive since it was removed.
- For nitrogen as an inert atmosphere, it showed a dramatic reduction in the max quasi-static pressure of the system. This proves that afterburn contributes extensively to the quasi-static pressure generated in an explosive event.

- The contributions of the afterburn in an explosive event occurring in an air atmosphere are shown to occur in the early time stages of the event as the pressure signal starts to differ as soon as there are any reflections occurring in the chamber. This shows that the shock reflecting off a boundary and mixing the external air into the fireball causes an increase in energy release and therefore an increase in pressure as soon as it occurs.
- When comparing the pressure traces between a test conducted in a pure nitrogen atmosphere to one conducted in an argon atmosphere, it is evident that the pressure in the argon atmosphere is increased compared to a nitrogen atmosphere. This is due to the increased density of the argon atmosphere, causing the shock wave speed to increase and allow the transfer of energy through the space more efficiently, allowing the pressure to be increased.

7.1.3 Thermochemical Modelling

- To create a fast-running predictive model, a chemistry based thermochemical model was built that predicts the maximum QSP of a system using energy releases of each chemical component of the system. To do this, the ideal gas assumptions were used as a guideline for the predictor, assuming that they would hold for the temperatures and pressures investigated.
- Once the predictor was created for the basic air trials of PE4 explosive charges, it was developed to include the use of PE10 and alternate atmospheres, ensuring that it would be robust when predicting alternate conditions.
- This method is based on the ideal gas equation, which itself is based on the following assumptions:
 - The gas particles have negligible volume.
 - The gas particles are equally sized and do not have intermolecular forces with other gas particles.
 - The gas particles move randomly in agreement with Newton's Laws of Motion (they move in straight lines).
 - The collisions between particles with other particles or the chamber walls are completely elastic (there is no energy loss).

Where in practice these assumptions are not realised, since the gas particles will occupy a certain volume of the chamber, each gas particle will not be equally sized post detonation, the particles will not move only in straight lines and the energy loss due to collision will not be zero. Though this is the case this ideal gas equation needed to be validated against an experimental test regime.

7.1.4 Infrared Thermometry

- To investigate the viability of using the ideal gas equation in the environment being used for these tests, a test regime that could measure the temperature directly during an explosive event was developed alongside the electrochemical engineering department at the university of Sheffield.
- This involved the use of an infrared thermometer that could measure temperature at high speeds. By using this in conjunction with pressure gauges to measure temperature and pressure from the same test, they could then be compared to each other and provide evidence of the ideal gas equations suitability.
- When comparing the results from the thermometer and the pressure measurements of the gauges, it was shown that other than the initial early time, the maximum QSP values agreed to a high level with those of the thermometer measurements using the ideal gas equation to convert them to the same variable.
- Early time differences between the thermometer measurements and the pressure gauge measurements are theorised to be due to the thermometer measuring the fireball temperatures as it expands, compared to the pressure gauges that measure the pressure at a singular point in the chamber. This will cause the temperature measurements to be higher initially than the pressure measurements due to the localised temperature of the fireball which dissipates after the fireball has occurred and then the thermometer measures the temperature of the chamber, as the pressure gauge measures the pressure of the chamber.
- This shows that for the maximum QSP predictor, the ideal gas equation is a suitable basis to use, as the pressures and temperatures when directly measured are at matching values when using the ideal gas equation to compare them.

7.1.5 Validation of the Model

- Once the ideal gas equation was determined to be suitable, the thermochemical model could then be used to compare to experimental results and validate it. This validation was completed by initially comparing tests of PE4 in air against the model of identical tests. These results showed that the predictor and measured pressures were very consistent for this initial validation trial.
- To ensure that the model is robust, it needed to be validated in other scenarios, not just a singular one. To do this, the model was altered to include the chemical composition of PE10, this meant that it could be used to predict PE10 and be compared to experimental data. This also showed high levels of agreement to experimental data, meaning it can be validated for two explosive types.

- Further robustness testing was then undertaken by altering the atmosphere in the model, changing it from standard air to nitrogen and argon. This changes the capabilities for afterburn energy to be released into the chamber, and hence reduces the pressure generation which accounts for the lack of afterburn energy in the system. This change when compared to tests conducted in a nitrogen or argon atmosphere again compare well with the experimental data, showing that even without afterburn this model can predict the maximum QSP pressures generated.
- This testing of the thermochemical model shows that it is possible to use this fast-running method to predict the maximum QSP in a confined explosion system through the use of chemical equations and energy releases as well as the ideal gas equation holding well enough to be used for such a model.

7.2 Future work

7.2.1 Non ideal explosives.

- Non-ideal explosives are of interest to protection engineers due to their use often in terror attacks. For this reason, it would be beneficial to conduct a similar regime of testing as the current one, but using explosives that are of a different composition and contain excess oxygen or large excesses of fuels to investigate their reactions to confinement.
- Some work on this has started to be undertaken through other projects at the University of Sheffield, investigating the QSP pressures generated by ANFO explosions and the influence of having excess oxygen in the explosive instead of excess fuels. Once completed, a journal article will be created to show the effects of non-ideal explosives and the differences that can be seen between the two.

7.2.2 The use of aluminised explosives that would increase the temperature.

- To investigate the effect of temperature increase on afterburn efficiency, the use of explosives containing aluminium powder as an additional fuel source. The additional fuel source would in theory provide additional energy in the early stages of the afterburn process dependant on the influence of this additional energy in the early stage.

- This would provide further information on the time frame that afterburn acts over. If the increased fuel content allows for the increased temperature that is expected by an aluminised explosive. A higher temperature in the early stages could allow for higher pressures for the early time shocks. This increased early pressure in theory would allow the maximum QSP to be increased over what you would expect from an equivalent mass of plastic explosive such as PE10 or PE4.
- The differences in the pressures would likely depend on the ratio of the aluminised explosive, so this could also be researched with aluminised explosives to see if the efficiency in a confined space requires a different ratio of explosive to aluminium than compared to free air explosives due to the confined nature.

7.2.3 Mitigation factors such as water and how these affect afterburn and QSP.

- The reduction and mitigation of explosive pressures is also of interest and could further be investigated. To do so a test series of plastic explosives could be performed where an explosive charge is surrounded by differing amounts of water. This water could be used to reduce the effects of afterburn on the pressure generation as it will quench the flames, taking energy out of the system.
- The water will also provide mitigation in the form of kinetic energy being reduced as the water requires work for it to be removed from around the charge. This would provide multiple methods for removing energy from the system so could provide an efficient way of removing energy from the system.

7.2.4 Further development of the model to include these facets.

- Once these additional tests have been completed, the data collected from them can be compared to the model, if the model can be altered to include the use of these different systems. This would then create a further use of the model that would expand its capabilities.
- If the model was expanded to include these assets it would require a lot more work to include these components as they would require adding new explosives as well as new atmosphere variations such as the water. Once this was created however, it would be a great tool for predicting confined explosive events.

7.2.5 DIC of confined chamber

- Investigation into what happens when one section of the chamber is no longer a rigid boundary and is instead a flexible surface, such as a thin aluminium plate. Using DIC technology, an investigation into the effects of confined blasts on a plate could be investigated and the differences between a rigid surface and a flexible plate could be determined in both QSP measurements as well as in plate deflections.
- This would allow investigations into the loading of members in confined areas that currently rely on modelling of fixed plates in open air scenarios to gain a more accurate understanding of the pressures and deflections that would be seen through a fully confined scenario.
- Once this capability was developed, it could then be used to test multiple shapes of clamped plates, as well as multiple shapes of chamber and confined pressures. This increase in understanding of plate deformation could then be included into the model to account for energy loss through work done to the plate, as long as rupture doesn't occur as it would then still contain the same moles of gas, just over a slightly larger volume.

7.2.6 Charge size to chamber volume expansion

- Further investigation into the different values of charge size and chamber volume ratios could be conducted. This would consist of examination of the mass to volume ratios where there is not enough oxygen for full afterburn but there is enough for partial afterburn, looking further at the choking effects of a lack of external oxygen and how this would affect the pressure profile of the explosive charges.
- It could also be investigated by using ratios where the energy release where the average temperature produced by the detonation would be lower, possibly reaching a point that the afterburn is stifled by the lack of temperature causing a lesser effect even though there may be available oxygen. This could be done through the use of small explosive charges in larger volumes, or also lowering the temperature of the testing rig so that the starting temperature is lower and more of the initial energy has to be used to raise that temperature before afterburn could occur.
- This could then show if the fireball can be self-sustaining in terms of temperature around itself before hitting a chamber wall where reflections would start to cause this afterburn, or if the dispersion of the fireball

temperature would be sent out into the surroundings faster, limiting the energy of the fireball and QSP.

Bibliography

- A. L. Kuhl, J. F. (1998). Confined Combustion of TNT Explosion Products in Air. *8th international colloquium on dust explosions*. Schaumburg, IL: Lawrence Livermore National Laboratory.
- A. Tyas, J. A. (2011). Prediction of clearing effects in far-field blast loading of finite targets. *Shock Waves*, 21(2), 111-119. doi:10.1007/s00193-011-0308-0
- Ahn, J.-K. D. (2017). Prediction of Near-Field Wave Attenuation Due to a Spherical Blast Source. *Rock Mechanics and Rock Engineering*, 50(11), 3085-3099.
- Akhavan, J. (2022). *The Chemistry of Explosives* (4th ed.). Vancouver: The Royal Society of Chemistry.
- Alex M. Remennikov, T. A. (2005). Modelling blast loads on buildings in complex city geometries. *Computers and Structures*, 83(27), 2197-2205.
- Anderson Jr CE, B. W. (1983). Quasi static pressure, duration and impulse for explosions in structures. *Int. J. Mech. Sci.*, 25(6), 455-464.
- Baker, W. E. (1983). *Explosion hazards and evaluation*. Amsterdam: Elsevier.
- Balakrishnan Kaushik, F. G. (2010). Numerical study of blast characteristics from detonation of homogeneous explosives. *Shock Waves*, 20(2), 147-162.
- Balakrishnan, K. (2010). Numerical study of blast characteristics from detonation of homogeneous explosives. *Shock Waves*, 147-162.
- Barnat, W. (2014). Experimental and numerical study of influence of incidence angle of shock wave created by explosive charge on the steel plate. *BULLETIN OF THE POLISH ACADEMY OF SCIENCES TECHNICAL SCIENCES*, 62(1), 151-163.
- Blastech Ltd. (2018). *Tyas(2018) MCM-ITP2 Task 11 – Blast testing - Final report. (Report No.BT-270-MBDA-P3-2v1.0.*
- Bogosian D., F. J. (2002). Measuring uncertainty and conservatism in simplified blast models. *30th Explosives Safety Seminar. 26*. Atlanta, Georgia: Department of Defense Explosives Safety Board.
- Borenstein, E. . (2009). Sensitivity analysis of blast loading parameters and their trends as uncertainty increases. *Journal of sound and vibration*, 321(3-5), 762-785.
- Brimblecombe, P. (1996). *Air Composition and Chemistry* . Cambridge University Press.
- C Knock, N. D. (2013). Blast waves from cylindrical charges. *Shock Waves*, 337-343.
- C. E. Anderson, W. B. (1983). QUASI-STATIC PRESSURE, DURATION, AND IMPULSE FOR EXPLOSIONS (e.g. HE) IN STRUCTURES. *International Journal of Mechanical Science*, 25(6), 455-464.
- C. Knock. (2016). Shock Waves from Hollow Cylinders. *29th International Symposium on Ballistics, 2: Explosion Mechanics*, pp. 1341-1349. Edinburgh, Scotland.

- C. Knock, N. D. (2015). Predicting Blast Waves from the Axial Direction of a Cylindrical Charge. *Propellants, Explosions, Pyrotechnics*, 40(2), 169-179.
- Catherine Johnson, P. M. (2018). Effect of Explosive Charge Geometry on Shock Wave Propagation. *Proceedings of the Conference of the American Physical Society Topical Group on Shock Compression of Condensed Matter*. St. Louis. doi:10.1063/1.5044977
- Cheval, K. L. (2003). Behavior of a Building Under Explosive Loading. *Proceedings of the ASME 2003 Pressure Vessels and Piping Conference. Problems Involving Thermal Hydraulics, Liquid Sloshing, and Extreme Loads on Structures, 16958*, pp. 165-173.
- Clarke, S. D. (2015). Geotechnical causes for variations in output measured from shallow buried charged. *International Journal of Impact Engineering*, 86, 274-283.
- Cooper, P. W. (2018). *Explosives Engineering*. John Wiley & Sons.
- Cranz, C. B. (1926). *Lehrbuch der Ballistik*. Berlin: Springer Germany.
- D. Farrimond, S. E. (2022). Time of arrival as a diagnostic for far-field high explosive blast waves. *International Journal of Protective Structures*, 13(2), 379-402. Retrieved from <https://journals.sagepub.com/doi/abs/10.1177/20414196211062923>
- D. G Farrimond, S. W. (2024). Experimental studies of confined detonations of plasticized high explosives in inert and reactive atmospheres. *Proceedings of the royal society A*, 480(2294). doi:<https://doi.org/10.1098/rspa.2024.0061>
- D. G. Farrimond, S. W. (2024). *Experimental Studies of Confined Plasticized High Explosive Detonations in Inert and Reactive Atmospheres*. Submitted to - Proceedings of the Royal Society A.
- Davison, L. (2008). *Fundamentals of Shock Wave Propagation in Solids*. Springer Science and Business Media.
- Dewey, J. (1964). The air velocity in blast waves from t.n.t. explosions. *the royal society of london. series A. mathematical and physical sciences*. 279, pp. 366-385. The Royal Society London.
- Doble Mukesh, A. K. (2005). *Biotreatment of industrial effluents*. Butterworth-Heinemann. doi:<https://doi.org/10.1016/B978-075067838-4/50019-1>.
- Edri I, Z. S. (2011). On Blast Pressure Analysis Due to a Partially Confined Explosion: I. Experimental Studies. *International Journal of Protective Structures*, 2(1), 1-20. Retrieved from <https://journals.sagepub.com/doi/abs/10.1260/2041-4196.2.1.1>
- Edri I.E., D. Y. (2019). TNT equivalency of different explosives in a confined space. *international symposium on the effects of munitions on structures*. Panama City, Florida.
- Edri, I. (2019). TNT equivalency of different explosives in a confined space. *international symposium on the effects of munitions on structures*. Panama City, Florida.
- Esparza, E. D. (1986). BLAST MEASUREMENTS AND EQUIVALENCY FOR SPHERICAL CHARGES AT SMALL SCALED DISTANCES. *international journal of impact engineering*, 4(1), 23-40. doi:[https://doi.org/10.1016/0734-743X\(86\)90025-4](https://doi.org/10.1016/0734-743X(86)90025-4).

- EURENCO. (2014, 08 18). *RDX NSH75 PE4*. EURENCO.
- Farrimond, D. G. (2023). Characterisation of Blast Loading from Ideal and Non-Ideal Explosives. *PhD Thesis*. University of Sheffield, U.K .
- Feldgun V.R., Y. K. (2016). Prediction of the quasi-static pressure in confined and partially confined explosions and its application to blast response simulation of flexible structures. *International Journal of Impact Engineering*, 90, 46-60. doi:https://doi.org/10.1016/j.ijimpeng.2015.12.001.
- Feldgun, V. Y. (2012). On Blast Pressure Analysis Due to a Partially Confined Explosion: II. Numerical Studies. *International Journal of Protective Structures*, 3(1), 61-79. Retrieved from https://journals.sagepub.com/doi/abs/10.1260/2041-4196.3.1.61
- Formby, S., & Wharton, R. (1996). Blast characteristics and TNT equivalence values for some commercial explosives detonated at ground level. *Journal of Hazardous Materials*, 50(2-3), 183-198. doi:https://doi.org/10.1016/0304-3894(96)01791-8.
- Fox, D. . (2011). The response of small scale rigid targets to shallow buried explosive detonations. *International Journal of Impact Engineering*, 38(11), 882-891. doi:https://doi.org/10.1016/j.ijimpeng.2011.05.009.
- Friedlander, F. G. (1946). The diffraction of sound pulses; diffraction by a semi-infinite plane. *Proceedings of the Royal Society A* (pp. 322-344). The Royal Society.
- Genetier, M. . (2014). Effect of the oxygen balance on ignition and detonation properties of liquid explosive mixtures. *Journal of Physics: Conference Series 500*. IOP Publishing. doi:10.1088/1742-6596/500/19/192001
- Glenn Randers-Pehrson, . K. (1997). *Airblast Loading Model for DYNA2D and DYNA3D*. MD, USA: ARMY RESEARCH LABORATORY.
- Griffiths, H. A. (1968). *Report of the inquiry into the collapse of flats at Ronan Point, Canning Town: presented to the Minister of Housing and Local Government*. HM Stationery Office.
- H.D.L. Patel, S. D. (2012). Human Body Projectiles Implantation in Victims of Suicide Bombings and Implications for Health and Emergency Care Providers: The 7/7 Experience. *Advancing Surgical Standards*, 313-317.
- Hopkinson, B. (1913). A Method of Measuring the Pressure Produced in the Detonation of High Explosives or by the Impact of Bullets. *Royal Society* , 411-413.
- Hopkinson, B. (1915). *British Ordnance Board Minutes*. Kew, UK: The national archives.
- Hryciów, Z. B. (2014). Influence of the shape of the explosive charge on blast profile. *Journal of KONES Powertrain and Transport*, 21(4), 169-176. doi:10.5604/12314005.1130466
- Hu Y, W. C. (2011). Characteristics of Confined Blast Loading in Unvented Structures. *International Journal of Protective Structures*, 2(1), 21-43. doi:10.1260/2041-4196.2.1.21

- Hyde, D. W. (1991). *Conventional weapons program (ConWep)*. Vicksburg, MS: US Army Waterways Experimental Station.
- I. Edri, V. F. (2013). Afterburning Aspects in an Internal TNT Explosion. *international Journal of Protective Structures*, 4(1), 97-116.
- Ian G. Cullis, J. S. (2010). Assessment of blast loading effects – Types of explosion and loading effects. *International Journal of Pressure Vessels and Piping*, 87(9), 493-503. doi:<https://doi.org/10.1016/j.ijpvp.2010.07.003>.
- J. A. Zukas, W. W. (2013). *Explosive Effects and Applications*. (1, Ed.) Aberdeen: Springer New York, NY. doi:<https://doi.org/10.1007/978-1-4612-0589-0>
- JACOBS, M. J. (1968). Chemistry of Detonations. I. A Simple Method for Calculating Detonation Properties of C-H-N-O Explosives. *THE JOURNAL OF CHEMICAL PHYSICS*, 48(1), 23-35. doi:10.1063/1.1667908
- Jai Prakash Agrawal, R. H. (2007). *Organic Chemistry of Explosives*. John Wiley & Sons.
- Kingery, C. N., & Bulmash, G. (1984). *Airblast parameters from TNT spherical air burst and hemispherical surface burst*, Technical Report ARBRL-TR-02555. Maryland USA: Ballistic research laboratory. Retrieved from <https://worldcat.org/title/867650613>
- Kinney, G., & Graham, K. (1985). *Explosive Shocks in Air* (2 ed.). NY, USA: Springer Berlin, Heidelberg. doi:<https://doi.org/10.1007/978-3-642-86682-1>
- Kuhl, A. L. (1998). *Confined combustion of tnt explosion products in air*. Livermore, CA, USA: Lawrence Livermore National Laboratory,.
- Kuhl, A. I. (2000). Effects of confinement on combustion of TNT explosion products in air. *28th International Symposium of Combustion*. Edinburgh, Scotland: Lawrence Livermore National Laboratory.
- KULITE SEMICONDUCTOR PRODUCTS, I. (2022, november 17). *HKM-375 Data sheet* . Retrieved from Kulite.com: <https://kulite.com//assets/media/2022/09/HKM-375-1.pdf>
- Kwak, H. S. (2015). *Disintegration of Carbon Dioxide Molecules in a Microwave Plasma Torch*. Seoul: Nature. doi:<https://doi.org/10.1038/srep18436>
- Langran-Wheeler C., S. E. (2021). Near-field spatial and temporal blast pressure distributions from non-spherical charges: horizontally-aligned cylinders. *International Journal of Protective Structures*, 12(4), 492-516. doi:10.1177/20414196211013443
- Langran-Wheeler, C. (2021). Near-field spatial and temporal blast pressure distributions from non-spherical charges: horizontally-aligned cylinders. *International Journal of Protective Structures*.
- Leonard, B. (2011). Alternative interpretations of the mole and the ideal gas equation. *Accreditation and Quality Assurance volume*, 16(11), 577-581. doi:10.1007/s00769-011-0822-x
- Le-Ping Zhou, B.-X. W.-F.-Z.-P. (2010). On the Specific Heat Capacity of CuO Nanofluid. *Advances in Mechanical Engineering*, 2. doi:10.1155/2010/172085

- Lobry, E. ,.-E. (2021). Tuning the Oxygen Balance of Energetic Composites: Crystallization of ADN/Secondary Explosives Mixtures by Spray Flash Evaporation. *Propellants, Explosives, pyrotechnics*, 46(3), 398-412. doi:<https://doi.org/10.1002/prop.202000090>
- Locking, P. (2011). The trouble with TNT equivalence. *26TH INTERNATIONAL SYMPOSIUM ON BALLISTICS*, (pp. 143-154). MIAMI, FL.
- M. Y. H. Bangash, T. B. (2005). *Explosion-Resistant Buildings: Design, Analysis, and Case Studies* (1 ed.). Springer. doi:<https://doi.org/10.1007/3-540-31289-7>
- McNesby, K. L. (2010). Afterburn Ignition Delay and Shock Augmentation in Fuel Rich Solid Explosives. *Propellants, Explosives, Pyrotechnics*, 35(1), 57-65. doi:<https://doi.org/10.1002/prop.200800084>
- McShane, G. ., (2013). A laboratory-scale buried charge simulator. *International Journal of Impact Engineering*, 62, 210-218. doi:<https://doi.org/10.1016/j.ijimpeng.2013.06.007>.
- Michael M. Swisdak, J. (1975). *EXPLOSION EFFECTS and properties part1 - explosions in air*. maryland: naval surface weapons centre.
- Milne, A. M. (2016). Modelling of complex blast. *International Journal of Protective Structures*, 7(3), 325-339. doi:10.1177/2041419616661431
- Netherton, M., & Stewart, M. (2008). Security risks and probabilistic risk assessment of glazing subject to explosive blast loading. *Reliability Engineering and System Safety*, 93(4), 627-638. doi:<https://doi.org/10.1016/j.ress.2007.03.007>.
- Obed Samuelraj Isaac, O. G. (2023). Blast wave interaction with structures – An overview. *International Journal of Protective Structures*, 14(4), 584-630. doi:10.1177/20414196221118595
- Ornellas, D. L. (1982). *Calorimetric Determinations of the Heat and Products of Detonation for Explosives: October 1961 to April 1982*. Lawrence Livermore National Laboratory.
- P. D. Smith, T. A. (1999). Clearing of blast waves from building facades. *Proceedings of the Institution of Civil Engineers: Structures and Buildings* , (pp. 193-199).
- Pepkin, V. a. (2007). Heat of Explosion of Commercial and Brisant High Explosives. *Combustion, Explosion, and Shock Waves*, 43(2), 212-218. doi:<https://doi.org/10.1007/s10573-007-0029-y>
- Pichandi, S. ., (2013). Fibrous and composite materials for blast protection of structural elements—A state-of-the-art review. *Journal of Reinforced Plastics and Composites*, 32(19), 1477-1500. doi:10.1177/0731684413498297
- Police, B. T. (2024, 10 15). *About Us - Our History*. Retrieved from British Transport Police: <https://www.btp.police.uk/police-forces/british-transport-police/areas/about-us/about-us/our-history/london-bombings-of-2005/>
- Poling, B. E. (2001). *The properties of gases and liquids* (5 ed.). American Chemical Society. doi:10.1021/ja0048634

- Proctor, J. F. (1972). *Internal blast damage mechanisms computer program*. Ohio: national technical information service. doi:<https://api.semanticscholar.org/CorpusID:108089336>
- Rayleigh, F. L. (1900). VI. The Law of Partition of Kinetic Energy. *The London, Edinburgh, and Dublin Philosophical Magazine and Journal of Science*, 49(296), 98-118. doi:<https://doi.org/10.1080/14786440009463826>
- Reisler, R. E. (1995). *MABS Monograph, Air Blast Instrumentation, 1943-1993 Measurement Techniques and Instrumentation Volume 1—The Nuclear Era—1945-1963*. Alexandria, VA: Defense Nuclear Agency.
- Reza Hedayati, M. S. (2016). 5 - Flat plate experimental tests. *Bird Strike*, 79-111. doi:<https://doi.org/10.1016/B978-0-08-100093-9.00005-4>
4<https://doi.org/10.1016/B978-0-08-100093-9.00005-4>
- Richard G. Stoner, B. W. (2004). The Attenuation of Spherical Shock Waves in Air. *Journal of Applied Physics*, 19, 670-678. doi:10.1063/1.1698189
- Rickman, D. ,. (2007). Development of an improved methodology for predicting airblast pressure relief on a directly loaded wall. *Journal of Pressure Vessel Technology*, 195-204.
- Rigby S., C. O. (2021). Spherical equivalence of cylindrical explosives: Effect of charge shape on deflection of blast-loaded plates. *International Journal of Impact Engineering*, 155. doi:10.1016/j.ijimpeng.2021.103892.
- Rigby SE, T. A. (2014). The Negative Phase of the Blast Load. *International Journal of Protective Structures*, 5(1), 1-19. doi:10.1260/2041-4196.5.1.1
- Rigby, S. R. (2020). Reflected Near-field Blast Pressure Measurements Using High Speed Video. *Experimental Mechanics*, 60(7), 875-888. doi:10.1007/s11340-020-00615-3
- S. Davis Herring, T. C.-J. (2010). Effects of void size, density, and arrangement on deflagration and detonation sensitivity of a reactive empirical bond order high explosive. *Physical Review B*. doi:<https://doi.org/10.1103/PhysRevB.82.214108>
- S. E. Rigby, T. A. (2014). Validation of semi-empirical blast pressure predictions for far field explosions - is there inherent variability in blast wave parameters? *6th International Conference on Protection of Structures against Hazards*. Sheffield.
- S.E Rigby, S. D. (2015). Angle of Incidence Effects on Far-Field Positive and Negative Phase Blast Parameters. *International Journal of Protective Structures*, 6(1), 23-42. doi:10.1260/2041-4196.6.1.23
- S.E. Rigby, A. T. (2014). A Numerical Investigation of Blast Loading and Clearing on Small Targets. *International Journal of Protective Structures*, 5(3), 253-274. doi:10.1260/2041-4196.5.3.253
- S.Paterson. (1955). The structure of the reaction zone in a detonating explosive. *Symposium on Combustion*, 5(1), 672-684. doi:10.1016/S0082-0784(55)80093-8.

- Salvado, F. C.-D. (2017). Confined explosions: The effect of compartment geometry. *Journal of Loss Prevention in the Process Industries*, 48, 126-144. doi:10.1016/j.jlp.2017.04.013.
- Shelton, F. H. (1988). *Reflections of a Nuclear Weaponeer*. Shelton Enterprises. Retrieved from <https://books.google.co.uk/books?id=B4zTQgAACAAJ>
- Shi, Y. . (2022). Experimental and numerical investigation of charge shape effect on blast load induced by near-field explosions. *Process safety and environmental protection*, 165, 266-277. doi:10.1016/j.psep.2022.07.018.
- Silvestrini, M. . (2009). Energy concentration factor. A simple concept for the prediction of blast propagation in partially confined geometries. *Journal of Loss Prevention in the Process Industries*, 22(4), 449-454. doi:10.1016/j.jlp.2009.02.018.
- Simoens, B. . (2015). Influence of the Shape of an Explosive Charge: Quantification of the Modification of the Pressure Field. *Central European Journal of Energetic Materials*, 12(2), 195-213.
- Sollier, A. . (2016). A novel method for the measurement of the von Neumann spike in detonating high explosives. *Journal of applied physics*. doi:10.1063/1.4955075
- Swisdak, M. M. (1994). *Simplified Kingery Airblast Calculations*.
- Sydney Meyers, E. S. (1990). Industrial explosives - a brief history of their development and use. *Journal of Hazardous Materials*, 23(2), 183-201. doi:https://doi.org/10.1016/0304-3894(90)85027-Z
- T.V. Bazhenova, L. G. (1984). Unsteady interactions of shock waves. *Progress in Aerospace Sciences*, 21, 249-331. doi:10.1016/0376-0421(84)90007-1.
- Tang L., S. R. (2018). Validation of Air3D for scaled experimental pressure and impulse data. *International Symposium on Military Aspects of Blast and Shock (MABS)*. The Hague, Netherlands.
- Tang, L. D. (2017). Reflections on Variability of Blast Pressure Measurement at Different Scales. *international symposium on the interaction of the effects of munitions with structures*. Bad Neuenahr - Ahrweiler. Retrieved from <https://api.semanticscholar.org/CorpusID:134034139>
- Taylor, S. G. (1949). The instability of liquid surfaces when accelerated in a direction perpendicular to their planes. I. 201(1065). doi:10.1098/rspa.1950.0052
- Taylor, S. G. (1950). The formation of a blast wave by a very intense explosion I. Theoretical discussion. *Proceedings of the Royal Society of London. Series A. Mathematical and Physical Sciences*, 201(1065), 159-174. doi:10.1098/rspa.1950.0049
- The Engineering Toolbox. (2024, January 19). *Carbon Dioxide - Specific Heat of Gas vs. Temperature*. Retrieved from The Engineering Toolbox: https://www.engineeringtoolbox.com/carbon-dioxide-d_974.html#gsc.tab=0

- The Engineering Toolbox. (2024, January 19). *Water Vapor - Specific Heat vs. Temperature*. Retrieved from The Engineering Toolbox: https://www.engineeringtoolbox.com/water-vapor-d_979.html
- Toolbox, T. E. (2024, 09 23). *Gases - Speed of Sound*. Retrieved from Engineering Toolbox: https://www.engineeringtoolbox.com/speed-sound-gases-d_1160.html
- Toolbox, T. E. (2024, 10 16). *Metals and Alloys Densities* . Retrieved from The Engineering Toolbox : https://www.engineeringtoolbox.com/metal-alloys-densities-d_50.html
- Toolbox, T. E. (2024, 10 16). *Specific Heat of Common Substances*. Retrieved from The Engineering Toolbox: https://www.engineeringtoolbox.com/specific-heat-capacity-d_391.html
- Trzcinski, W. (2006). On some methods of determining the detonation energy of explosives. *Archive of Combustion*, 55-62.
- Tyas A, J. J. (2016). Experimental studies of the effect of rapid afterburn on shock development of near-field explosions. *International Journal of Protective Structures.*, 7(3), 452-465. doi:10.1177/2041419616665931
- Tyas, A. ,. (2016). Experimental studies of the effect of rapid afterburn on shock development of near-field explosions. *International Journal of Protective Structures*, 7(3), 452-465. doi:10.1177/2041419616665931
- Tyas, A. (2018). Near-field High Explosive Blast Loading: The Challenges for Measurement and Prediction. *5th International Conference on Protective Structures*. Poznan, Poland. Retrieved from <https://eprints.whiterose.ac.uk/137946/>
- UFC-3-340-02. (2008). *Structures to resist the effects of accidental explosions*. Washington: US department of defence.
- Urbanski, T. (1964). *Chemistry and Technology of Explosives* . Warszawa: Pergamon Press.
- V.R. Feldgun, Y. K. (2011). A simplified model with lumped parameters for explosion venting simulation. *International Journal of Impact Engineering*, 38(12), 964-975. doi:10.1016/j.ijimpeng.2011.08.004.
- W. A. Trzcinski, S. C. (2007). Studies of Free Field and Confined Explosions of Aluminium Enriched RDX Compositions. *Propellants, Explosives, Pyrotechnics*, 502-508.
- Walter, P. L. (2004). *Air Blast and the Science of Dynamic Pressure Measurements*. Texas Christian University, Engineering Faculty . Depew, NY: Measurement Specialist/PCB Piezotronics, Inc. Retrieved October 2024, from https://www.pcb.com/contentstore/MktgContent/LinkedDocuments/Technotes/TN-31-0714_Air_Blast_Lowres.pdf
- Wang, L.-Y. ,.-M. (2019). Compensation method for infrared temperature measurement of explosive. *Thermochimica Acta*, 680. doi:10.1016/j.tca.2019.178342.

- Waples, D. W. (2004). A Review and Evaluation of Specific Heat Capacities of Rocks, Minerals, and Subsurface Fluids. Part 1: Minerals and Nonporous Rocks. *Natural Resources Research*, 13(2), 97-122. doi:10.1023/B:NARR.0000032647.41046.e7
- Weibull, H. R. (1968). Pressures recorded in partially closed chambers at explosion of TNT charges. *Annals of the New York Academy of Sciences*, 152(1), 357-361. doi:10.1111/j.1749-6632.1968.tb11987.x
- Whittaker, J. S. (2019). Blast-Wave Clearing for Detonations of High Explosives. *Journal of Structural Engineering*, 145(7).
- Wisotski, J. (1965). *Characteristics of Blast Waves Obtained From Cylindrical High Explosive Charges*. Denver: Denver Research Institute.
- Wu C., G. F. (2010). Investigation of Air-Blast Effects from Spherical-and Cylindrical-Shaped Charges. *International Journal of Protective Structures*, 1(3), 345-362. doi:10.1260/2041-4196.1.3.345
- Wu Chengqing, M. L. (2013). Experimental and numerical investigation of confined explosion in a blast chamber. *Journal of Loss Prevention in the Process Industries*, 26(4), 737-750. doi:10.1016/j.jlp.2013.02.001
- Xiangshao Kong, H. Z. (2019). An experimental study on the mitigation effects of fine water mist on confined-blast loading and dynamic response of steel plates. *International Journal of Impact Engineering*, 134. doi:10.1016/j.ijimpeng.2019.103370
- Xiao, W. ,. (2020). Influence of charge shape and point of detonation of high explosive cylinders detonated on ground surface on blast-resistant design. *International Journal of Mechanical Sciences*, 181. doi:10.1016/j.ijmecsci.2020.105697

Appendix 1

	A	B	C	D	E	F	G	H	I	J	K	L	M
1	Mass of PE4	0.05 kg		AIR_Initial					Det+Defl RDX				
2	%RDX	87		V	0.275 m ³				RDX	C3_H6_N6_O6+1.5O2->3CO2+3H2O+3N2			
3	%Paraffin Wax	13		M_air	0.336875 kg				Mass	0.0435 kg			
4		43.5	0.195858	P0	100000 Pa				Mols	0.195858			
5		6.5	0.018429	T0	288 K				Gas Produced				
6	Energy release			Mol air	11.48498 mol				CO2	0.587573 mol			
7	RDX Det	6178 kJ/kg		MolN2	8.967471	0.251205771			H2O	0.587573 mol			
8	RDX Def	3820 kJ/kg		Mol O2	2.406103	0.076995296			N2	0.587573 mol			
9	Paraffin Wax Def	42000 kJ/kg		Mol CO2	0.004594	-0.000202182			O2	-0.29379 mol			
10	Total energy release	707.913 kJ		MolAr	0.10681	0.004160048			CO	0 mol			
11	Total energy	776.4916				0.332563296							
12	Implied Ideal Gas Peak Temp	2364.804 K		E0	68.57855 kJ								
13	Implied QSP	843.2627 kPa		Mol Air Tot	11.48498								
14	T (user input to avoid circular re	843.3 K			68578.55								
15													
16	TNT Energy release per kg	14983 kJ		Air molar mass	N2	0.02187255							
17	TNT equivalent mass of charge	0.047248 kg			O2	0.006704							
18					CO2	0.000017604							
19		434.9	0.385659		Ar	0.000362216							
20		541.7	0.234793			0.028956371							
21		707.913											

N	O	P	Q	R	S	T	U	V
Defl of Paraffin Wax				Final Mol: Mol		Mass (kg)	Molar mass (kg/mol)	
Mineral OC25_H52+38O2 -->25CO2+26H2O				CO2	1.052924784	0.046339	0.04401	
Mass	0.0065 kg			H2O	1.066761098	0.019218	0.018015	
Mols	0.018430305 mol			N2	9.555044365	0.267665	0.028013	
Gas Produced				O2	1.411964816	0.045183	0.032	
CO2	0.460757627 mol			CO	0	0	0.02801	
H2O	0.479187932 mol			Ar	0.1068103	0.00416	0.038948	
N2	0 mol			SUM (n)	13.19350536	0.382565	0.028996	
O2	-0.700351594 mol			Check Sun	13.19350536	0.386875		
				Average Molar Mass		0.028996	kg/mol	
Mol Weig g/mol								
RDX	222.1							
Min Oil	352.7							
PE4	239.078			0.586826425				
3819.900946								

Appendix 2

Mass upper and lower bounds PE10 Air

mass	volume	initial temp	qsp	% error
0.0995	275	280	150.5	-4.32295
0.0105	275	280	164	4.259377
0.0195	275	280	276.5	-2.12389
0.0205	275	280	288.4	2.088496
0.0295	275	280	390.5	-1.38889
0.0305	275	280	401.5	1.388889
0.0395	275	280	497.9	-1.03359
0.0405	275	280	508.3	1.033592
0.0495	275	280	600.3	-0.82604
0.0505	275	280	610.3	0.826037

Volume upper and lower bounds PE10 Air

mass	volume	initial temp	qsp	% error
0.01	273.8	280	158.3	0.635728
0.01	277.8	280	156.3	-0.63573
0.02	273.8	280	284.2	0.60177
0.02	277.8	280	280.7	-0.63717
0.03	273.8	280	398.4	0.606061
0.03	277.8	280	393.6	-0.60606
0.04	273.8	280	506.2	0.61618
0.04	277.8	280	500.1	-0.5963
0.05	273.8	280	609	0.611267
0.05	277.8	280	601.7	-0.59475

Temperature upper and lower bounds PE10 Air

mass	volume	initial temp	qsp	% error
0.01	275	273.15	158.5	0.640578
0.01	275	292.15	155.2	-1.33503
0.02	275	273.15	284.4	0.672566
0.02	275	292.15	279.1	-1.20354
0.03	275	273.15	398.6	0.656566
0.03	275	292.15	391.6	-1.11111
0.04	275	273.15	506.3	0.636056
0.04	275	292.15	497.8	-1.05347
0.05	275	273.15	608.9	0.594746
0.05	275	292.15	599.2	-1.00776

Mass upper and lower bounds PE10 N2

mass	volume	initial temp	qsp	% error
0.0995	275	280	65.3	-4.67153
0.0105	275	280	71.7	4.671533
0.0195	275	280	125.7	-2.17899
0.0205	275	280	131.3	2.178988
0.0295	275	280	179.5	-1.42779
0.0305	275	280	184.7	1.427787
0.0395	275	280	229.4	-1.07805
0.0405	275	280	234.3	1.034929
0.0495	275	280	276.6	-0.86022
0.0505	275	280	281.3	0.824373

Volume upper and lower bounds PE10 N2

mass	volume	initial temp	qsp	% error
0.01	273.8	280	69	0.729927
0.01	277.8	280	68.1	-0.58394
0.02	273.8	280	129.3	0.622568
0.02	277.8	280	127.7	-0.62257
0.03	273.8	280	183.2	0.604064
0.03	277.8	280	181	-0.60406
0.04	273.8	280	233.3	0.603708
0.04	277.8	280	230.5	-0.60371
0.05	273.8	280	280.7	0.609319
0.05	277.8	280	277.3	-0.60932

Temperature upper and lower bounds PE10 N2

mass	volume	initial temp	qsp	% error
0.01	275	273.15	68.9	1.468379
0.01	275	292.15	67.9	-0.87591
0.02	275	273.15	129.4	0.700389
0.02	275	292.15	127	-1.16732
0.03	275	273.15	183.5	0.768808
0.03	275	292.15	179.8	-1.26304
0.04	275	273.15	233.6	0.733075
0.04	275	292.15	228.9	-1.29366
0.05	275	273.15	281	0.716846
0.05	275	292.15	275.6	-1.21864

Mass upper and lower bounds PE4 N2

mass	volume	initial temp	qsp	% error
0.0995	275	280	59.8	-4.77707
0.0105	275	280	65.8	4.77707
0.0195	275	280	116.5	-2.2651
0.0205	275	280	121.9	2.265101
0.0295	275	280	168.1	-1.46542
0.0305	275	280	173.1	1.465416
0.0395	275	280	2164	889.4833
0.0405	275	280	221.1	1.097394
0.0495	275	280	262.3	-0.86924
0.0505	275	280	266.8	0.831444

Volume upper and lower bounds PE4 N2

mass	volume	initial temp	qsp	% error
0.01	273.8	280	63.2	0.636943
0.01	277.8	280	62.4	-0.63694
0.02	273.8	280	120	0.671141
0.02	277.8	280	118.5	-0.58725
0.03	273.8	280	171.7	0.644783
0.03	277.8	280	169.6	-0.58617
0.04	273.8	280	220.1	0.640146
0.04	277.8	280	217.4	-0.59442
0.05	273.8	280	266.2	0.604686
0.05	277.8	280	263	-0.60469

Temperature upper and lower bounds PE4 N2

mass	volume	initial temp	qsp	% error
0.01	275	273.15	63	1.597428
0.01	275	292.15	62.3	-0.79618
0.02	275	273.15	119.9	0.587248
0.02	275	292.15	118.1	-0.92282
0.03	275	273.15	171.7	0.644783
0.03	275	292.15	168.7	-1.11372
0.04	275	273.15	220.2	0.685871
0.04	275	292.15	216.2	-1.14312
0.05	275	273.15	266.4	0.680272
0.05	275	292.15	261.6	-1.13379